Institut für Erd- und Umweltwissenschaften
Mathematisch-Naturwissenschaftliche Fakultät
Universität Potsdam

LATE PALEOZOIC BASIN ANALYSIS OF THE LOPPA HIGH AND FINNMARK PLATFORM IN THE NORWEGIAN BARENTS SEA:

Integration of seismic attributes and seismic sequence stratigraphy

Jhosnella Sayago

Kumulative Dissertation zur Erlangung des akademischen Grades
Doktor der Naturwissenschaften (Dr. rer. Nat.)
in der Wissenschaftsdisziplin Geologie

Eingereicht an der
Mathematisch-Naturwissenschaftlichen Fakultät der
Universität Potsdam

Potsdam, June 2014

ABSTRACT

The subsurface upper Palaeozoic sedimentary successions of the Loppa High half-graben and the Finnmark platform in the Norwegian Barents Sea (southwest Barents Sea) were investigated using 2D/3D seismic datasets combined with well and core data. These sedimentary successions represent a case of mixed siliciclastic-carbonates depositional systems, which formed during the earliest phase of the Atlantic rifting between Greenland and Norway. During the Carboniferous and Permian the southwest part of the Barents Sea was located along the northern margin of Pangaea, which experienced a northward drift at a speed of ~2–3 mm per year. This gradual shift in the paleolatitudinal position is reflected by changes in regional climatic conditions: from warm-humid in the early Carboniferous, changing to warm-arid in the middle to late Carboniferous and finally to colder conditions in the late Permian. Such changes in paleolatitude and climate have resulted in major changes in the style of sedimentation including variations in the type of carbonate factories. The upper Palaeozoic sedimentary succession is composed of four major depositional units comprising chronologically the Billefjorden Group dominated by siliciclastic deposition in extensional tectonic-controlled wedges, the Gipsdalen Group dominated by warm-water carbonates, stacked buildups and evaporites, the Bjarmeland Group characterized by cool-water carbonates as well as by the presence of buildup networks, and the Tempelfjorden Group characterized by fine-grained sedimentation dominated by biological silica production.

In the Loppa High, the integration of a core study with multi-attribute seismic facies classification allowed highlighting the main sedimentary unconformities and mapping the spatial extent of a buried paleokarst terrain. This geological feature is interpreted to have formed during a protracted episode of subaerial exposure occurring between the late Palaeozoic and middle Triassic. Based on seismic sequence stratigraphy analysis the palaeogeography in time and space of the Loppa High basin was furthermore reconstructed and a new and more detailed tectono-sedimentary model for this area was proposed.

In the Finnmark platform area, a detailed core analysis of two main exploration wells combined with key 2D seismic sections located along the main depositional profile, allowed the evaluation of depositional scenarios for the two main lithostratigraphic units: the Ørn Formation (Gipsdalen Group) and the Isbjørn Formation (Bjarmeland Group). During the mid-Sakmarian, two major changes were observed between the two formations including (*1*) the variation in the type of the carbonate factories, which is interpreted to be depth-controlled and (*2*) the change in platform morphology, which evolved from a distally steepened ramp to a homoclinal ramp.

The results of this study may help supporting future reservoirs characterization of the upper Palaeozoic units in the Barents Sea, particularly in the Loppa High half-graben and the Finnmark platform area.

ZUSAMMENFASSUNG

Die unterirdischen Sedimentabfolgen des oberen Paläozoikums des Loppa High Halbgrabens und der Finnmark-Plattform in der norwegischen Barentssee (südwestliche Barentssee) wurden mit 2D/3D-Seismik Datensätzen untersucht, welche mit Bohrungs-und Kerndaten kombiniert wurde. Diese Sedimentabfolgen stellen einen Fall von gemischten siliziklastischen-karbonatischen Ablagerungssystemen dar, die während der ersten Phase des Atlantiks-Riftings zwischen Grönland und Norwegen gebildet wurden. Während des Karbons und Perms war der südwestliche Teil der Barentssee entlang des Nordrand von Pangäa lokalisiert, der einen Drift nach Norden mit einer Geschwindigkeit von ~ 2-3 mm pro Jahr erlebte. Diese allmähliche Verschiebung in der paläolatitudinalen Position spiegelt sich durch Veränderungen in den regionalen klimatischen Bedingungen wider: von warm-feuchten im frühen Karbon, zu warm-ariden im mittleren bis späten Karbon und schließlich zu gemäßigten-kalten Bedingungen im späten Perm. Solche Änderungen in Paläolatitude und Klima führten zu größeren Veränderungen im Sedimentationsstil, einschließlich Variationen in der Karbonatausfällungsart.

Die obere paläozoische Sedimentfolge umfasst vier Hauptablagerungseinheiten, in chronologischer Reihenfolge, die Billefjorden-Gruppe, welche von siliziklastischen Ablagerungen in durch extensionale Tektonik gesteuerten Keilen dominiert wird, die Gipsdalen-Gruppe, die von Warmwasser-Karbonaten, „stacked buildups" und Evaporiten dominiert wird, die Bjarmeland-Gruppe, von Kaltwasser-Karbonaten als auch durch die Anwesenheit von „buildup-networks" charakterisiert, und die Tempelfjorden-Gruppe, die durch feinkörnige Sedimentation, dominiert durch biologische Produktion von Kieselsäure, gekennzeichnet.

In der Loppa High war es durch die Integration einer Kernstudie mit einer Multi-Attribut Klassifizierung der seismischen Fazies möglich, die wichtigsten sedimentären Diskordanzen hervorzuheben und die räumliche Ausdehnung eines verborgenen Paläokarstsystems zu kartieren. Diese geologische Besonderheit soll sich während einer lang-anhaltenden Episode der subaerischen Exposition gebildet haben, die zwischen dem späten Paläozoikum und mittleren Trias auftrat. Basierend auf der Analyse seismischer Sequenzstratigraphie, wurde die Paläogeographie des Loppa High Beckens im Hinblick auf Zeit und Raum weiterhin umgebaut und eine neue und es wurde ein detaillierteres tektonisch-sedimentäres Modell für diesen Bereich vorgeschlagen.

Im Bereich der Finnmark-Plattform konnte durch eine detaillierte Bohrkernanalyse zweier Explorationsbohrungen in Kombination mit seismischen 2D-Schlüssel-Sektionen, die sich entlang des Hauptablagerungsprofils befindet, Ablagerungsszenarien für die beiden wichtigsten lithologischen Einheiten bewertet werden: die Ørn Formation (Gipsdalen Gruppe) und die Isbjørn Formation (Bjarmeland-Gruppe). Im mittleren Sakmarian wurden zwei wichtige Änderungen zwischen den beiden Formationen beobachtet, einschließlich (1) der Veränderung in der Art der Karbotausfällungen, welche als Tiefen-abhängig beschrieben wird, und (2) die Veränderung der Plattformmorphologie, die sich von einer distal steilen Rampe zu einer homoklinalen Rampe entwickelte.

Die Ergebnisse dieser Studie können dazu beitragen, zukünftige Reservoir-Charakterisierungen der Einheiten des oberen Paläozoikum in der Barentssee zu unterstützen, vor allem im Loppa High Halbgraben und dem Finmmark Plattformbereich.

CONTENTS

3. Late Paleozoic seismic sequence stratigraphy and paleogeography of the Loppa High in the Norwegian Barents Sea

4. Facies and seismic analysis from the late Carboniferous–early Permian Finnmark carbonate Platform (southern Norwegian Barents Sea): a new assessment of the carbonate factories and depositional geometries

LIST OF FIGURES

LIST OF TABLES

Acknowledgements

1

INTRODUCTION

1.1. Objectives and scope of the study

The study of the upper Paleozoic sedimentary successions in the subsurface of the Norwegian Barents Sea remains a key objective in the economical development of the area. Their investigation has not been as exhaustive as in the overlying Mesozoic and Cenozoic sedimentary deposits due to several factors, which include the uneconomic results from the wells drilled in the 80's, the limited well data available reaching these deposits and the degradation of the seismic signal/noise ratio at those depths. However, in the Russian sector of the Barents Sea many wells have tested productive lower Permian-Carboniferous reservoirs (e.g., Zhemchugova and Schamel, 1994).

In the year 2000, a renewed exploration phase in the Norwegian Barents Sea started with the acquisition of 3D seismic surveys as well as collaborative geological projects between oil companies and academic research groups. From these efforts two main oil discoveries were made in the Norwegian Barents Sea: one in the Hammerfest Basin and one the Nordkapp Basin, both were associated to sediments of Mesozoic age. Additionally, the investigation of the upper Paleozoic units have also gained from this exploration phase and the number of related publications have increased over the last decade (e.g., Larssen et al., 2002; Elvebakk, 2003; Hunt et al., 2003; Lindstrom, 2003; Carrillat et al., 2005; Larssen et al., 2005; Stemmerik and Worsley, 2005; Colpaert et al., 2007; Rafaelsen et al., 2008; Fisher et al., 2010; Sayago et al., 2012; Ahlborn et al., 2014). During the year 2013 the first economical oil discovery in Permian carbonates rocks was drilled in the Norwegian Barents Sea (www.npd.no).

The present research thesis aims to improve our understanding of the upper Paleozoic units in the Barents Sea and its main objectives are:

(1) To map the extension of karstified areas in the upper Paleozoic units of the Loppa High and explain their origin.

(2) To reconstruct the late Paleozoic palaeogeography and propose a detailed tectono-sedimentary model, in time and space, for the Loppa High half-graben.

(3) To discuss various depositional scenarios for the middle Sakmarian shifting in the carbonate factories and platform morphology observed at the boundary between the two main upper Paleozoic formations (Ørn and Isbjørn) of the Finnmark Platform.

(4) To test unconventional seismic interpretation techniques, such multi-attribute seismic facies classification in areas where 3D seismic data are available but where well data are sparse.

The analysis of subsurface sedimentary deposits relies in the integration of 2D/3D seismic surveys, well data including geophysical well logs, facies analysis derived from cored rocks, ditch- and sidewall- samples; all complemented by the study of outcrops analogues. In the present study the main data used are 2D/3D seismic surveys combined with exploration wells (three in the Loppa High area and two in the Finnmark Platform area)

(Figure 1). The results and models attained in this thesis must be pondered at the resolution and scale of the seismic data and age control available. The vertical resolution of the seismic data for the studied intervals can fluctuates between 20 m to 315 m, depending on the seismic signal frequency. The age control remains mostly at the stage level and is obtained from published data, which were accordingly cited. This investigation should, therefore, be considered as a regional study.
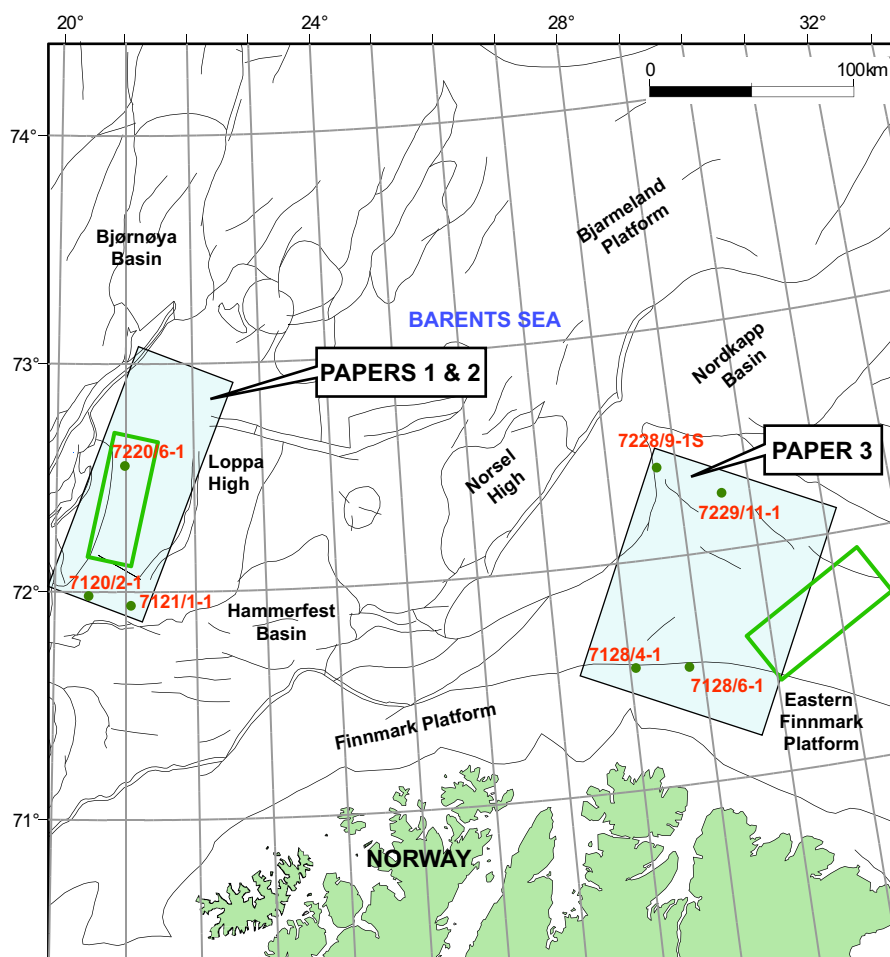
Figure 1. Location map of the study area in the Norwegian sector of the Barents Sea. The main two study areas are enclosed by blue polygons. Used 3D seismic surveys (green rectangles) and exploration wells are also shown. The main geological provinces and structural lineaments in the subsurface of the Norwegian Barents Sea are shown. This map was generated in Petrel™ with data provided by Edison Oil& Gas.

1.2. General geological setting

During the late Paleozoic, the southwest part of the Barents Sea was located along the northern margin of Pangaea and was affected by the early rifting of the Atlantic arm between Greenland and Norway, which generated a structural style characterized by half-graben geometries (e.g., Golonka and Ford, 2000; Stemmerik and Worsley, 2005). A rifting event in the middle Carboniferous (Bashkirian) (Stemmerik and Worsley, 1989; Stemmerik et al., 1991) contributed to fault-controlled subsidence and formation of basins, along the rift axis,

such as the Nordkapp and Trømso basins in the Barents Sea (e.g., Stemmerik et al., 1999). The gentler subsiding platforms such as the Finnmark Platform and the structurally active blocks such as the Loppa High became sites of a mixed siliciclastic-carbonate deposition, which gradually evolved toward pure shallow-marine deposition with predominance of carbonates from the middle Carboniferous until the late Permian (e.g., Stemmerik and Worsley, 1989, 2005). Furthermore, the northward drift of the northern margin of Pangaea induced changes in climatic conditions from warm-humid in the early Carboniferous, to warm-arid in the middle to late Carboniferous, and finally to colder conditions in the late Permian (e.g., Beauchamp and Desrochers, 1997; Stemmerik and Worsley, 2000; Beauchamp and Baud, 2002; Stemmerik and Worsley, 2005). The induced climatic change is reflected in the style of sedimentation and type of biogenic production during each time period. In each of the following chapters a detailed geological setting and stratigraphy is presented for the discussed study areas.

1.3. General methodology

3D Multi-attribute seismic study, seismic sequence stratigraphy, and core analysis are the main tools employed in this investigation. A 3D multi-attribute study allows revealing information from the seismic data, which cannot be observed using conventional seismic interpretation methods. The most significant seismic attributes are combined into an artificial neural network to automatically separate different seismic facies in an interval, horizon or complete 3D seismic cube (e.g., Coléou et al., 2003; Linari et al., 2003; Tebo and Hart, 2005).

For the Loppa High area, the 3D multi-attribute seismic facies classification allowed discriminating the various seismic facies related to seismic discontinuities along the 3D seismic survey. When correlated with the lithofacies identified in the core analysis (from well 7220/6-1, Figures 1 and 3.4), the resulting seismic facies were showed to represent sedimentary unconformities. 3D volume rendering technique allowed mapping the spatial extent of the unconformities and then the probable mechanisms about their origin were discussed. Seismic sequence stratigraphic analysis allowed evaluating the basin infill evolution from the early Carboniferous to the late Permian in the Loppa High half-graben and assesses the potential local tectonic controls –including uplift, rotation, and subsidence (Bosence et al., 1998; Cross et al., 1998; Sharp et al., 2000; Bosence, 2005)– of the overall morphology of the seismic sequences. Furthermore, the seismic sequence stratigraphic analysis allowed the palaeogeography for key intervals of time during the late Paleozoic to be reconstructed.

For the Finnmark Platform area, a core analysis from two exploration wells (7128/4-1 and 7128/6-1, Figures 1 and 4.1) along with a key 2D seismic line, allowed re-evaluating the depositional scenarios of the main lithostratigraphic units. Furthermore, new drivers are proposed to explain the variability of the carbonate factories as well as of the platform morphologies observed across the boundary between the two main lithostratigraphic units (i.e., Ørn and Isbjørn Formations).

1.4. The cooperation between Edison Oil & Gas and the University of Potsdam

This PhD thesis was funded by a collaborative research project between the Edison Oil & Gas (Norway branch) and the Sedimentology Group at the Institute of Earth- and Environmental Sciences from the University of Potsdam, as part of the growing exploration phase in different sectors of the Norwegian Barents Sea. The main goal of this cooperation

was to enhance our understanding of the local tectono-stratigraphic evolution of the upper Paleozoic sedimentary units in Barents Sea with special focus on the Loppa High and the Finnmark Platform areas. Edison Oil & Gas and the Norwegian Petroleum Directorate provided the raw data, which comprised 2D/3D seismic surveys as well as well and core data.

1.5. Organization of the thesis

This PhD thesis is organized in several chapters. Chapters 2, 3, and 4 are research papers, which integrate the main results of this work. Chapter 2 (paper I) shows conventional seismic interpretation, 3D multi-attribute seismic facies classification, and core analysis in the Loppa High area (Figure 1). This multidisciplinary analysis allowed mapping the extent of karstified areas, which affected the crest of the upper Paleozoic units in the Loppa High. Such karstification processes occurred during a protracted episode of multiple subaerial exposures extending from the late Paleozoic and middle Triassic. The large extent of the mapped karstified terrain (12 km in width x 46 km in length) suggests that this buried erosive morphology may represent a coalesced collapsed paleocave system. This study additionally refined the description of the Loppa High half-graben including its structural position. Furthermore it allowed detecting the main seismic facies related to sedimentary unconformities within the upper Paleozoic units. Paper I was published by the *American Association of Petroleum Geologist* (Sayago, J., Di Lucia, M., Mutti, M., Cotti, A., Sitta, A., Broberg, K., Przybylo, A., Buonaguro, R., Zimina, O., 2012, Characterization of a deeply buried paleokarst terrain in the Loppa High using core data and multi-attribute seismic facies classification: *AAPG Bulletin*, v. 96, No. 10, p. 1843-1866, doi: 10.1306/02271211137).

Chapter 3 (paper II) focused on a detailed seismic sequence stratigraphic analysis of the upper Paleozoic units in the Loppa High (Figure 1). This study allowed a better understanding of the late Paleozoic stratigraphic evolution of the Loppa High. The palaeogeography of key time intervals was reconstructed and discussed in terms of local tectonic deformations, global sea-level oscillations, and climatic changes. Paper II has been submitted to the journal *Marine and Petroleum Geology* (Sayago, J., Di Lucia, M., Mutti, M., Sitta, A., Cotti, A., Frijia, G., Late Paleozoic seismic sequence stratigraphy and palaeogeography of the Loppa High in the Norwegian Barents Sea, submitted to *Marine and Petroleum Geology*).

Chapter 4 (paper III) evaluated the variations of carbonate factories and depositional geometries of upper Paleozoic units (Ørn and Isbjørn Formations, middle Sakmarian boundary) from the Finnmark Platform area (Figure 1). Paper III is in preparation for the *American Association of Petroleum Geologist* (Di Lucia, M., Sayago, J., Frijia, G., Mutti, M., Cotti, A., Sitta, A., Facies and seismic analysis from the late Carboniferous-early Permian Finnmark carbonate platform (southern Norwegian Barents Sea): a new assessment of the carbonate factories and depositional geometries).

2

CHARACTERIZATION OF A DEEPLY BURIED PALEOKARST TERRAIN IN THE LOPPA HIGH BY USING CORE DATA AND MULTI-ATTRIBUTE SEISMIC FACIES CLASSIFICATION

Sayago J., Di Lucia M., Mutti M., Cotti A., Sitta A., Broberg K., Przybylo A., Buonaguro R., Zimina O.

Abstract

The recognition of paleokarst in subsurface carbonate reservoirs is not straightforward, as conventional seismic interpretation alone is generally not sufficient to discriminate karstified areas from their surroundings. In the Loppa High (Norwegian Barents Sea), a protracted episode of subaerial exposure occurring between the late Paleozoic and mid-Triassic time – upper Permian to Anisian – resulted in significant overprinting of the previously deposited carbonate units. Here, we map the extension of the karstified areas using an integrated approach consisting of (1) a core study of critical paleokarst intervals; (2) a 3D seismic stratigraphic analysis; and (3) a 3D multi-attribute seismic facies classification. A core retrieved in the flat-topped Loppa High revealed breccia deposits at least 50 m thick, which probably resulted from cave collapses following the burial of the karst terrain. The seismic facies classification was tested on a 3D cube to (1) discriminate the respective seismic facies related to the breccia deposits compared with other seismic facies and (2) to estimate their spatial extent. Seismic facies analysis suggest that breccias occupied the topmost area of the structural high, extending up to 12 km in width, 46 km in length, and tens of meters in thickness. The inference of such a large amount of breccia suggests that a significant part of this terrain was derived from the amalgamation of successive cave-development events – including periods of subaerial exposure and subsequent burial and collapse – resulting in a 'coalesced collapsed-paleocave system'. Previous observations from the Loppa High revealed the presence of karst plains associated with sinkholes, caves and other dissolution phenomena associated with the breccia facies, further suggesting that a large volume of carbonate rocks in this area was affected by subaerial exposure and karstification. Our integrated approach and proposed karstification model could be applied to similar sedimentary basins that accommodate deeply buried carbonate successions affected by protracted episodes of subaerial exposure, where only few wells as well as 3D seismic data are available.

2.1 Introduction

The identification and prediction of subsurface paleokarst signatures are important challenges in carbonate-reservoir exploration (Feazel, 2010). Karst processes spanning near-surface weathering to deep burial dissolution have affected numerous carbonate-rock sequences intervals that host petroleum-prone deposits (Hardage et al., 1996; Loucks, 1999;

Purdy and Waltham, 1999; Feazel, 2010). Some hydrocarbon reservoirs that have significant production may be paleokarst-related. These include the early to late Paleozoic carbonates of west Texas (Kerans, 1988), the lower Cretaceous carbonates of Mexico (Viniegra and Castillo-Tejero, 1970), the lower Ordovician carbonates of Bohai Bay in China and the Devonian to Mississippian carbonates in Kazakhstan (Gunn, 2004).

It is known that 40% or more of recoverable hydrocarbons in carbonate deposits are trapped at stratigraphic unconformities, and in most cases, they are of karst origin (Ford and Williams, 2007). Such unconformities in buried paleokarst can vary strongly in size, shape and extension, depending on the carbonate substrate, the former karst processes and their resulting dissolution features. Fritz et al. (1993) stated that several prolific oilfields consist of a number of minor karst-related unconformities stacked in longer depositional sequences. The unconformities with the greatest spatial extent have been documented as irregular, entirely buried karst terrains, such as the Liuhua field in South China (Yuan, 1991; Heubeck et al., 2004), the El Paso field in Texas (Wright et al., 1991), and the Rospo Mare field in the Adriatic Sea (Soudet et al., 1994).

The vast majority of paleokarst-related reservoirs are thought to have been derived from near-surface karstification processes (*i.e.*, epigenic karst) in carbonates that subsequently were subjected to burial compaction and further diagenesis. Near-surface karstification in carbonate terrains results from the dissolution of carbonates by the action of mildly acidic water (meteoric or mixtures of meteoric and marine waters). The resulting morphologic karst features are controlled by both intrinsic and extrinsic factors (James and Choquette, 1984). The predominant intrinsic factors are the original mineralogy, grain size, initial permeability and the porosity of the affected rocks. Conversely, extrinsic factors correspond to the type of climate as well as the duration of exposure (James and Choquette, 1984). The combined action of both intrinsic and extrinsic factors leads to dissolutional excavation and the development of highly irregular terrains, cave passages and cave systems. A cave passage is defined as the cavernous conduit (commonly not larger than 8 m wide), including its neighboring walls and ceiling (Curl, 1986; Ford, 1988; White, 1988), while a cave system includes a three-dimensional network of cave passages (White, 1988; Palmer, 1991).

Frequent collapses of cave-passage walls and ceilings are inherent to the development of caves in carbonate rocks (White and White, 1969). These collapses of rock masses are related to vertical stresses – due to an increase in overburden by the overlying strata – and a reduction in tensile strength (White, 1988). The main products of these collapses are different breccia types, such as monomitic-pack and -float breccias (e.g., Warren, 2006), derived from chaotic break-down as well as cave-ceiling and cave-wall collapses (White and White, 1969; Kerans, 1988; Loucks and Handford, 1992; Lucia, 1995; Loucks and Mescher, 1997). In addition, as burial processes start when the cave system subsides into the subsurface, relict collapsed cave passages may collapse again, inducing further brecciation of preexistent breccias. It is believed that most karst-related reservoirs – due to their large extents that often reach hundreds to several thousands of meters across – are formed by the amalgamation of numerous collapsed paleocave systems (Purves et al., 1992; Canter et al., 1993; Lucia, 1995; Tinker et al., 1995; Loucks and Mescher, 1997; McMechan et al., 1998; Loucks, 1999). Overall, the combination of near-surface karstification and burial processes commonly produce complex reservoir architectures with strong spatial heterogeneities.

Assessing the spatial distribution of subsurface karst-related features is key to understanding post-depositional processes that have overprinted depositional sedimentary units, in addition to providing important information on reservoir potential and forecasting of drilling-related issues such as 'thief zones'. Moreover, it is also crucial to characterize the

sediments infilling the karst-formed cavernous areas, which, in some cases, might trap important quantities of hydrocarbons (e.g., Warren, 2006; Ford and Williams, 2007).

Previous studies in the Loppa High (Norwegian Barents Sea; Figure 2.1), based on 3D seismic analysis, have recognized major stratigraphic hiatuses – at the top basement, top
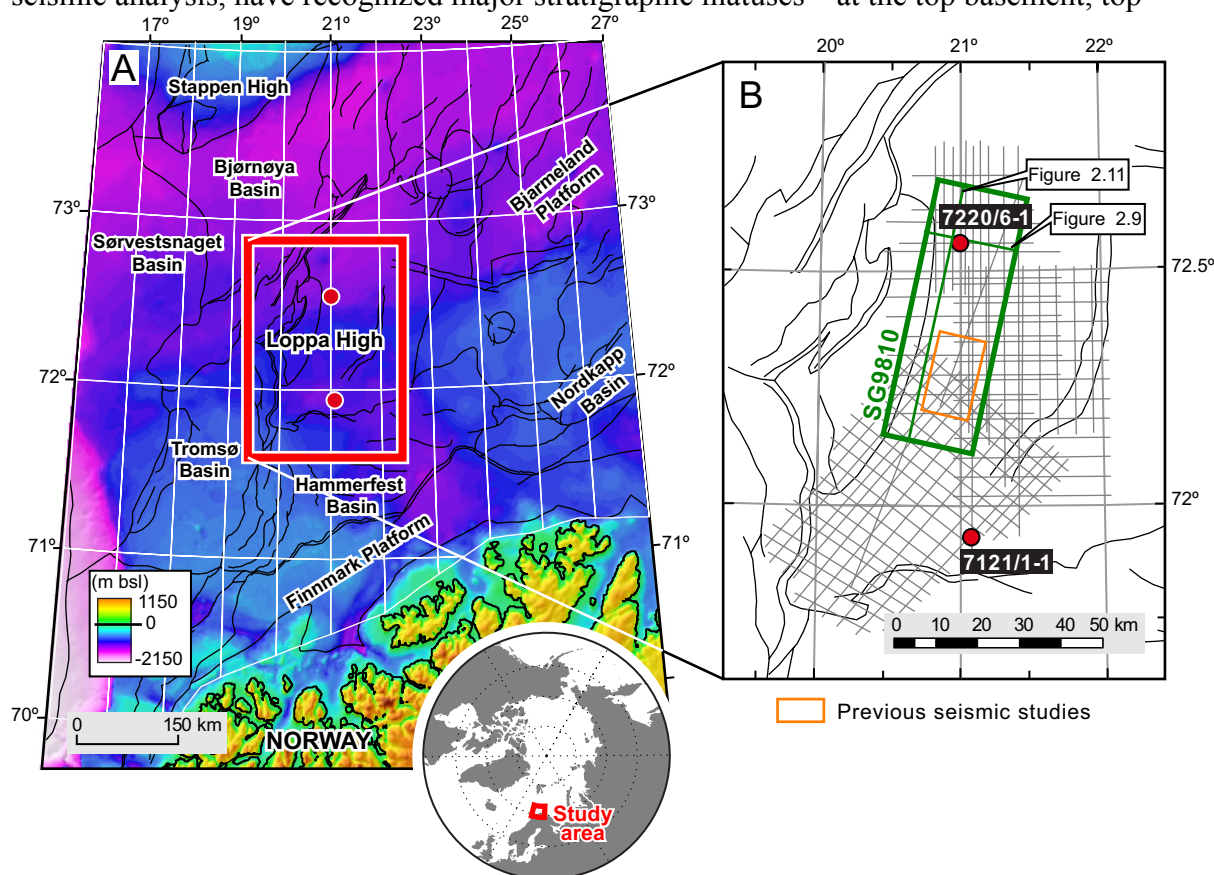
Figure 2.1 (A) Bathymetric map of the Norwegian Barents Sea with major structural lineaments (black lines) and basins. (B) 3D seismic survey SG9810, exploration wells 7220/6-1 and 7121/1-1, 2D seismic lines used to map the top Bjarmeland Group reflector to the 3D survey. Inset rectangle shows location of previous studies. Inset map shows location of the area at a larger scale.

Gipsdalen Group and top Bjarmeland Group – as well as the presence of paleokarst features (Elvebakk et al., 2003; Hunt et al., 2003; Carrillat et al., 2005; Fisher et al., 2010) (Figure 2.2). However, these previous studies have been focused in a sub-cube of the available 3D seismic data (Figure 2.1) without additional support from well data. In our study, we map the spatial distribution of the late Paleozoic-Early Triassic karst-related deposits at a larger scale and focus on the entire area covered by the available 3D survey. We used an integrated approach combining core analysis, 3D seismic mapping and multi-attribute seismic facies classification, which allowed us to estimate the probable maximum spatial extent of the karst-related deposits. Furthermore, comparing our observations with available outcrop analogues allowed us to hypothesize about the role of evaporites in the development of the buried paleokarst system in the Loppa High.

Our results, in combination with previously published data (Elvebakk et al., 2002; Elvebakk et al., 2003; Carrillat et al., 2005; Fisher et al., 2010), provide new constraints on the Loppa High karst and its subsequent burial history. Furthermore, the integrated approach may aid in the characterization of paleokarst in other areas where 3D seismic data is available and wells are sparse.

Figure 2.2 Main stratigraphic units in the Loppa High, position of well 7220/6-1 and available core. (A) Sketch shows the position of the well 7220/6-1 in the Loppa High structure and the main units penetrated. The carbonate interval is lying over the basement and capped by Triassic shales. (B) Simplified stratigraphic log of the upper Paleozoic succession of the Loppa High (adapted from Larssen *et al.* 2002); legend of rock types at the base. Time scale from Ogg *et al.* (2008). (C) Main units penetrated by the well 7220/6-1 and location of studied core. Gamma-ray log shows the change from Triassic shales to the underlying carbonate interval at SB2 and the contact between the carbonates and basement rocks at SB1. Note the increase in gamma-ray values at the lower part of the Gipsdalen Group, representing the interbedding of carbonates and siliciclastics. See the locations of SB1 and SB2 in Figure 2.3. KTG = Kapp Toscana Group. TG = Tempelfjorden Group. BG = Bjarmeland Group. GG = Gipsdalen Group. SB = sequence boundary.

2.2 Geological setting of the Loppa High

The Loppa High is a marked isolated structural high near the southwestern margin of the Norwegian Barents Sea (Figure 2.1). The Loppa High is bounded by the Hammerfest Basin to the south and by the Tromsø and the Bjørnøya basins to the west (Gabrielsen et al., 1990). To the east and northeast, it grades into the Bjarmeland Platform (Figure 2.1). The Loppa High evolved as a positive structural element of the Atlantic rift arm between Greenland and Norway during the late Paleozoic (Stemmerik and Worsley, 1989; Stemmerik et al., 1999; Golonka and Ford, 2000; Stemmerik and Worsley, 2005) and from Late Jurassic–Early Cretaceous rifting (Stemmerik et al., 1999).

The Loppa High was a site of shallow-water carbonate deposition from the mid-Carboniferous until the Late Permian (*e.g.*, Stemmerik et al., 1999). The carbonate units in the Loppa High comprise two major stratigraphic units, the Gipsdalen and Bjarmeland groups (Figure 2.2). The Gipsdalen Group was deposited in a marine carbonate-ramp succession during mid-Carboniferous to Early Permian time (Larssen et al., 2002). Transgressive clastics and mixed siliciclastic and carbonates characterize its base, while warm-water carbonates, including stacked build-ups, dominate its top (Elvebakk et al., 2002; Hunt et al., 2003; Carrillat et al., 2005). Additionally, the presence of evaporites suggests deposition during warm semi-arid to arid conditions (Steel and Worsley, 1984; Stemmerik, 2000). Furthermore, the occurrence of stacked rhythmic shelf deposits, often terminated by subaerial surface exposures, indicates sedimentation controlled by high-frequency and high-amplitude relative sea-level fluctuations (*e.g.*, Stemmerik and Worsley, 1989; Stemmerik et al., 1998; Worsley et al., 2001). Conversely, the Bjarmeland Group reflects deposition along a steepened ramp characterized by more open marine conditions, which developed during the Early Permian (late Sakmarian to the Artinskian) (Larssen et al., 2002). Carbonate production for this latter group was characterized by a temperate cool-water environment, including bryozoan-dominated build-ups (Blendinger et al., 1997; Ehrenberg et al., 1998a; Stemmerik et al., 1999).

The strata of both groups dip to the east and are truncated by an angular unconformity towards the western crest (Figures 2A, 2B). During subaerial exposure, erosion of ~350–500 m of strata (in the western part of the high) and karst processes significantly altered these carbonate units (Stemmerik et al., 1999; Elvebakk et al., 2003; Hunt et al., 2003). Regarding the karstification, Elvebakk et al. (2003) proposed three main mechanisms responsible for karst processes of the Loppa High: (1) high-frequency subaerial exposures related to glacio-eustatic sea-level changes; (2) subaerial exposures and karstification associated with third- and second-order sequence boundaries such as the one delimiting the Gipsdalen and Bjarmeland groups; and (3) protracted exposure and the formation of a major unconformity between the late Permian and the Anisian, lasting approximately 25 My.

2.3 Material and methods

2.3.1 Core study

The Statoil vertical exploration well 7220/6-1 (Figures 2.1, 2.2), with a total depth of 1540 m, was used for calibrating stratigraphic markers for seismic stratigraphy. From the same well, we logged and described 52.5 meters of available core (Figure 2.2 C). Core coverage was limited to the investigated carbonate interval, and therefore, other detailed

lithostratigraphical and sedimentological studies from adjacent areas in the Barents Sea were incorporated to augment our data and support our interpretation (Stemmerik and Worsley, 1989; Stemmerik et al., 1995; Ehrenberg et al., 1998a; Stemmerik et al., 1999; Stemmerik and Worsley, 2000; Larssen et al., 2002; Stemmerik and Worsley, 2005; Rafaelsen et al., 2008).

2.3.2 3D seismic stratigraphic framework

The 3D seismic volume (SG9810) used for this study encompasses an area of ~960 km^2 (Figure 2.1). It has a bin size of 25 × 25 m, a sampling interval of 4 ms and a record length of 6 sec. The frequency spectra extracted from the seismic survey vary from 15 to 30 Hz, with a peak around 25 Hz for the deeply buried Paleozoic section. Due to the high seismic P-wave velocities greater than 4500 m/s, the vertical resolution in the carbonate interval of interest is ~45 m. Seismic vertical scales are given in two-way traveltime (TWT), while well-depth data are given in meters below kelly bushing (KB).

The seismic-well calibration was performed by constructing synthetic seismograms with a wavelet statistically extracted from the 3D seismic volume. This critical step allowed anchoring the lithologic units to the seismic units. The stratigraphic markers 'top basement' and 'top Gipsdalen' were calibrated from well 7220/6-1, and the 'top Bjarmeland' was calibrated using the Esso Exploration and Production Norway well 7121/1-1R, which is located outside the current 3D survey (Figure 2.1). The top basement and top Gipsdalen horizons were mapped by using manual and automated interpretation in the 3D seismic volume (Figures 2.3, 2.4). The top Bjarmeland was mapped by tracing the seismic reflector, calibrated from well 7121/1-1R, trough adjacent 2D seismic lines connected to the 3D survey (Figure 2.1). The seismic mapping resulted in the construction of a 3D seismic stratigraphic framework of reference, where the lateral extent and structural situation of main stratigraphic units inside the 3D survey were established (Figures 2.3, 2.4).

2.3.3 3D multi-attribute seismic facies classification

A 3D automated seismic facies classification was subsequently applied, to separate the response of different seismic facies in the 3D seismic cube, by combining different seismic attributes (*i.e.*, mathematical transforms of the seismic data) in an artificial neural network (Coleou et al., 2003; Linari et al., 2003; Carrillat et al., 2005; Tebo and Hart, 2005; Farzadi, 2006; Herrera et al., 2006; Baaske et al., 2007; Farzadi and Hesthammer, 2007). The classification method used here has been successfully applied for reservoir characterization (*e.g.*, Coleou et al., 2003; Linari et al., 2003; Carrillat et al., 2005; Farzadi, 2006; Herrera et al., 2006; Farzadi and Hesthammer, 2007). The workflow involved several steps that are summarized in Figure 2.5 and described below.

Figure 2.3 Seismic lines showing the interpretation in the 3D seismic survey. Inset map shows the location of the lines. (I) SSW-NNE line along the longer axis of the 3D survey, note distribution of seismic sequences; GG is present in the entire area, while the BG is eroded at the crest of the structure. (II) - (VI) seismic lines show the thickness variation of GG and BG inside the 3D area. GG = Gipsdalen Group. BG = Bjarmeland Group. SB = Sequence boundary. SB1 = top basement. SB2 = top Gipsdalen. SB3 = top Bjarmeland.
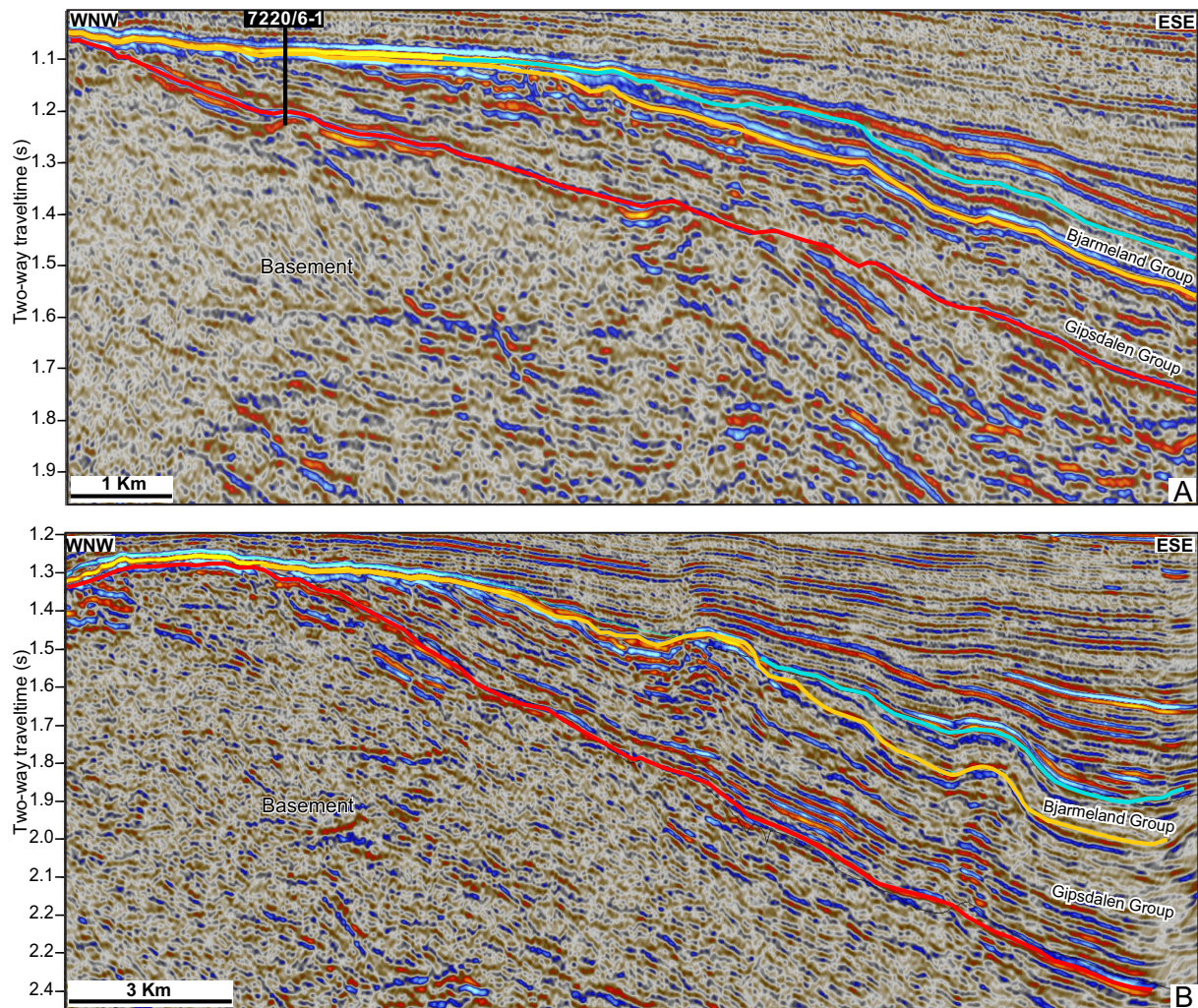
Figure 2.4 Seismic stratigraphic framework construction of the Loppa High. (A) Zoom of Line III from Figure 2.3. **(B)** Zoom of Line V from Figure 2.3. Note truncation of units towards the crest of the Loppa High. Color-coding in Figure 2.3.
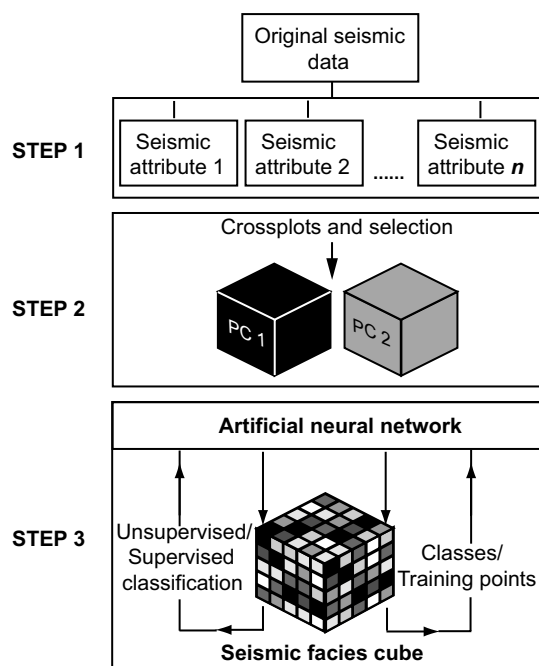
Figure 2.5 Schematic workflow of the seismic facies classification process using an Artificial Neural Network (ANN). Step 1 involves generation and examination of seismic attributes. Step 2 includes cross-plots and selection of seismic attributes with further PCA. The PCs selected are shown in Table 3. Step 3 comprises the unsupervised and supervised classification using the ANN. Seismic classification is an iterative process in which the number of classes, training data (in case of supervised mode) and seismic attributes can be modified to obtain the best results. PCA = Principal Component Analysis. PC = Principal Component. ANN = Artificial Neural Network.

Step 1: generation and examination of seismic attributes

The first step of the multi-attribute classification study was the computation of seismic attribute volumes. Eighteen seismic attributes covering the whole range of seismic information were computed (e.g., time, amplitude, frequency and attenuation) (Brown, 1996). Following the methodology presented by Baaske et al. (2007), these attributes were visually evaluated and compared to the known geological model to find representative geological trends and correlations. The geological and mathematical significance of each selected attribute was supported by key studies (Taner et al., 1979; White, 1991; Barnes, 1993; Brown, 1996; Chen and Sidney, 1997; Gastaldi et al., 1997; Lewis, 1997; Raeuchle et al., 1997; Skirius et al., 1999; Hart and Balch, 2000; Barnes, 2001; Carr et al., 2001; Meldahl et al., 2001; Banchs and Michelena, 2002; Sarg and Schuelke, 2003; Tebo and Hart, 2005; Farzadi, 2006; Baaske et al., 2007; Barnes, 2007; Chopra and Marfurt, 2007; Farzadi and Hesthammer, 2007), aiding the pre-selection of the seismic attributes (Table 1). Following the approach of Barnes (2007), attributes with geological and geophysical meaning were systematically preferred to attributes with purely mathematical meaning.

Seismic attribute	Basic seismic information	Event continuity	Lithology	Structures	Fluid content	Sequence boundaries	Rock properties	Stratigraphic features
Apparent polarity	Sign of seismic trace	✓✓				✓✓		
Gradient magnitude	Amplitude	✓✓		✓✓		✓		
Reflection intensity	Amplitude	✓✓	✓✓			✓✓		
RMS amplitude	Amplitude			✓	✓✓			
First derivative	Amplitude							✓
Instantaneous quality	Amplitude				✓			
Envelope	Total energy of the seismic trace			✓		✓✓		
Cosine of instantaneous phase	Phase	✓✓		✓✓		✓✓		✓✓
Instantaneous bandwidht	Frequency						✓✓	✓
Instantaneous frequency	Frequency		✓✓				✓✓	
Dominant frequency	Frequency						✓✓	
Instantaneous phase	Phase	✓✓		✓✓		✓✓		
Chaos	Chaoctiness of seismic signal	✓✓		✓✓				
Variance	Structural information	✓✓		✓✓		✓✓		
Relative acoustic impedance	Apparent acoustic contrast			✓	✓✓	✓✓		
Local structural dip	Dip of seismic events	✓		✓✓				
Local structural azimuth	Azimuth of seismic events			✓✓				
Attenuation	Frequency	✓		✓	✓✓		✓✓	

Good indicator   ✓✓
Medium indicator   ✓
RMS = Root mean square

Table 1. Eighteen calculated seismic attributes for the study. Table shows the geophysical and geological significance of each seismic attribute.

Step 2: cross-plots and selection of seismic attributes

To avoid data redundancy, seismic attributes were further selected using a cross-plot technique, which examines the independence of each attribute with respect to the others (Barnes, 2007). Figure 2.6 shows a portion of the analyzed cross-plots. Pairs of seismic attributes that were linearly correlated with each other (e.g., Figure 2.6 C, 2.6 D) were redundant, and only one attribute of each pair was retained. Conversely, independent seismic attributes, *i.e.*, unrelated to the others were favored for the seismic classification (e.g., Figure 2.6 A, 2.6 B).

The cross-plot technique provided six optimal seismic attributes among eighteen originals. These attributes include envelope, dominant frequency, chaos, gradient magnitude, instantaneous bandwidth and variance. Table 2 summarizes each of these seismic attributes in regards to their seismic information, type and applicability in this study. However, as we observed that both variance and chaos attributes were predominantly capturing structural information (*i.e.*, fault traces) for the area of interest, we discarded them from the classification process to avoid bias.

The redundancy of attributes was further optimized by applying a principal component analysis (PCA) to the four selected attributes (Hotelling, 1933; Jolliffe, 2002). The first two principal components (PC1 and PC2) (Table 3) with the highest variance were finally selected for the seismic facies classification.
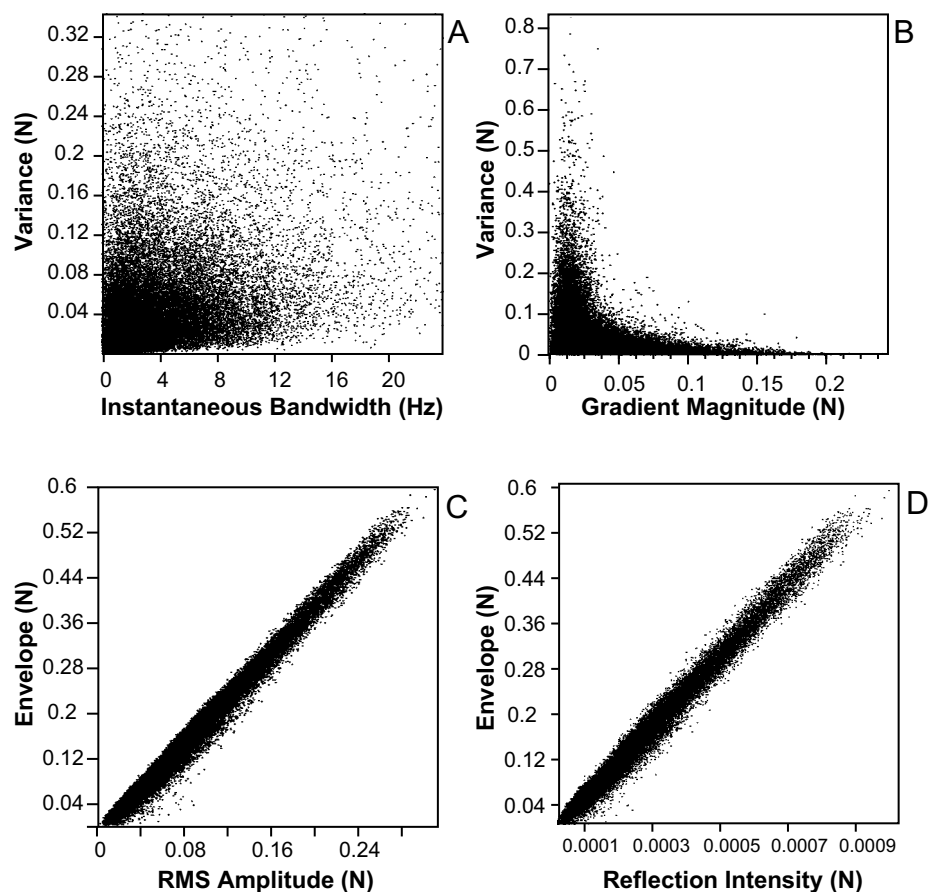
Figure 2.6 Some of the cross-plots of seismic attributes performed in the study. (A) and (B) show a scatter correlation among them; therefore, they represent different seismic properties and may be selected for the classification process. (C) and (D) show lineal correlation, meaning that they are in essence identical; therefore, only one seismic attribute of those should be selected for the classification process (see text for detailed explanation). Hz= Hertz. RMS= Root Mean Square. N=Normalized.

Seismic attribute	Basic seismic information	Type of seismic attribute	Application in this study
Envelope	Energy of the seismic trace	Complex trace attribute	Acoustic impedance contrast and detection of major lithological changes and sequence boundaries
Dominant frequency	Frequency	Complex trace attribute	Time varying spectral properties of seismic data
Chaos	Chaoctiness of seismic signal	Stratigraphic attribute	Recognize chaotic texture in seismic data
Gradient magnitude	Amplitude sensitive	Structural attribute	Determine regions of weak coherent signal from the ones with significant reflectivity and signal strenght
Instantaneous bandwidth	Frequency	Complex trace attribute	Time varying spectral properties of seismic data. Good indicator of lower frequency areas
Variance	Structural information	Structural / stratigraphic attribute	Isolate edges from the input data set

Table 2. Detailed description of the six seismic attributes chosen from the cross-plot analysis indicating basic seismic information, type of seismic attribute and the application in this study. Chaos and Variance were not considered in the classification process (see text for explanation).

A. Unsupervised classification

Principal Component	Eigenvalues	Contribution (%)	Cumulative (%)
PC 1	2.1773	54.43	54.43
PC 2	1.3551	33.88	88.31
PC 3	0.2878	7.19	95.50
PC 4	0.1799	4.50	100

B. Supervised classification

Principal Component	Eigenvalues	Contribution (%)	Cumulative (%)
PC 1	1.9702	49.25	49.25
PC 2	1.4797	36.99	86.25
PC 3	0.5042	12.60	98.85
PC 4	0.0460	1.15	100

Table 3. Principal component analysis (PCA). (A) For unsupervised classification. (B) For supervised classification. Each table shows the contribution of principal components (PC) to the maximum variability of the multidimensional dataset. The PCs with the highest eigenvalues (close to 1 or higher) were selected for the classification process. In both cases, the first two PC were selected. PC = Principal Component.

Step 3: unsupervised & supervised seismic facies classification
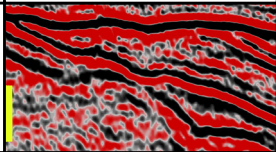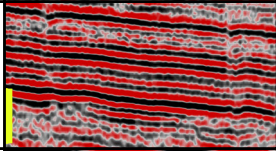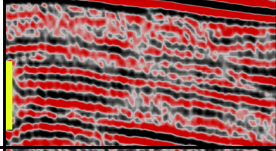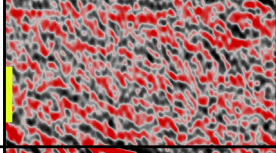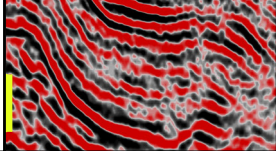
A seismic facies classification can be applied in unsupervised or supervised mode (e.g., Coleou et al., 2003; Linari et al., 2003; Saggaf et al., 2003; Carrillat et al., 2005; Baaske et al., 2007; Corradi et al., 2009). In the unsupervised mode, the natural clustering of the data is obtained by combining different seismic attributes into the artificial neural network (Figure 2.5). For the unsupervised classification, five classes were selected as the number of output facies.

In the supervised mode, sets of different seismic facies (*i.e.*, training data) were selected in the 3D survey and used to train the artificial neural network (Table 4). Subsequently, the artificial neural network predicts target seismic facies in the remaining regions (*i.e.*, outside the given training data) (Barnes, 2001; Saggaf et al., 2003; Carrillat et al., 2005). The supervised classification was performed in the first instance in a smaller sub-cube of the seismic data. After several iterations, satisfactory results were obtained, and then the supervised classification was applied to the entire 3D cube.

Geobody extraction

To better examine the spatial extent of the seismic facies in the 3D survey, a volume rendering technique that uses an opacity control to illuminate features of interest was applied in each classified volume (unsupervised and supervised). Those illuminated features were finally extracted as 3D objects ('geobody extraction technique', Schlumberger[TM]). The extraction methodology relied on connectivity threshold values among adjacent voxels (volumetric pixels). Each voxel is compared with its neighbors using a user-defined connectivity threshold value. However, as some areas of the 3D cube may be characterized by a large number of isolated voxels, they may have not been extracted in the final geobody.

Seismic-well calibration, three-dimensional seismic interpretation, multi-attribute seismic facies classification and 3D object-extraction were performed with the software Petrel 2010.1 (Schlumberger[TM]).

Seismic Facies	Reflection geometry	Amplitude characteristic	Spatial distribution	Example (Vertical bars represent 100 ms)
SF1	Parallel continuous	High amplitude	Occurs mainly at the crest of the structural high and at the top of basement	
SF2	Parallel continuous	Medium- to low amplitude	Occurs mostly towards the flanks of the Loppa High	
SF3	Parallel discontinuous	Medium- to low amplitude	In overlying Triassic clastics and some areas of the carbonate intervals	
SF4	Chaotic	Low amplitude	Present at the core of the build-ups and in the basement	
SF5	Semi-parallel dipping discontinuous	Medium amplitude	Occurs mostly in the slopes of build-ups	

Table 4. Seismic facies textures (training data) selected to train the artificial neural network for the supervised classification.

2.4 Results and interpretation

2.4.1 Core study

Four different types of lithofacies were identified in the analyzed core, which recovered strata from the upper part of the Gipsdalen Group (Ørn Formation) (Figure 2.2C). The lithofacies are described below; photographs of the samples are shown in Figure 8, and their locations on the core are depicted in Figure 2.7:

1) **'Fine dolomitic lithofacies' (FDL)** (Figures 2.7, 2.8A) comprises fine yellowish-brownish marly dolomites, interpreted as dolomitic replacement of micritic textures (carbonate mudstones). Millimetric to centimetric irregular nodules of anhydrite and chert are occasionally observed, whereas the biotic content is rare. Millimetric to centimetric layers of greenish shales and silts, occurring mostly within the lower part of the fine dolomitic beds, appear as stylonodular films. No visible porosity characterizes this lithofacies.

2) **'Coarse dolomitic lithofacies' (CDL)** (Figures 2.7, 2.8B) is made of coarse yellowish-brownish dolomite, interpreted as dolomitic replacement of bioclastic muddy textures (wackestone-packstone) and microbial laminites. Anhydrite and chert nodules are present. The faunal content comprises bryozoans, small gastropods, crinoids, undefined molluskan shell fragments, undifferentiated algae and benthic foraminifers. The top of some beds shows microbial laminites, cross-cut by vertical centimetric cavities, indicating the

former presence of roots (Figure 2.8B). Abundant microvuggy and less intergranular and fracture porosity is observed.

3) **'Monomict dolomitic packbreccias' (MDP)** (Figures 2.7, 2.8C, 2.8D) constitutes crackle- to rubble- sediment-filled chaotic breccias. Clasts are made of FDL and CDL, described above. Pebble- to cobble-sized-clasts dominate; boulder sizes are rare. The clasts are mostly angular to sub-angular. Clast contact varies from smoothed- to solution-rounded. As secondary components, chert, quartz, anhydrite and pyrite are present, with sizes < 5 cm. The space between the clasts is filled by dolomite replacing the depositional matrix and green silts and shales. The contact between these breccias and the underlying beds is sharp and characterized by centimetric green shale layers. Microvuggy and minor intergranular and fracture porosity is present.

4) **'Monomict dolomitic floatbreccias' (MDF)** (Figures 2.7, 2.8E) contain few indistinct beds (< 2.5 m) composed of FDL and CDL clasts, matrix-supported by green shales and silts. Few clasts (< 5 cm) of chert, quartz and anhydrite are present. Pyrite nodules were also observed. The roundness and size of the clasts resemble the MDP lithotype. Visible microvuggy, minor intergranular and fracture porosity are visible.

Two major lithologic intervals were identified in the core on the basis of bedding patterns. The interval number 1 (1202-1186 m) (Figure 2.7) shows the alternation of metric-thick beds (< 2 m) of dolomites and breccias. The interval number 2 (1186-1149.5 m) comprises pack- and float-breccia deposits (Figure 2.7).

The two major intervals are interpreted to reflect 1) dolomitized inner ramp deposits of an intertidal to supratidal shallow-lagoon and sabkha environment and 2) solution-collapse breccia deposits, superimposed on the in situ strata. The observed significant breccia deposits – characterized by the presence of the following: 1) rubble- and pack-breccias; 2) chaotic fabrics; 3) thin intervals of insoluble residuals at the base of the brecciated interval; 4) general coarsening-upwards trends of the brecciation; 5) a higher degree of compaction (from float- to packbreccias) upwards; and 6) a decreasing occurrence of insoluble residuals upwards – suggest a solution-collapse origin (Warren, 2006) that was probably produced during phases of cave development and cave collapse associated with karst systems (cf. DeHass and Jones, 1989; Entzminger and Loucks, 1992; Loucks and Handford, 1992; Tinker et al., 1995; Loucks and Mescher, 1997; McMechan et al., 1998; Loucks, 1999). We hypothesize that the inferred caves formed by dissolution of marine carbonates and evaporites during phases of emergence associated with sea-level lowstands. Analogous to present-day karst landscapes, the formation of those cavities was accompanied by the collapse of cave walls and ceilings during later burial compaction.

2.4.2 3D seismic stratigraphic framework

A 3D seismic stratigraphic framework for the Loppa High was built by first calibrating the available well and seismic data. The 'top basement' and 'top Gipsdalen' unconformities recorded in the well 7220/6-1 correlated with seismic amplitude troughs from the 3D seismic data at depths of ~1483 m and ~1138 m, respectively. The 'top Bjarmeland' unconformity in the well 7121/1-1 R (see Figure 2.1 for location) correlated with a seismic amplitude peak at a depth of ~3502 m.
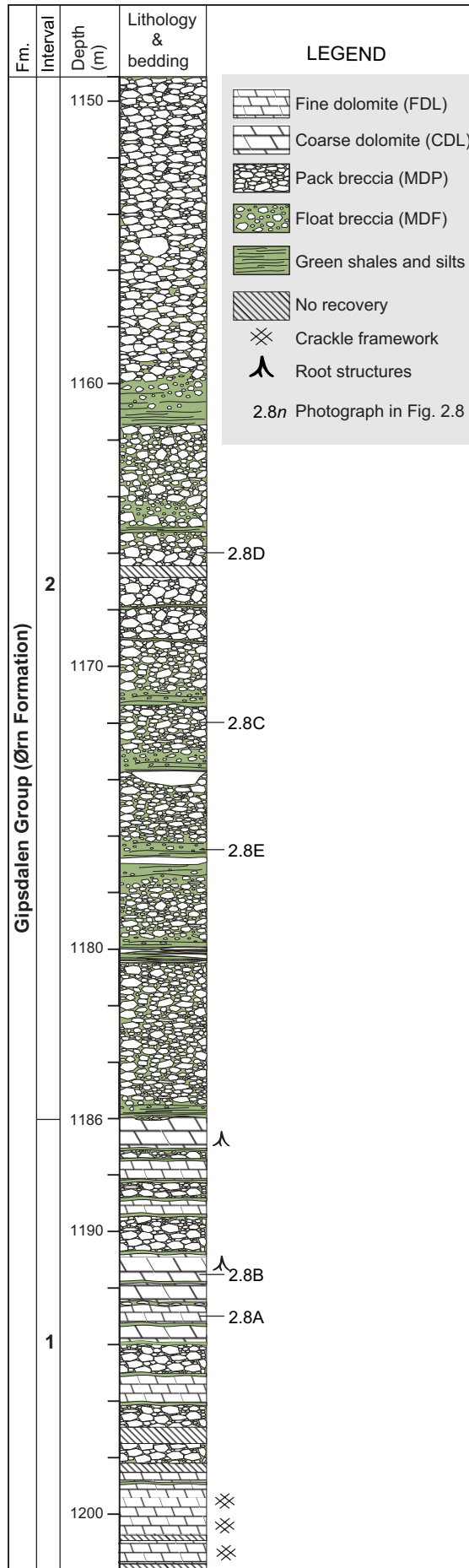
Figure 2.7 Schematic lithostratigraphic log of the studied cored interval from well 7220/6-1. Two major lithological intervals are recognized. Interval 1 shows the alternation of dolomitic beds and breccias. Interval 2 constitutes float- and pack-breccia deposits. See Figure 2.8 (A) - (E) for photographs of the core lithofacies. Dolomitic clasts making up the breccias are not to scale. FDL = Fine dolomitic lithofacies. CDL = Coarse dolomitic lithofacies. MDP = Monomict dolomitic packbreccias. MDF = Monomict dolomitic floatbreccias.

Figure 2.8 Lithofacies from the cored interval of the well 7220/6-1. (A) Fine dolomite and anhydrite nodules (An) from the "Fine dolomitic lithofacies" (FDL), alternated with irregular clayley and silty laminae (1192.9 m). (B) Coarse porous dolomite of the "Coarse dolomitic lithofacies" (CDL), finely alternated with microbial laminites and characterized by the presence of root structures (see arrows) (1191 m). (C) Dolomitic rubble packbreccias from the "Monomict dolomitic packbreccias" lithofacies (MDP) (1172 m). (D) Highly compacted dolomitic crackle packbreccias from the "Monomict dolomitic packbreccias" lithofacies (MDP). Note the presence of millimetric residual anhydrite fragments (1166 m). (E) Dolomitic floatbreccias from the "Monomict dolomitic floatbreccias" lithofacies (MDF). Dolomitic clasts float in a green clayley matrix (1176.4 m).
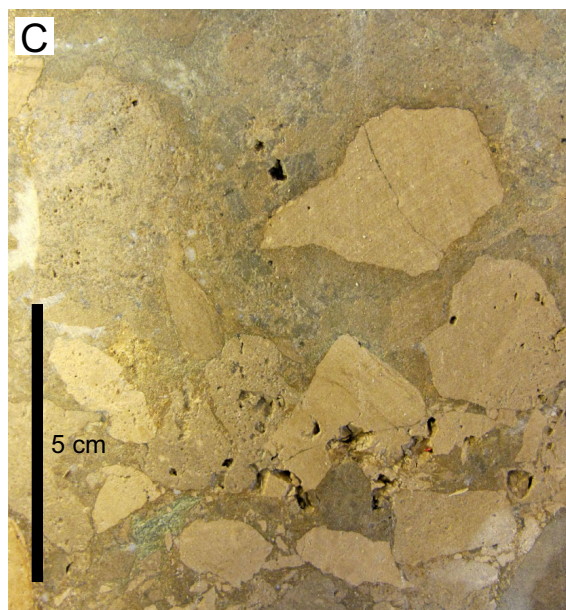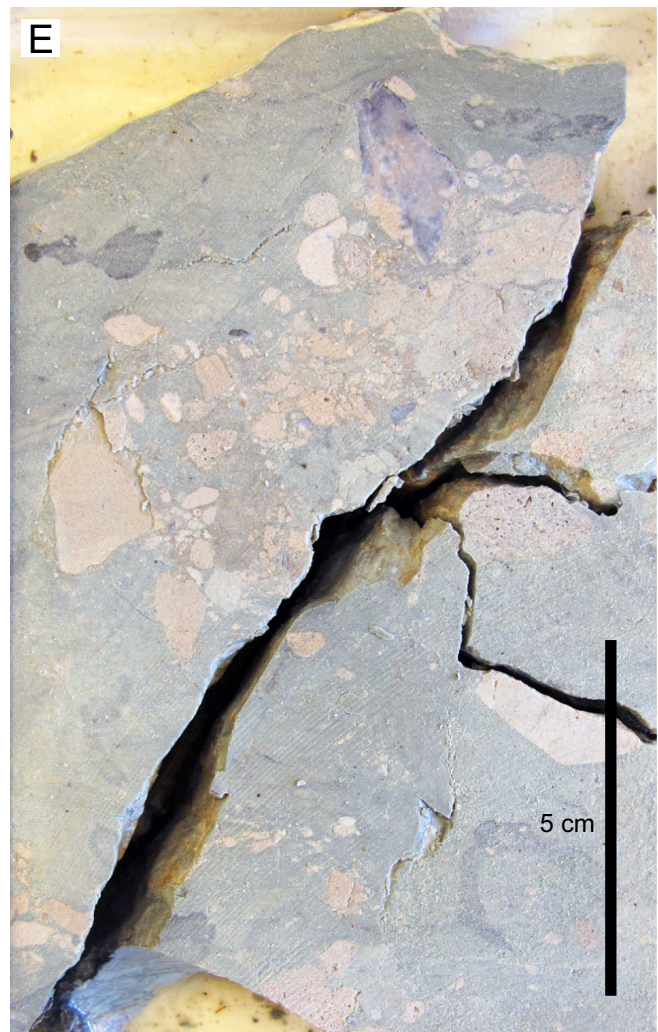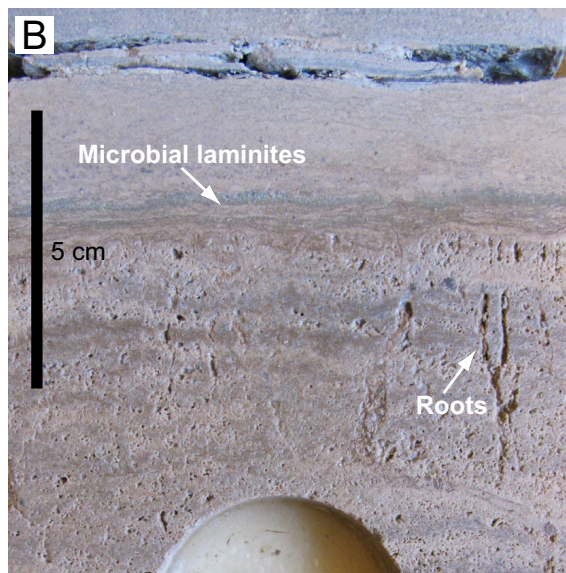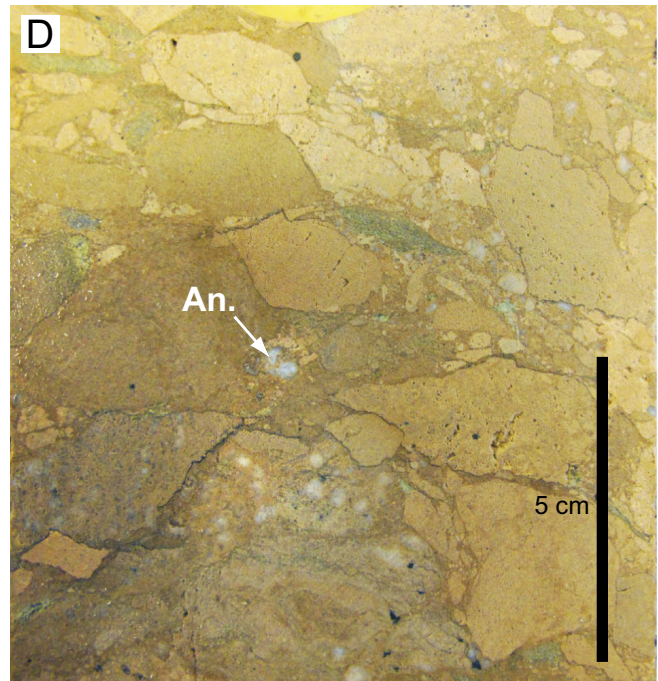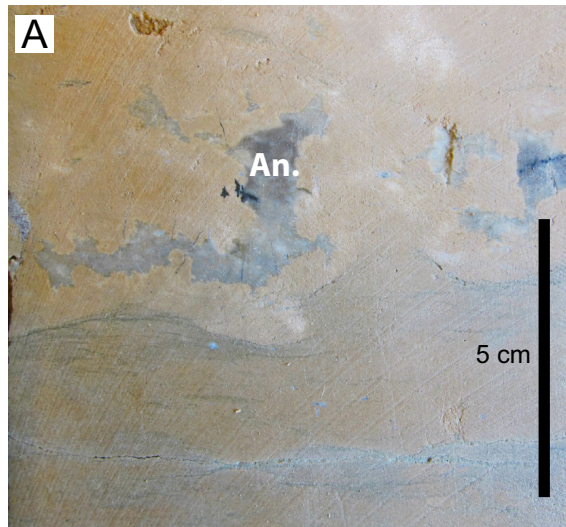
The constructed 3D seismic stratigraphic framework shows evidence of variable thickness for both the Gipsdalen and Bjarmeland groups within the 3D volume investigated in this study (Figures 2.3, 2.4). From west to east, the Gipsdalen Group ranges from 0 to ~1012.5 m (0 to 450 ms) in thickness, while the Bjarmeland Group ranges from 0 to ~225 m (0 and 100 ms) in thickness, assuming an interval seismic-wave velocity of 4500 m/s. Both the Gipsdalen and Bjarmeland groups are composed mainly of carbonate rocks and separated from each other by a marked unconformity (Figures 2.3, 2.4).

The current structural configuration of the Loppa High resulted from a complex geological history encompassing several phases of uplift and subsidence, followed by tilting and erosion (e.g., Stemmerik et al., 1999). Overall, the sedimentary units on the Loppa High dip towards the east, as uplift of this structural high was accentuated towards the western part of the structure (Larssen et al., 2002).

2.4.3 3D multi-attribute seismic facies classification

The objective of this seismic classification was to separate the response of the breccia facies, as observed in core from well 7220/6-1, from the other surrounding seismic facies to define the probable maximum extension of karst-related fabrics in the Loppa High.

The results of the unsupervised and supervised classification are shown for the inline 8353 in Figures 2.9C and 2.9D, respectively. An enlargement in the area of the well 7220/6-1 is further displayed in Figures 2.10A and 2.10B. The seismic facies selected for the classification are shown in Table 4. In both classifications, the output seismic facies (SF) are labeled with different identification and color codes (Figures 2.9C, 2.9D). Accordingly, SF1, SF2, SF3, SF4, and SF5 are yellow, pink, dark blue, green, and light blue, respectively. We will focus our interest on two main seismic facies: SF1 and SF2. Indeed, in both classifications, SF1 was the seismic facies matching the brecciated interval described in core 7220/6-1 (see above). Therefore, we associated SF1 with breccia deposits. Moreover, SF1 and SF2 appeared closely related, especially in the supervised classification. We associated SF2 with major stratigraphic unconformities.

Unsupervised classification

In the unsupervised classification (Figures 2.9C, 2.10A, 2.11A), SF1 was well depicted in the main stratigraphic unconformities. SF1 was present in the flat-topped carbonate interval but also in the vicinity of the main seismic reflectors, occupying the outer slopes of the structural high, *i.e.*, 'top Basement', 'top Gipsdalen', and 'top Bjarmeland' (arrows in Figures 2.9C, 2.11A). The unsupervised classification displayed strongly chaotic patterns, especially in the basement area, with a complex alternation of SF2, SF3, SF4, and SF5.

Supervised classification

To accomplish the supervised classification, the seismic facies (SF) (training-data) selection phase was a key step (Table 4). These seismic facies were selected based on the intensity of the amplitude reflections: *i.e.*, parallel high amplitude (SF1), parallel medium amplitude (SF2), and parallel discontinuous low amplitude (SF3). Two additional sets of seismic facies (*i.e.*, chaotic (SF4) and dipping discontinuous (SF5)) were added to map concave-up structures and their edges (Table 4).

In the supervised classification and at the scale of the whole 3D seismic survey, SF1 is mostly concentrated on the crest of the Loppa High (Figures 2.9D, 2.10B, 2.11D) where it correlated with the parallel high amplitude training points (Table 4). Conversely, SF2 was restricted to the slopes of the structural high, highlighting the main seismic boundaries, and it was correlated with parallel medium amplitude training points. On the other hand, SF3 was mostly present in the Triassic shales, although it was also observed in some areas of the carbonate interval and correlated with the parallel discontinuous low-amplitude training points. SF4 is associated with chaotic seismic patterns, and SF5 is not well depicted in the classification results (probably because the seismic attributes selected were not able to discern such target seismic facies). SF4 and SF5 are associated with chaotic and dipping discontinuous training points, respectively (Table 4).

Differences between the two seismic classifications

Both the unsupervised and the supervised classification revealed similar patterns (Figures 2.9, 2.10, 2.11). However, we found significant differences in the results of the two methods. Concerning SF1, the spatial extent of this facies was the largest, but it was also the most diffuse in the unsupervised classification where it reached the outer slopes of the Loppa High (Figures 2.11A, 2.11B, 2.11C). In contrast, it was only restricted to the topmost areas in the supervised classification (Figures 2.11D, 2.11E, 2.11F). According to the available core, breccia deposits were also found (1) restricted in the topmost carbonate units and (2) in a proximal position on the Loppa High. Thus, we conclude that the SF1 (corresponding to the parallel high amplitude seismic facies) in the supervised classification was the best estimation for the spatial extension of the breccia deposits in the 3D cube. One possible explanation for this observation is that a strong acoustic impedance contrast is generated over a wide area because lower velocity breccias are encased between a seal of Triassic shales (above) and higher velocity bedded carbonates (below) (Figure 2.7). Concerning SF2, their appearance remained ubiquitous and diffuses in the unsupervised classification, while it was systematically associated with the main seismic unconformities in the supervised classification (Figures 2.9, 2.10, 2.11). Therefore, we conclude that only the supervised classification provided robust information to delineate the main seismic unconformities (*i.e.*, SF2) and clearly isolated them from the breccia deposits (*i.e.*, SF1).
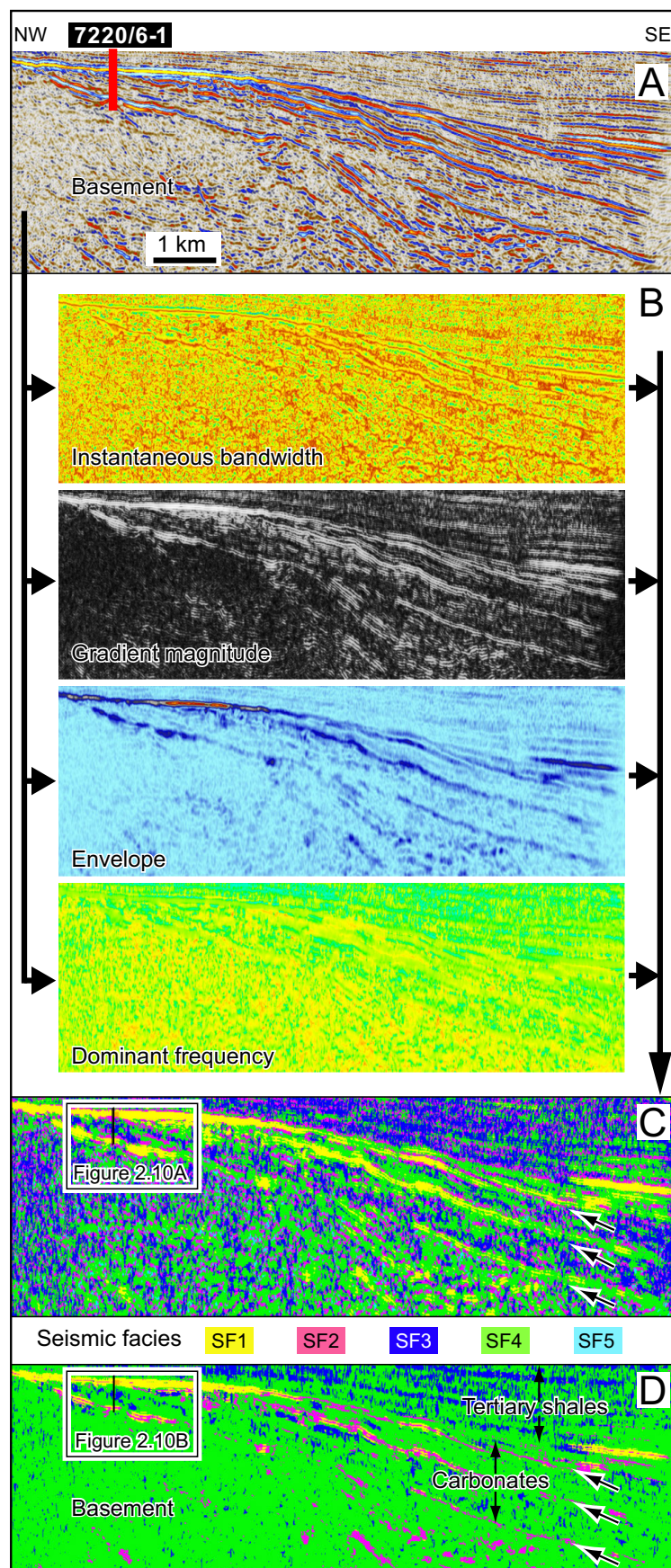
Figure 2.9 Multi-attribute seismic facies classification. (A) Inline 8353 of the original seismic data with well 7220/6-1. (B) Four seismic attributes calculated for the classification (instantaneous bandwidth, gradient magnitude, envelope and dominant frequency). (C) Unsupervised classification results for the inline 8353. SF1 is present in the flat-topped carbonate interval but also in the vicinity of the main seismic reflectors occupying the outer slopes of the structural high, *i.e.*, 'top Basement', 'top Gipsdalen', and 'top Bjarmeland' (white arrows). Strongly chaotic patterns and complex alternation of SF2, SF3, SF4 and SF5 are observed. (D) Supervised classification results for the inline 8353. SF1 is mostly concentrated in the topmost area (crest) of the Loppa High where it correlates with the Parallel High Amplitude training points (Table 4). SF2 is restricted to the slopes of the structural high, highlighting the main seismic boundaries. SF = Seismic facies.
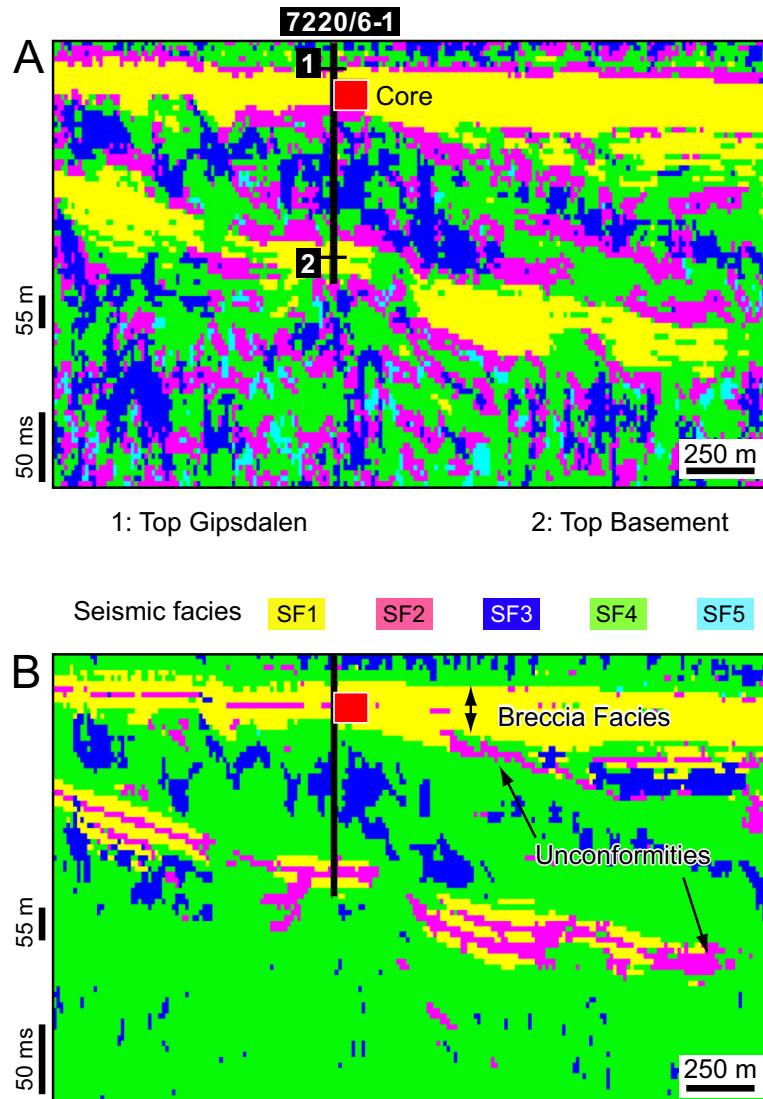
Figure 2.10 Zoom of classification results for inline 8353 close to well 7220/6-1 indicating well path, main well tops and core position. (A) Results of unsupervised classification showing distribution of SF1. (B) Results of supervised classification with a better demarcation of the breccia facies, represented by SF1, and unconformities represented by SF2. SF = Seismic facies.
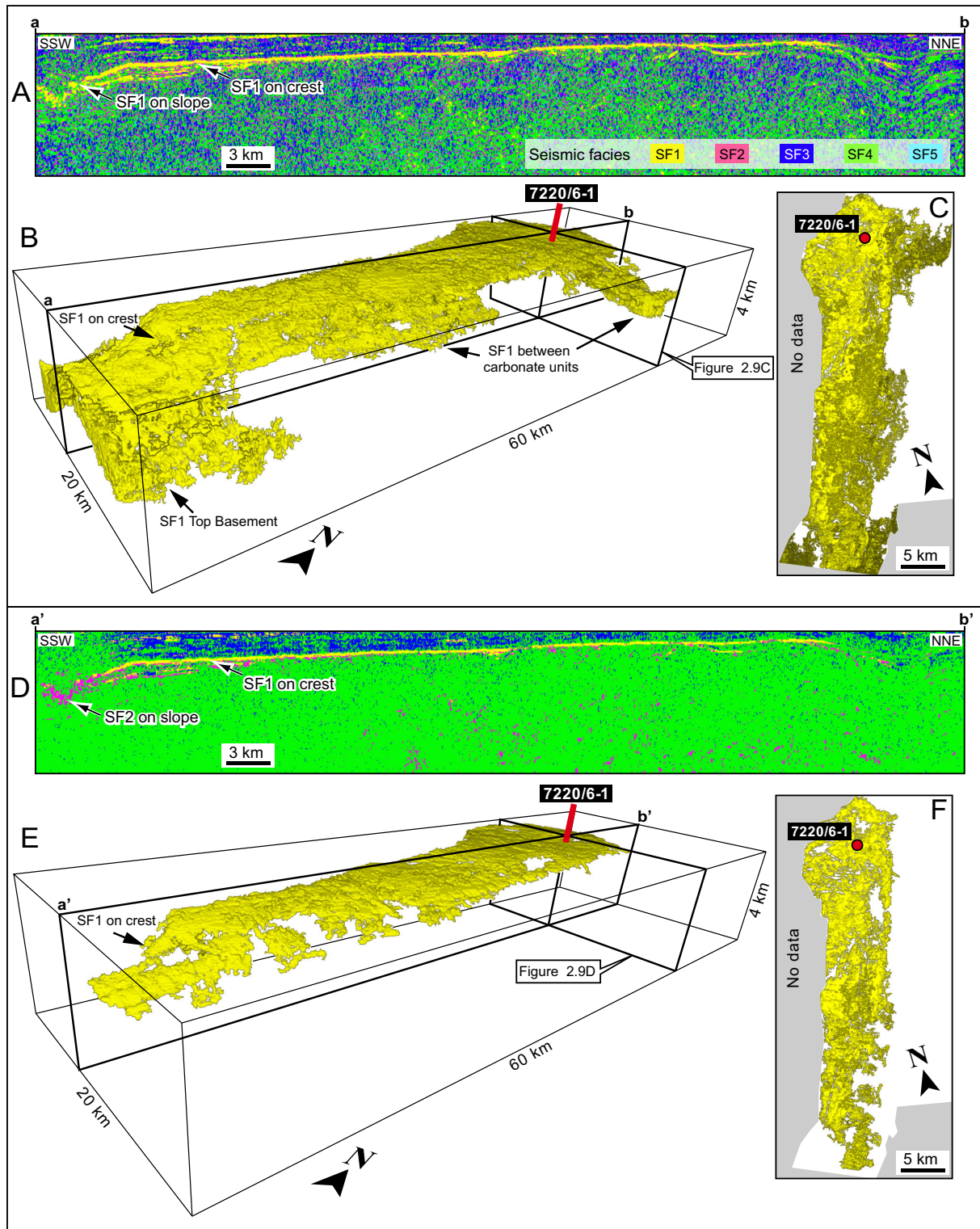
Figure 2.11 (A) Cross-line 5065 of 3D survey (oriented SSW-NNE) showing results of the UC. (B) 3D geobody extraction of SF1 from UC. SF1 observed at the flat-topped crest, at the limit between the two main carbonate units, and at some areas of the top basement. Position of well 7220/6-1, intersection of cross-line and figure 2.9C is shown. (C) Map view of SF1 in UC. (D) Cross-line 5065 (oriented SSW-NNE) of the SC. (E) 3D geobody extraction of SF1 from SC. Distribution of SF1 restricted to the crest of the structure. Position of well 7220/6-1, cross-line and figure 2.9D is shown. (F) Map view of SF1 in SC. SF = Seismic facies. UC = Unsupervised classification. SC = Supervised classification.

2.5 Discussion

Previous studies in the Loppa High recognized the presence of paleokarst features (Elvebakk et al., 2003; Hunt et al., 2003; Carrillat et al., 2005; Fisher et al., 2010). By examining a sub-cube of the 3D seismic survey (see Figure 2.1 for location of previous studies), Carrillat et al. (2005) described sinkholes with diameters < 240 m as well as subsurface passages of up to ~1.3 km long and ~450 m wide. Similarly, using dip maps and velocity analysis, Hunt et al. (2003) noted the presence of paleokarst–highlighted by low-velocity zones below the 'top Paleozoic' unconformity as well as features such as sinkholes, canyons and karst valleys along the crest of the Loppa High.

The integration of well and core data with 3D multi-attribute seismic facies classification provided additional information on the distribution of breccia deposits and stratigraphic unconformities related to paleokarst terrains in the Loppa High. The core analysis revealed the predominance of breccias in the upper and proximal part of the Gipsdalen Group. These sedimentary deposits were interpreted to have been derived from paleocave systems related to karst processes. The 3D seismic facies classification allowed to map the seismic facies related to breccia deposits at the scale of the 3D survey in the Loppa High (Figures 2.11, 2.12).

Below, we provide a potential scenario, which may help explain the formation of the extensive accumulations of breccias identified in our core and seismic facies classification.

A 'Coalesced Collapsed-Paleocave system' in the Loppa High?

The core description provided important information on the local vertical extent of the breccia deposits, but it provided no information on their spatial extent. Conversely, the supervised seismic facies classification, which was viewed to be the most accurate of the two tested seismic classifications (see above), provided an estimation of the spatial extent of the seismic facies SF1 in the Loppa High. Seismic facies SF1 was related to the breccia deposits found in the analyzed core. SF1 reached 40–50 km in length, 10–12 km in width, and 10–150 m in thickness (Figure 2.11E). However, due to the limitation of the method and dataset (i.e., lack of additional calibration points, deep depth of burial and the resolution of the seismic) the areal extent of breccia deposits in the Loppa High (cf. SF1, Figures 2.11F, 2.12) is only indicative and should be taken with caution.

The inferred large volume and spatial extent of the breccia deposits, which occupy virtually the entire proximal areas of the Loppa High, are incompatible with the formation of simple paleocave collapse systems. For example, Loucks (1999) reported on the size of cave passages in the four largest epigenic modern caves in United States (Crystal Cave, Blue Spring Cave, McFail's Cave, and Skull Cave). Cave passages, in these environments, reached ~5–10 m in width and were up to ~1–5 m high in the majority of the measurements. Similarly, cave passages size reported for the Mammoth Cave (Kentucky, USA), the longest mapped cave in the world, shows widths ranging generally from ~1–3 m (with a maximum of

20 m) and heights in the order of ~30 m (Palmer, 1981; Palmer, 1989; Quinlan and Ewers, 1989; Granger et al., 2001).

If the breccia deposits mapped in the Loppa High were related to paleokarst systems, only dissolution processes of greater magnitude rather than simple isolated cave formation and collapse could have produced them. A possible explanation is that these extensive breccia deposits derived from the coalescence of several collapsed-paleocave systems *sensu* Loucks (1999). Previous studies have documented the existence of brecciated zones of great extent reaching up to several thousand meters wide in many collapsed-paleocave systems (e.g., Purves *et al*., 1992; Canter *et al*., 1993; Lucia, 1995; Tinker *et al*., 1995; Loucks and Mescher, 1997; McMechan *et al*., 1998).

Moreover, it has been documented that areas affected by extensive karstification were often associated with composite unconformities (Esteban, 1991; Wright *et al*., 1991; Canter *et al*., 1993; Lucia, 1995; Mazullo and Chilingarian, 1996; Loucks, 1999). Composite unconformities are produced during several second- or third-order transgressive-regressive cycles, when prolonged exposure is interrupted by renewed marine transgression. Karstification processes will occur during each cycle of exposure, and the newly formed karst will also affect previously karstified rocks. The effects of such processes can be observed today in different regions comprising tropical carbonate deposition including the Belize shelf (e.g., Purdy, 1974) and the Great Barrier Reef (Hopley, 1982), where paleokarst landforms are reoccupied by renewed reefal growth and carbonate deposition.

Hence, the cave systems will subsequently collapse and coalesce during burial to form a 'coalesced collapsed-paleocave system' (Loucks, 1999). The extent and density of cave passages is therefore larger than the one produced during a single unconformity.

During exposure, cave passages may form, become inactive subsequently and, afterwards, be partially filled with sediments during the next marine transgression. Following several transgressive-regressive cycles, several tens of meters (vertically) of closely stacked cave passages may develop and extend over a broad area. During the subsequent burial, the cave system may subside, leading to wall and ceiling collapse, which ultimately produces a variety of breccia deposits (e.g., crackled- and mosaic- chaotic breccia) and fractures. Rebrecciation, in turn, may occur when collapsed cave passages collapse again due to renewed karstification at lower karst hydrographic base levels, which is followed by burial and subsidence.

Comparison with an outcrop analogue

A direct outcrop analogue was studied in the Billefjorden Trough (Central Spitsbergen) by Eliassen and Talbot (2005). Wide areas covered by carbonate breccias were described and further interpreted as the result of gravitational collapse into cavities, formed mainly by the dissolution of gypsum and anhydrite beds, in the Minkinfjellet Formation.

In the Loppa High, brecciation may also be controlled by the dissolution of evaporitic rocks in the Gipsdalen Group (e.g., Stemmerik et al., 1999; Larssen et al., 2002; Hunt et al., 2003). Moreover, based on seismic studies and regional stratigraphic data, Elvebakk *et al*. (2003) suggested that brecciation may have occurred in the Loppa High following the dissolution of evaporitic beds – leading to cave development – within the Gipsdalen Group.

Core data from well 7220/6-1 analyzed in this study confirmed that nodules of anhydrite were present between the breccia clasts (Figures 2.8A, 2.8C). Thus, it is conceivable that brecciation in the Loppa High may have been partly controlled by the dissolution of evaporitic layers and subsequent collapses of overlying carbonate deposits.

Top Paleozoic
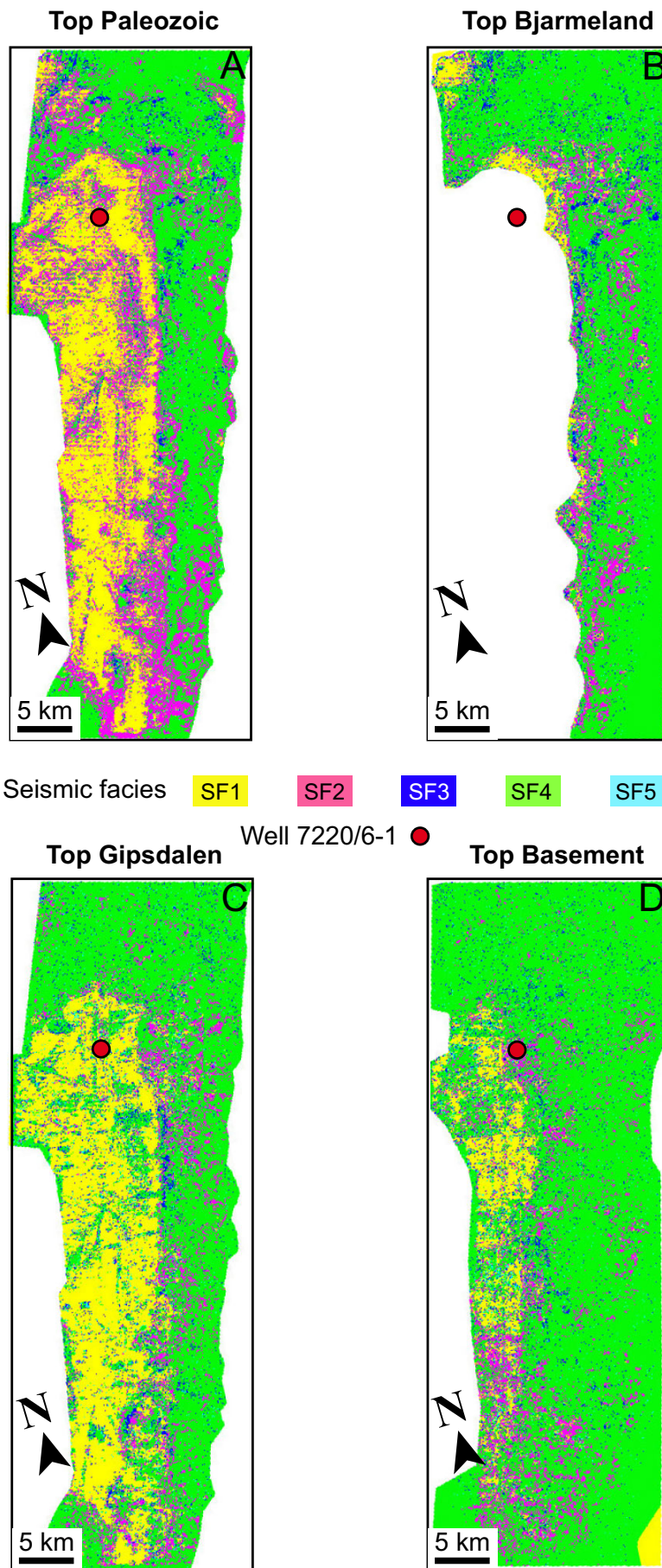
Top Bjarmeland

Figure 2.12 2D maps from the supervised classification showing the distribution of different seismic facies. (A) Top Paleozoic horizon. Note the extension of the seismic facies 1 (SF1) along the crest of the Loppa High. (B) Top Bjarmeland horizon, which is not present at the crest of the Loppa High. (C) Top Gipsdalen horizon also shows the presence of the SF1 at the crest of the Loppa High. (D) Top Basement horizon shows scattered presence of SF1.

Seismic facies   SF1   SF2   SF3   SF4   SF5

Well 7220/6-1 ●

Top Gipsdalen

Top Basement

2.6 Conclusion

Our study, based upon an integrated approach and including the use of core data, conventional seismic interpretation and seismic facies classification, helped to characterize a deeply buried paleokarst terrain in the Loppa High of the Norwegian Barents Sea. The core data indicated that ~50 m thick breccia-dominated deposits occupied the proximal part of this isolated structural high. Sedimentary facies analysis suggests that these breccia deposits formed during phases of cave development (due to dissolution of carbonate and evaporitic rocks) and cave collapse associated with karst systems. Conventional seismic interpretation allowed us to build an initial stratigraphic framework and to depict the present structural situation of the area. The seismic facies classification approach in both unsupervised and supervised mode was used to map the spatial extension of breccia deposits related to karstification processes, as well as other sedimentary unconformities and surrounding seismic facies in the investigated interval.

We estimated, with the 3D seismic facies classification that the breccia deposits occupied an area 40–50 km long and 10–12 km wide and were locally 10–150 m thick. Moreover, they were restricted to the highest part of the Loppa High. Consideration of our data along with those from previous studies leads us to propose that the large volume of breccia deposits mapped in the late Paleozoic carbonates represented an extensive 'coalesced collapsed-paleocave system'. Furthermore, comparison with an outcrop analogue suggested that brecciation in the Loppa High may have been produced also by the dissolution of evaporitic layers, inducing the collapse of overlying carbonate deposits.

As this study is the first in the Loppa High area in which core data are calibrated with a 3D seismic facies classification analysis, further data are needed to test and validate our results. Finally, such an approach may be applied to other areas (including the Barents Sea) where 3D seismic and core data are available to estimate and map karst-related deposits.

3

LATE PALEOZOIC SEISMIC SEQUENCE STRATIGRAPHY AND PALEOGEOGRAPHY OF THE LOPPA HIGH IN THE NORWEGIAN BARENTS SEA

Sayago J., Di Lucia M., Mutti M., Sitta A., Cotti A., Frijia G.

Abstract

The Loppa High (SW Barents Sea) is a half-graben structure, which developed during the late Paleozoic when the earliest phase of the Atlantic rifting between Greenland and Norway occurred. The southwest of the Barents Sea, located at the northern margin of Pangaea during the Carboniferous and Permian, was characterized by a structural style of half-graben geometries. The northward drift of the northern Pangaea triggered changes in regional climatic conditions that are reflected in the preserved sedimentary deposits. 2D/3D seismic combined with well and core data were used to define depositional seismic sequences and to develop a model of the stratigraphic evolution of the Loppa High. Based on the geometry of the defined seismic sequences and the character of observed sedimentary facies, a paleogeographic reconstruction of the key stages in the Loppa High evolution is also proposed and discussed in relation to local tectonic, global sea-level oscillations, and climatic changes. A total of seven seismic sequences, ranging from clastic-dominated to transitional clastic-carbonate sedimentation followed by an evaporitic drawdown phase, then shifting to carbonate-dominated sequences and finally capped by silica- and chert-dominated deposits, have been defined and represent the basin evolution from synrift to postrift sequences. Tectonics processes associated with the half-graben development are the principal controls in the overall 3-D morphology of the defined sequences. Sea-level fluctuations and climate changes have modified the biotic evolution and were responsible of the small-scale features inside each sequence.

3.1 Introduction

The sedimentary deposits of late Paleozoic age beneath the western Barents Shelf have been studied for three decades (Stemmerik and Worsley, 1989; Palmlöv, 1995; Stemmerik and Worsley, 1995; Stemmerik et al., 1998; Stemmerik et al., 1999; Stemmerik and Worsley, 2000; Larssen et al., 2002; Elvebakk et al., 2003; Samuelsberg et al., 2003; Larssen et al., 2005; Stemmerik and Worsley, 2005a). However, they have received less attention than the overlying sedimentary deposits of Mesozoic and Cenozoic age. Indeed, the overall loss of interest in upper Paleozoic sedimentary deposits following the first results from the exploration wells drilled in the area in the late 80's (Stemmerik et al., 1999), the limited number of wells studied reaching these deposits, and the degradation of the seismic signal with depth have limited the investigations of these sedimentary deposits. However,

Stemmerik et al. (1999) and Hunt et al. (2003) among other authors have highlighted the importance of the upper Paleozoic sedimentary deposits in the Loppa High in terms of reservoir prospectivity and suggested that a renewed interest in the area could help finding feasible reservoirs that have been overlooked in the past. Here, we intend to enhance the understanding of the late Paleozoic tectono-sedimentary evolution of the Loppa High over an area of ~3722 km^2 (Figures 3.1 and 3.2). Our new study complements others from the same area (e.g., Cecchi, 1993; Palmlöv, 1995; Ehrenberg et al., 1998a; Stemmerik et al., 1998; Stemmerik et al., 1999; Ehrenberg et al., 2000; Elvebakk et al., 2002; Larssen et al., 2002; Samuelsberg et al., 2003; Larssen et al., 2005; Colpaert et al., 2007; Rafaelsen et al., 2008), and represents the first detailed seismic stratigraphic analysis with particular focus to the sedimentary succession ranging from early Carboniferous to late Permian in the Loppa High. Previous studies in the area established the main lithostratigraphic subdivision of the southern Norwegian Barents Sea including the Billefjorden, Gipsdalen, Bjarmeland and Tempelfjorden groups (Larssen et al., 2002; Larssen et al., 2005; Bjørkesett, 2009). Nevertheless, further lithostratigraphic subdivisions and high-resolution mapping of the seismic sequences remained limited in the area. Here, we recognized and mapped a total of seven seismic sequences in the Loppa High (Figures 3.3B and 3.5) using 2D/3D seismic and well-log/core data, constructed time-thickness maps (isochrones) of each unit and ultimately reconstructed the paleogeography of the studied area for key time slices.

The subsurface of the Barents Sea region comprises two main geological provinces (see Figure 2 in Worsley et al. (2008)): the eastern province with the South and North Barents basins characterized by low tectonic activity since the Carboniferous and the development of a regional sag basin during the late Carboniferous and Permian (Stemmerik and Worsley, 1989; Gabrielsen et al., 1990; Dengo and Røssland, 1992; Cecchi, 1993; Bugge et al., 1995; Stemmerik and Worsley, 1995; Gudlaugsson et al., 1998), and the western province where the Loppa High is located, which was tectonically more active, i.e., affected by faulting, block-rotation, uplift, and erosion during the Permian and Triassic (e. g., Stemmerik and Worsley, 1989; Gabrielsen et al., 1990; Gudlaugsson et al., 1998)).

The mid-Carboniferous rifting led to development of fault-controlled basins, isolated platforms and structural blocks (Stemmerik et al., 1991). Distinct depositional trends were described among the sedimentary deposits from individual platforms and blocks (Stemmerik and Worsley, 1989; Stemmerik et al., 1999). Differences in tectonic history are thought to have driven variations in deposition among different areas. The Loppa High is an eastward-tilted and elongated fault block forming a half-graben in the subsurface of the western margin of the Barents Sea. Starting from the early Carboniferous, it underwent several phases of uplift, subsidence, tilting and erosion, and has accommodated a sedimentary succession of up to 5-km-thick covering the upper Paleozoic to the Cenozoic time interval (e.g., Larssen et al., 2002; Larssen et al., 2005).

The upper Paleozoic succession of the Loppa High consists of a mixed siliciclastic-carbonate depositional system, which developed on a rotating and subsiding fault-block in a rift basin. Within such a setting, the initial stage of rifting is defined by siliciclastic sedimentation along the hanging wall of main faults, areas that later evolve as sub-basins with predominant clastic deposition (Sharp et al., 2000; Bosence, 2005). Conversely, carbonate deposition with
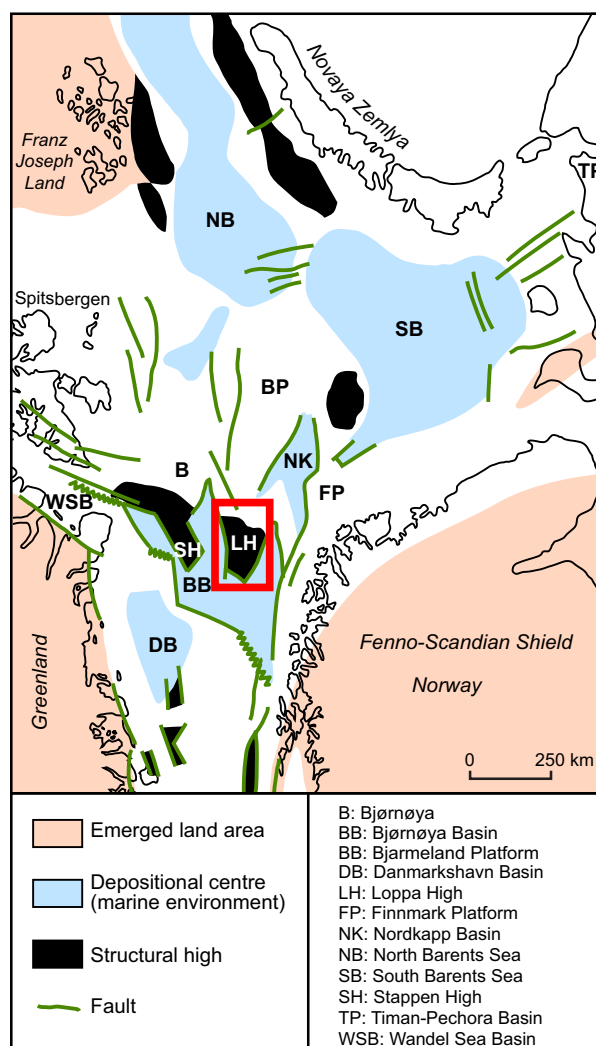
Figure 3.1 Pre-drift reconstruction of the northern margin of Pangaea during the late Paleozoic (modified after Stemmerik and Worsley 2005).

rimmed-margins and depositional sequences truncated by sedimentary or tectonic unconformities may occur in the footwall areas and in the hanging wall dipslopes (Bosence et al., 1998; Cross et al., 1998; Bosence, 2005). Such depositional systems with mixed sedimentation, which occurred within fault blocks of rift basins, have been previously described in various areas such as the Red Sea, Gulf of Suez, and Gulf of Aden (Burchette, 1988; James et al., 1988; Bosence et al., 1998; Cross et al., 1998; Purser and Bosence, 1998; Bosence, 2005). Similar depositional systems observed within fault blocks associated to rifting may be also found within fault blocks associated to the development of passive margins (Bosence, 2005).

In the Loppa High area, additionally to the interplay between local tectonic processes and global sea-level changes other paleo-environmental processes have also imprinted this sedimentary basin throughout the late Paleozoic (e.g., Stemmerik et al., 1998; Stemmerik et al., 1999). Indeed, the northward movement of the Pangaea is thought to have altered the regional climatic and hydrographic conditions (e.g., Golonka and Ford, 2000; Stemmerik, 2000). One of the effects was the shifting from warm-humid conditions in the early Carboniferous (Viséan to Serpukhovian) to warm-arid in the mid- to late-Carboniferous (Bashkirian to Sakmarian age); towards temperate and then cool-water during the Permian

(Artinskian to Urzhumian age). All these climatic changes influenced the facies development as well as early diagenetic processes (e.g., Stemmerik, 1997; Larssen et al., 2005; Stemmerik and Worsley, 2005a; Worsley, 2008). A broad understanding of these climate-related forcing mechanisms has been acquired by studying the well exposed outcrops of the upper Paleozoic sedimentary deposits in Bjørnøya, North and East Greenland, Svalbard, Sverdrup Basin in Arctic Canada and the Timan Pechora Basin (e.g., Steel and Worsley, 1984; Beauchamp, 1993; Stemmerik and Larssen, 1993; Stemmerik et al., 1995; Beauchamp and Desrochers, 1997; Stemmerik, 1997; Stemmerik et al., 1998; Stemmerik, 2000; Worsley et al., 2001).
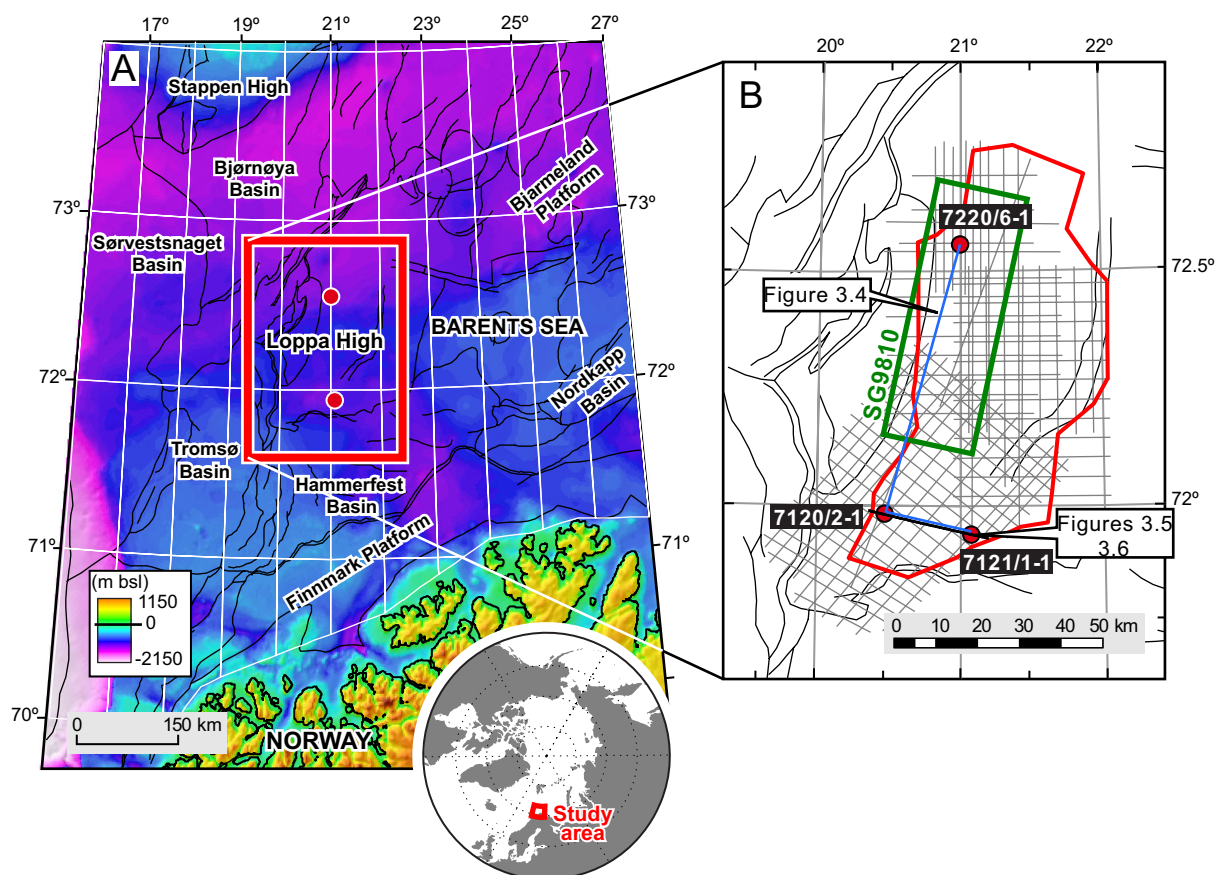
Figure 3.2 (A) Bathymetric map of the Norwegian Barents Sea, with major structural elements (modified from Sayago *et al*. 2012). (B) Location of the 2D/3D seismic data used in this study and location of exploration wells 7220/6-1, 7120/2-1 and 7121/1-1. m bsl = meters below sea level.

In our study, the detailed stratigraphic analysis of the seismic architecture allowed us to propose the tectono-sedimentary evolution for the Loppa High area during the late Paleozoic. We divided the upper Paleozoic units into seven the depositional seismic sequences, based on seismic sequence stratigraphic analysis. We integrated the available biostratigraphic data from the wells and the correlation framework across depositional seismic sequences to question the age of the first appearance of evaporitic deposits in the half-graben of the Loppa High. Finally, we inferred the development of three coeval margins, during the deposition of the carbonates units, with three different depositional styles, which probably resulted from differential subsidence between the hanging wall and footwall of the developing half-graben.

3.2 Geological setting: the Barents Sea and the Loppa High

3.2.1 Regional Structural Setting

During the Late Paleozoic, the area occupied by the Barents Sea was located at the northern margin of Pangaea and belonged to an extensive continental shelf with a west-east orientation. The shelf included, from west to east, the Sverdrup Basin of Arctic Canada, the North Greenland, the Norwegian Barents Sea and the Arctic Russia (Golonka and Ford, 2000; Stemmerik and Worsley, 2005a)(Figure 3.1). During the late Paleozoic, the central part of the shelf – including the Barents Sea, North Greenland and Spitsbergen area – was affected by the development of two rift arms (Stemmerik and Worsley, 2005a). The Atlantic rift arm between Greenland and Norway extended to the northeast throughout the Central Barents Sea (Figure 3.1) with a structural style characterized by half-graben geometries (Gudlaugsson et al., 1998). Conversely, the Arctic rift arm expanded to the west between Greenland and Spitsbergen (Gudlaugsson et al., 1998).

The principal late Paleozoic rifting event developed in the mid-Carboniferous (Bashkirian) and mid- to late- Permian (Artinskian-Kazanian)(Stemmerik and Worsley, 1989; Stemmerik et al., 1991). The first rifting event contributed to fault-controlled subsidence and formation of depocenters, along the rift axis, such as the Nordkapp, Trømso and Danmarkshavn basins (Figure 3.1) (Stemmerik et al., 1999). Following a marine transgression in the late Bashkirian these depocenters became a place of deep-water deposition (Stemmerik and Worsley, 1989; Stemmerik et al., 1999).

The more gently subsiding platforms such as Bjarmeland and Finnmark, and tectonically active structures, such as the Stappen High and Loppa High became sites of shallow marine deposition, with predominance of carbonates, from the mid-Carboniferous until the Late Permian. These deposits were intermittently interrupted by subaerial exposure surfaces (Stemmerik and Worsley, 1989; Stemmerik et al., 1991; Stemmerik and Worsley, 2005a; Sayago et al., 2012).

The structuring of the Caledonian basement seems to have influenced the rift development, especially from its main structural trends (NE-SW, N-S and NW-SE) (Doré, 1991). The NE-SW trend is the most significant and defines the orientation of some of the basins and structural highs such as the Nordkapp Basin and Loppa High (Figure 3.1) (Stemmerik and Worsley, 1989; Gabrielsen et al., 1990; Gudlaugsson et al., 1998).

Between the early Carboniferous and late Permian (from ~340 to ~260 Ma), the continental shelf was moving northwards at a speed of ~2–3 mm per year (from ~20°N to ~45°N) (Scotese and McKerrow, 1990). This gradual shift in paleolatitudinal position is reflected by changes in regional climatic conditions: from warm-humid in the early Carboniferous, changing to warm-arid in the mid- to late-Carboniferous and finally to temperate conditions in the late Permian. Such changes in paleolatitude and climate have also induced major changes in climate and therefore in the style of carbonate sediments being produced (Beauchamp and Desrochers, 1997; Stemmerik and Worsley, 2000; Beauchamp and Baud, 2002; Stemmerik and Worsley, 2005a).

3.2.2 The Loppa High

3.2.2.1 Structural setting

The Loppa High is one of the several buried structural highs located in the Barents Shelf. It is located near the southwestern margin of the Norwegian Barents Sea (Figure 3.2A). Several geologic basins such as the Hammerfest, Trømso and Bjørnøya bound the Loppa High to the south, southwest and west respectively; to the east it heads towards the Bjarmeland platform (Figure 3.2A) (e.g., Gabrielsen et al., 1990). The late Paleozoic tectonic activity across south-western part of the Barents Sea, which resulted in the evolution of the Loppa High, has been previously described (Faleide et al., 1984; Rønnevik and Jacobsen, 1984; Gabrielsen and Faerseth, 1989; Stemmerik and Worsley, 1989; Gabrielsen et al., 1990; Dengo and Røssland, 1992; Bugge and Fanavoll, 1995; Bugge et al., 1995; Gudlaugsson et al., 1998).

Previous studies, using 3D seismic data from the Loppa High area and well data from adjacent areas (e.g., Stemmerik et al., 1999; Elvebakk et al., 2003; Hunt et al., 2003; Carrillat et al., 2005) have interpreted an acoustic basement overlaid by a sedimentary package constituted of mixed carbonate/siliciclastic and carbonate sediments of late Carboniferous to mid-Permian age (e.g., Larssen et al., 2002). These sediments are dipping to the east and truncated at their top, exhibiting a strong angular unconformity towards the western crest of the Loppa High (Figures 3.4A and 3.5B). Protracted late Permian subaerial exposure led to intensive karstification processes – indicated by the presence of drainage systems, canyons, sinkholes, irregular topography and collapse breccia – that have significantly affected the carbonate sedimentary units (e.g., Stemmerik et al., 1998; Stemmerik et al., 1999; Elvebakk et al., 2003; Hunt et al., 2003; Sayago et al., 2012).

3.2.2.2 Stratigraphy

The Loppa High encompasses four major lithostratigraphic units from the early Carboniferous to the late Permian: Billefjorden, Gipsdalen, Bjarmeland and Tempelfjorden groups (e.g., Stemmerik, 1997; Dallmann, 1999; Stemmerik, 2000; Beauchamp and Baud, 2002; Larssen et al., 2002; Lindstrom, 2003; Larssen et al., 2005)(Figure 3.3A). The Billefjorden Group (Viséan to Serpukhovian) (Lindstrom, 2003) is a second-order sequence deposited in humid climatic conditions with sedimentation of continental fluvial deposits to marginal marine deposits (Gjelberg, 1981; Steel and Worsley, 1984). The Gipsdalen Group (late Bashkirian to early Sakmarian) is a second-order sequence deposited in warm semiarid to arid climatic conditions. It is characterized by mixed siliciclastic and carbonates at the base, while warm-water carbonates with abundant build-ups and presence of evaporites characterized its top (Steel and Worsley, 1984; Stemmerik, 2000; Elvebakk et al., 2002).

The Bjarmeland (late Sakmarian to Artinskian) was deposited during a temperate climate in open marine conditions; the sediments are typical of a cool-water carbonate factory characterized by Bryozoans, *tubiphytes*, foraminifera, brachiopods, bivalves and crinoids (Blendinger et al., 1997; Ehrenberg et al., 1998a; Stemmerik et al., 1999). The Tempelfjorden Group (middle-Kungurian to Urzhumian) comprises the youngest upper Paleozoic sedimentary deposits in the Loppa High. The sedimentation occurred in cold-water and basinal environments with siliceous sponge organisms as the dominant fauna (e.g., Ehrenberg et al., 1998a).
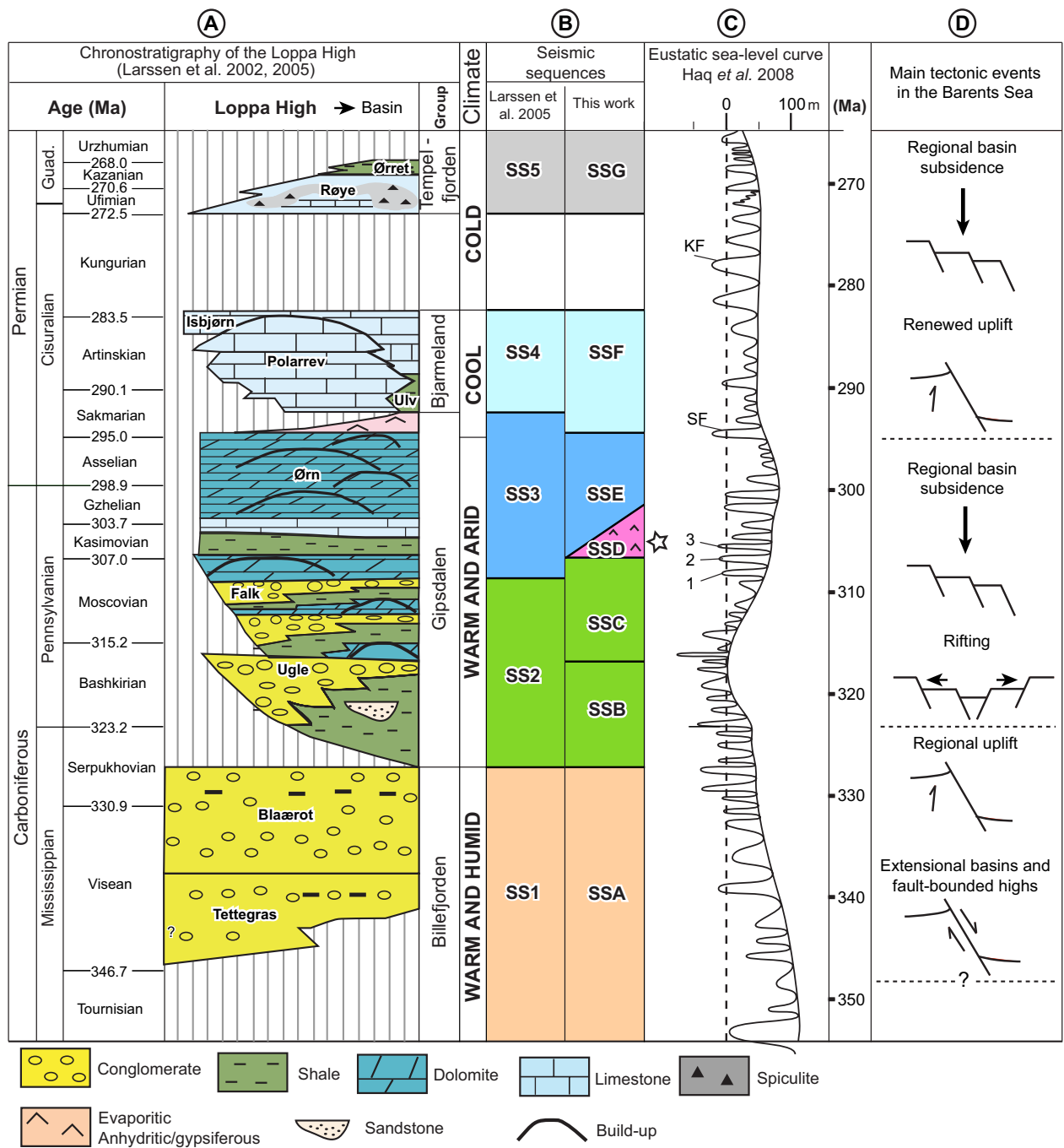
Figure 3.3 (A) Upper Palaeozoic lithostratigraphic units in the Loppa High. The age-scale has been adjusted to a linear scale, in order to compare it with the sea-level curve. The lithostratigraphic units are based on data from Larssen et al. (2002, 2005). (B) Comparison of the seismic sequences from the previous work of Larssen et al. (2002, 2005) and this work. The star symbol besides the SSD denotes the position of the new suggested evaporitic basin. (C) Eustatic sea-level curve of Haq et al. (2008). Numbers 1, 2, 3 represent three low-stand cycles during the Kasimovian. SF= Sakmarian flooding. KF= Kungurian flooding. (D) Main tectonic events in the Barents Sea and in the Loppa High area. Data based on data from (Gabrielsen, 1984; Gabrielsen et al., 1990; Stemmerik et al., 1991; Stemmerik et al., 1999; Stemmerik and Worsley, 2005a; Worsley, 2008).

3.3 Data and Methods

3.3.1 Seismic and well data

The area of study covers an area of 3722 km^2 (red polygon in Figure 3.2B). The seismic sequence analysis was performed using the available dataset of 2D/3D commercial seismic provided by Edison Oil&Gas Norway. The 2D seismic surveys included lines of different signal/noise ratios. For the interval of interest, the frequency spectra for the 2D lines ranges from 5 to 50 Hz. Due to the high P-wave velocities ranging between 4000 to 6300 m s^{-1}, the seismic resolution is in the order of 20–315 m. The 3D seismic volume (SG9810) used covers an area of ~960 km^2 (Figure 3.2B) and its frequency spectra – extracted from the seismic – is of 20–30 Hz for the target formation, with a peak of 25 Hz. The seismic resolution for the studied interval is of approximately ~45 m, assuming P-wave velocities larger than 4500 m s^{-1}. Seismic vertical scales are given in milliseconds (ms) two-way traveltime (TWT).

Data from three exploration wells (7120/2-1, 7121/1-1, and 7220/6-1) have been utilized for the calibration of the seismic stratigraphy and for age-control and facies evaluation (Figures 3.2B and 3.4). The data consisted of geophysical logs, cores and public released data from the Norwegian Petroleum Directorate. Construction of synthetic seismograms using the sonic and density logs allowed performing the seismic-well tie. Depth of the well data is given in meters below mean sea level (m bsl).

Seismic attributes such variance, cosine of phase, second derivative (Schlumberger™) were applied to the seismic lines in order to guide the interpretation process. In areas with poor resolution the seismic attributes helped to enhance the reflector terminations and structural delineations, also highlight depositional features and discontinuities. The seismic interpretation process was achieved with the software Petrel 2010.1 (Schlumberger™).

Time-thickness maps (isochrones) were constructed in order to visualize the distribution of the sediments and the main depocenters in each of the studied sequences. Based on the seismic data and the core data from the wells, Paleogeographic maps were inferred in an attempt to reconstruct the Loppa High paleo-environments during key stages of development.
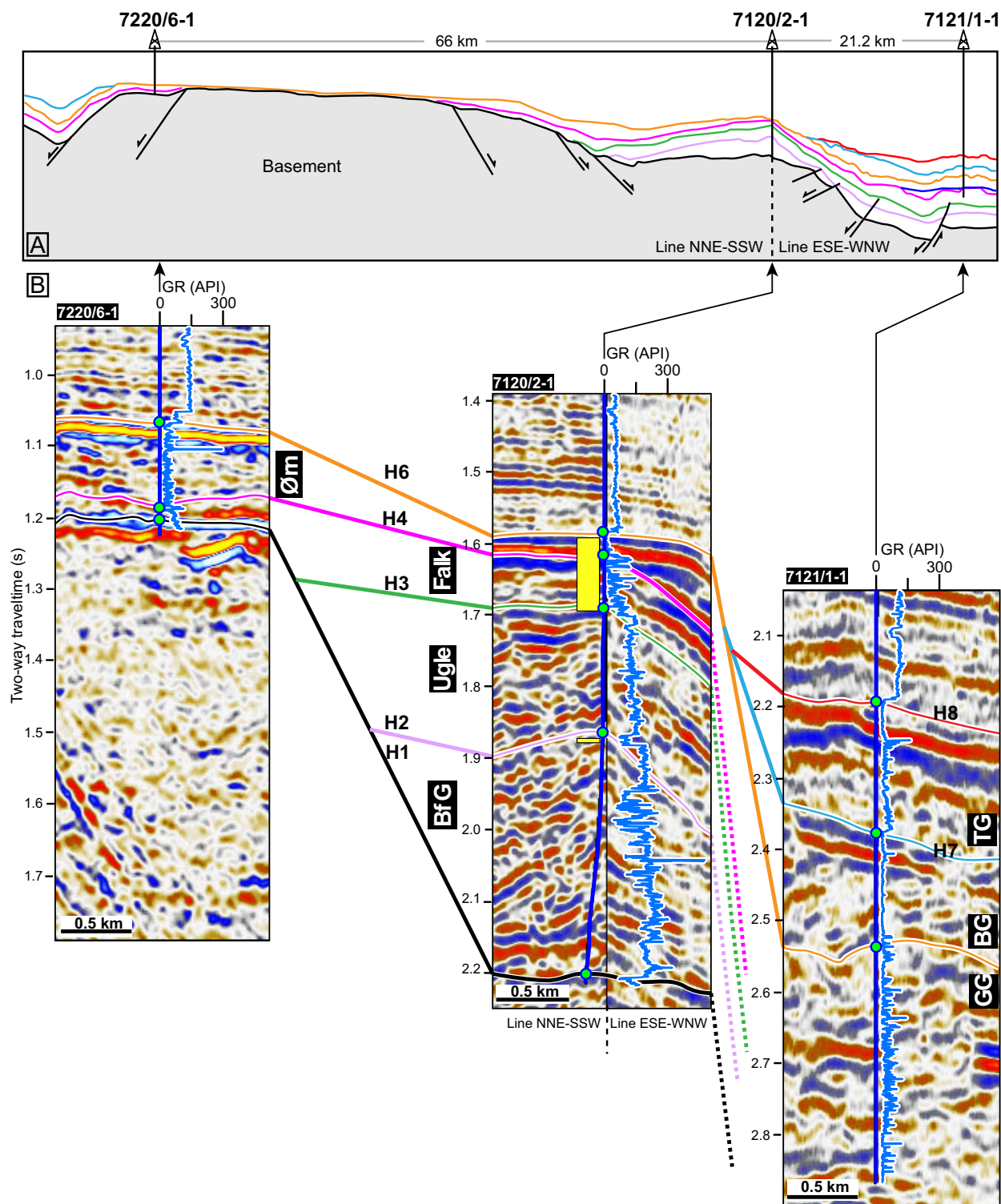
Figure 3.4 (A) Cross-section among the three exploration wells 7220/6-1, 7120/2-1, 7121/1-1 and distance among wells. For transect location see Figure 3.2B. (B) Stratigraphic gamma-ray well log correlation. Note the truncation/thinning of the sequences towards the crest of the Loppa High. Bf G = Billefjorden Group. GG = Gipsdalen Group. BG = Bjarmeland Group. TG = Tempelfjorden Group. Hn = horizon n (n = 1 – 8). Core intervals are presented in yellow.
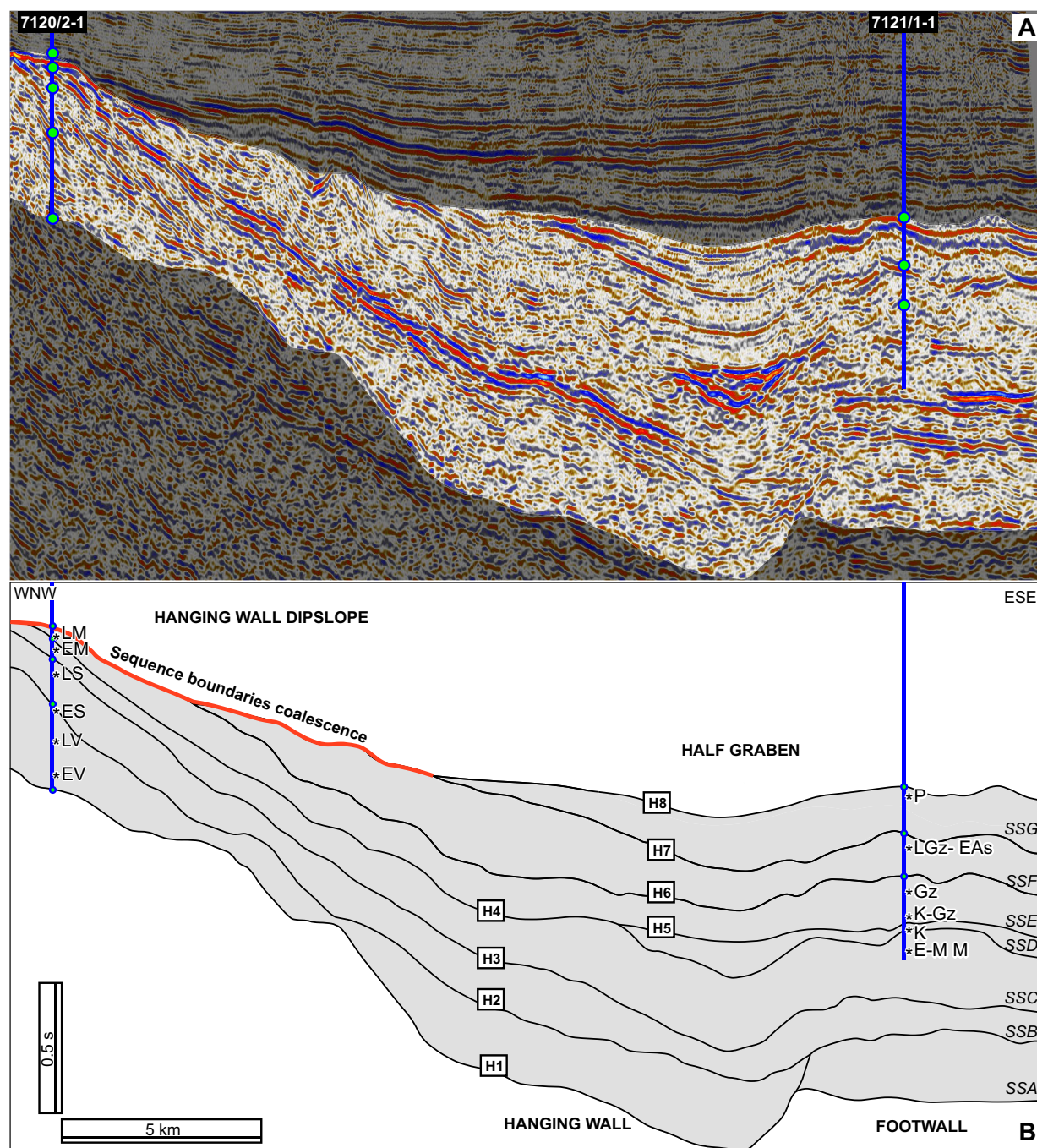
Figure 3.5 (A) Seismic line SG8737-102 showing the half-graben geometry of the Loppa High (see Figure 3.2B for line location). (B) Seismic sequences A to G interpreted in the Loppa High (see text for discussion). Available biostratigraphic ages are marked along the well paths (Alsgaard et al., 1987; Bugge et al., 1995; Stemmerik et al., 1995; Ehrenberg et al., 1998; Ehrenberg et al., 2000; Larssen et al., 2002; Lindstrom, 2003; Larssen et al., 2005). EV = Early Viséan, LV = Late Viséan, ES = Early Serpukhovian, LS = Late Serpukhovian, EM = Early Moscovian, LM = Late Moscovian, E-M M = Early–Middle Moscovian, K = Kasimovian, K–Gz = Kasimovian–Gzhelian , Gz = Gzhelian, LGz–EAs = Late Gzhelian–Early Asselian, P = Permian. Note the wedge geometry of the studied interval and the coalescence of the sequence boundaries towards the hanging wall dipslope. SSn = Seismic sequence n (n = A – G). Hn = horizon n (n = 1 – 8).

3.4 Results and interpretation

3.4.1 Sequence stratigraphic analysis

In this study we used the general sequence stratigraphic subdivision of the upper Paleozoic succession of the Barents Sea established by previous studies (Stemmerik and Worsley, 1989; Cecchi, 1993; Stemmerik et al., 1995; Ehrenberg et al., 1998a; Stemmerik et al., 1999; Stemmerik and Worsley, 2000; Larssen et al., 2002; Larssen et al., 2005; Stemmerik and Worsley, 2005a; Rafaelsen et al., 2008). In a regional seismic study, Larssen et al. (2002, 2005, their figure 5a) have identified five seismic sequences in the upper Paleozoic succession of the Loppa High. Cecchi (1993) based on higher-resolution studies of well and outcrops data, have identified third- and higher- order depositional sequences, which included lowstand, transgressive and highstand system tracts. In our study, such system tracts remained hardly resolved due to the seismic resolution at the investigated target depth.

Across the studied time interval, we identified and mapped seven seismic sequences, starting from seismic sequence A (SSA) at the bottom and reaching seismic sequence G (SSG) at the top (Figure 3.5). The observation of geometrical associations of the strata and parameters such as reflection terminations, stacking patterns, amplitude changes and bounding discontinuities were taking into account to define each seismic sequence (Mitchum et al., 1977; Vail and Mitchum, 1977) (Neal and Abreu, 2009). The bounding discontinuities are marker reflectors that represent breaks in deposition at the seismic scale and can be regionally mapped. The rank-order designation of these sequences is defined by their approximate durations (Vail and Mitchum, 1977), determined by the available age-control. The seven seismic sequences oscillate in the range of second-order for sequences A, E, F and G and third-order for sequences B, C and D (Figures 3.3 and 3.5).

In general for all the interpreted seismic sequences, the disruption of reflectors and low signal/noise ratio in many of the seismic lines is ascribed to the depth of the studied interval, complex nature of the preserved sediments and loss of high frequencies with depth.

3.4.2. Seismic sequences: description and interpretation

1. Seismic Sequence A (SSA) – early Viséan to early Serpukhovian

SSA is limited between horizon 1 (H1) and horizon 2 (H2) (Figures 3.4 and 3.5). This sequence is found only in the southernmost part of the studied area (Figure 3.6E). It has a variable time-thickness ranging from 0 to 563 ms TWT. H1 is expressed as an angular truncation of the basement reflectors (Figure 3.6D). This contact represents a major unconformity in the Loppa High as well as in other areas of the Barents Sea (e.g., Larssen et al., 2002; Samuelsberg et al., 2003). In the well 7120/2-1, H1 corresponds to the base of the Billefjorden group, which overlies a metamorphosed rock of the Caledonian basement (Figure 3.4) (Gabrielsen, 1984; Gabrielsen et al., 1990; Gudlaugsson et al., 1998).

The SSA comprises wedges, ranging from ~3 to ~12 km in length, with internal divergent reflectors of chaotic signature and low- to medium- amplitude (Figures 3.6B and 3.6C). Flattening at the top of H2 was applied to remove the effects of post-depositional deformation and better depict the thickness variation of each wedge (Figure 3.6C). The main fault (F1), dipping to the west, limits the half-graben of the Loppa High and shows indication of activity during the deposition of SSA (Figure 3.6B). The fault movement is inferred by the thickening of the strata in the immediate hanging wall of the F1, which led to the formation of a 'major wedge' (Figure 3.6B). Additionally, typical hanging wall synrift

geometries, known as *aggradational footwall-derived fans* and characterized by divergent sediment wedges (Prosser, 1993; Sharp et al., 2000), are observed adjacent to the F1 (Figure 3.6B). All of the observed wedges likely represent the syn-tectonic filling of small-scale half-grabens formed during the ongoing early- to mid-Carboniferous rifting in the area (Stemmerik, 2000; Larssen et al., 2002; Samuelsberg et al., 2003; Larssen et al., 2005; Stemmerik and Worsley, 2005b).

In the well 7120/2-1 the sediments encountered corresponding to SSA consist of different types of breccias and conglomerates bodies overlying a layer of siltstones and mudstones; volcanic clasts are also present in significant amount. The depositional environment is associated to alluvial fans and braided rivers systems, with associated nearby volcanic activity (Larssen et al., 2002). Based on palynological data the Billefjorden group has been dated as early Viséan to early Serpukhovian in age in well 7120/2-1 (Lindstrom, 2003).
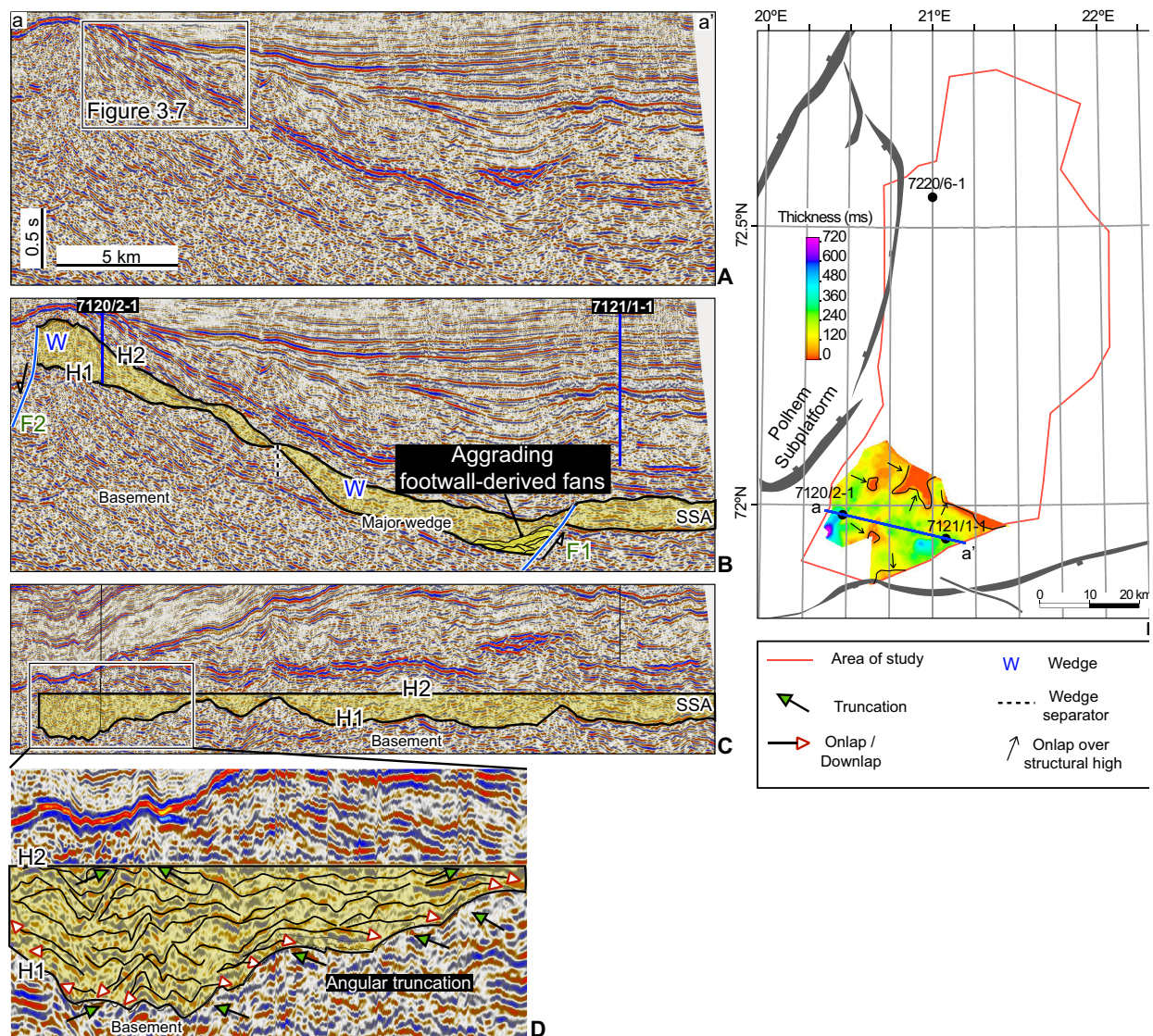
Figure 3.6 Interpretation of SSA between H1 and H2. The SSA is only crossed by well 7120/2-1. (A) Seismic line SG8737-102. (B) Interpretation showing different wedges- thicknesses along the profile, note the presence of aggrading footwall-derived fans in the hanging wall adjacent to the fault plane of Fault 1 (F1). (C) Flattened seismic line at the H2 showing in detail the thickness variation of the unit. (D) Enlargement of the wedge geometry (rectangle in C) displaying clear reflectors configuration (onlap/downlap) above and below H1. (E) Time-thickness map of SSA showing that the unit is restricted to the southwest of the studied area. The unit reaches a thickness of 563 ms TWT. W = wedge. SSA = seismic sequence A.

2. Seismic Sequence B (SSB) – late Serpukhovian to early Bashkirian

SSB is bounded by H2 and horizon 3 (H3) (Figure 3.4 and 3.5). As for SSA, its spatial extent is confined to the southernmost part of the studied area. Its time-thickness varies between 0 to 370 ms TWT (Figure 3.7C). The seismic data shows angular truncation of reflectors at the top of the SSA (Figure 3.7B), which can be related with an unconformity attributed to a regional uplift during the Serpukhovian (e.g., Bugge et al., 1995; Stemmerik et al., 1998). The internal configuration of the SSB exhibits medium- to high- amplitude values of well-bedded reflectors. In the hanging wall dipslope, lens-like features are present (Figure 3.7B) and have been interpreted as *offlapping hanging wall-derived fans* (Prosser, 1993; Sharp et al., 2000). The top of SSB (H3) corresponds to the top of the Ugle formation in the well 7120/2-1 (Figures 3.3 and 3.4) (Larssen et al., 2002; Larssen et al., 2005). Like SSA, SSB represents the filling of half-graben extensional formed during the ongoing mid-Carboniferous rifting in the area. The SSB is dominated by cycles of conglomerates grading upwards to siltstones with caliche nodules ontop and have been interpreted to reflect shallow subaqueous debris flows of alluvial fans and fan deltas (Gjelberg et al., 1985) deposited in continental and marginal marine environments. Lindstrom (2003), based on palynological data from well 7120/2-1, provided a late Serpukhovian to early Bashkirian age for the sedimentary deposits correlative to SSB.

3. Seismic Sequence C (SSC) – late Bashkirian to early Moscovian

SSC is bounded by H3 and horizon 4 (H4) (Figures 3.5 and 3.8). The SSC is present in nearly all the studied area and its time-thickness increases gradually from the west to the east from 0 ms to 700 ms TWT (Figure 3.9A). The base of SSC (H3) truncates the underlying reflectors of SSB in some areas, in other cases the transition appears conformable (Figures 3.8A and 3.8B). The SSC comprises a lower unit of parallel high-amplitude reflectors onlapped by an upper unit of low-amplitude reflectors (Figures 3.8A and 3.8B); the maximum observed westward extent of the onlapping unit is shown in Figure 3.9A. Seismic mounds are observed along the 2D seismic sections in the proximal and distal zones of the profile.

There are not indications of fault activity during the deposition of SSC. The top of SSC (H4) corresponds to the top of the Falk formation in the wells 7120/2-1 and 7220/6-1 (Figure 3.4) and according to our interpretation the well 7121/1-1 probably penetrated the distal part of the SSC (Figure 3.5).

The cored interval of the well 7120/2-1 corresponding to SSC includes cycles of continental conglomerates and nearshore deposits changing upwards to shelf carbonates interbedded with marine shales. The contact of lithofacies, within the SSC sediments, is sharp and bounded by exposure surfaces represented by caliche horizons (Gjelberg et al., 1985; Stemmerik et al., 1998; Larssen et al., 2002; Larssen et al., 2005). The ditch samples and sidewall cores of the well 7121/1-1 for the SSC interval consists of alternations of dolomitic limestone, anhydrite and siltstone (Alsgaard et al., 1987). The sidewall core sediments of the well 7220/6-1 for the SSC shows an intercalation of sandstones and limestones intervals (Edison, 2011).

The upward change from high to low amplitude reflectors within the SSC may reflect the seismic response of intercalated siliciclastic-carbonate sediments overlaid by carbonate sediments. This effect is also perceived in the gamma-ray logs that shows overall lower values and a noisy pattern due to the intercalation siliciclastic-carbonates (Larssen et al., 2002) (Figure 3.4). The presence of exposure surfaces in the most proximal well 7120/2-1 indicates repeated exposure and flooding of the uppermost area of the hanging wall. Such exposure surfaces are not observed in the more distal well 7121/1-1 signifying that the lowermost area of the hanging wall and the footwall of the Loppa High half-graben may have not been exposed although experiencing shallow-water conditions.

The Falk formation corresponds to the first pulses of marine transgression recorded in the Loppa High during a period of high-frequency and high-amplitude sea level changes (Figure 3.3) (Bugge et al., 1995; Ehrenberg et al., 1998a; Stemmerik et al., 1998; Stemmerik et al., 1999; Stemmerik and Worsley, 2000; Larssen et al., 2002; Samuelsberg et al., 2003; Larssen et al., 2005). The most abundant fossils consist of fusulinids, brachiopods, crinoids and corals; in less abundance are the Paleoaplysinid plates and phylloid algae (Larssen et al., 2002). Palynological data from well 7120/2-1 suggest an early Moscovian age for the upper part of the Falk formation (Lindstrom, 2003), although the top and base of the formation is expected to be diachronous as result of the marine transgression (Larssen et al., 2002; Larssen et al., 2005).
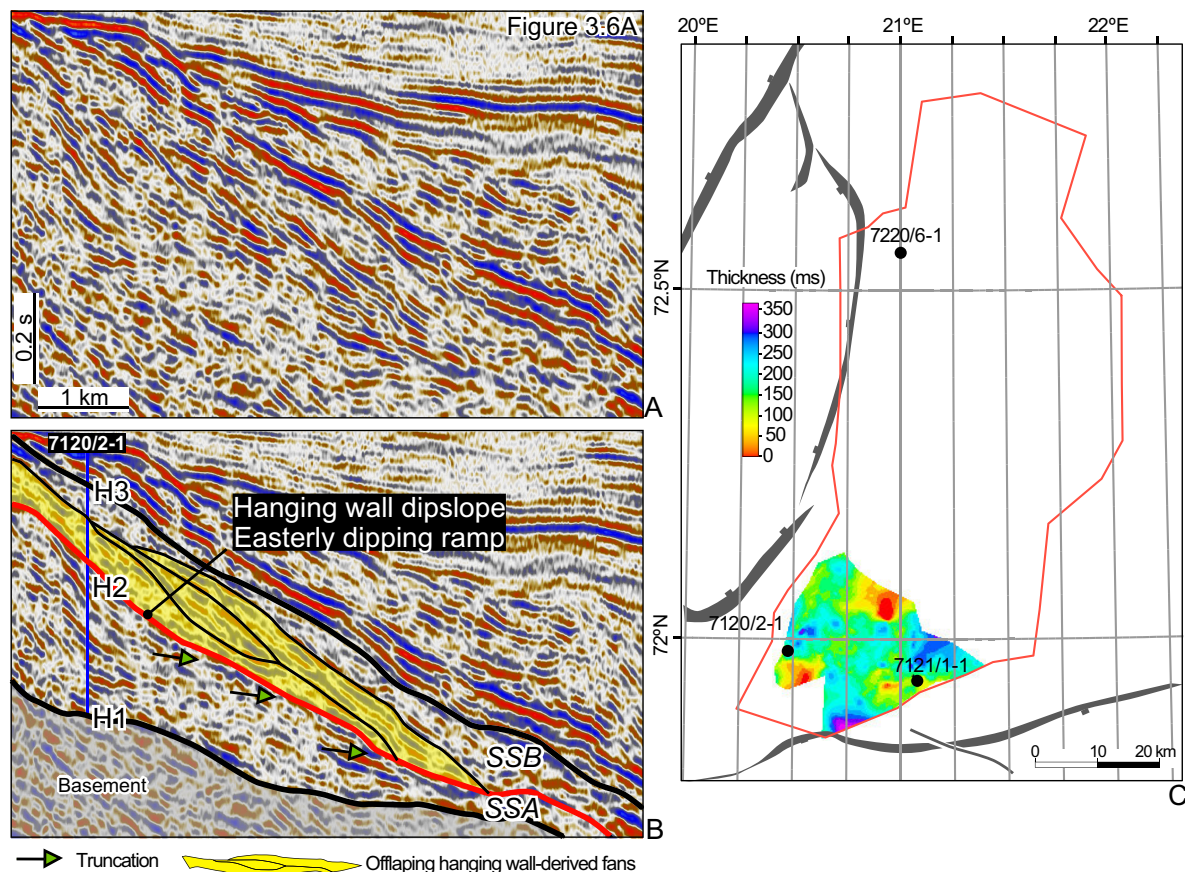
Figure 3.6A

Figure 3.7 Interpretation of SSB between H2 and H3 penetrated by well 7120/2-1. (A) Enlargement from figure 6A. (B) Interpreted seismic line with offlapping hanging wall derived fans in the uplifted/rotating dipslope of the hanging wall. Note the truncation of the reflectors below H2, which represents an unconformity surface. (C) Time-thickness map of SSB showing that the unit is restricted to the southwest of the studied area and reaches a thickness of 370 ms TWT. See text for details. SS*n* = Seismic sequence *n* (*n* = A – B).
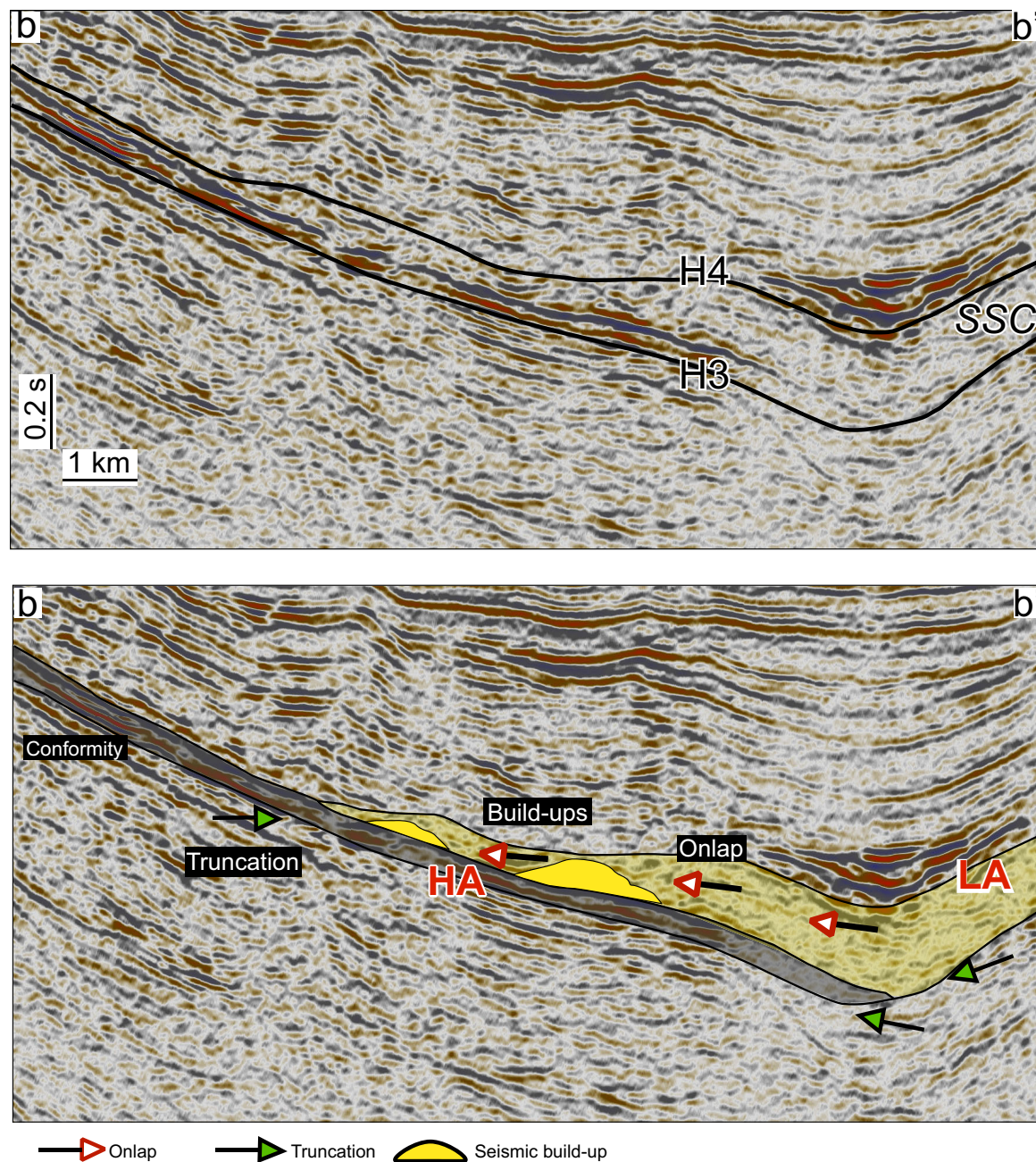
Figure 3.8A Interpretation of the Low Amplitude (LA) and High Amplitude (HA) bands from line NH8306-410 (b-b'), note the onlapping terminations of LA on HA. The base of SSC truncates underlying reflectors in some localized areas while conformity is observed in other areas. Observed seismic build-ups are shaded in yellow. The SSC increases thickness towards the southeast.
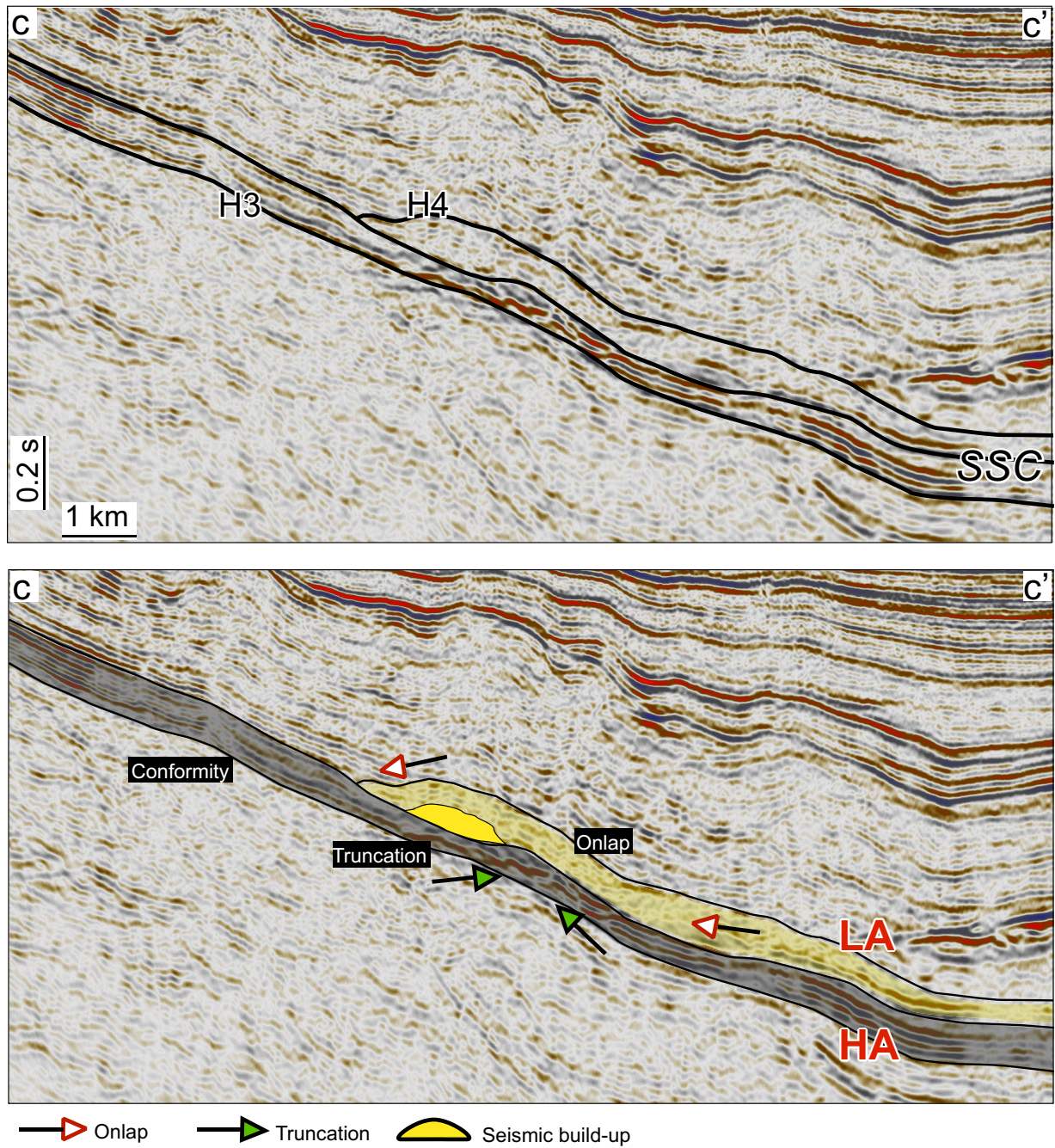
Figure 3.8B LA and HA bands observed in the seismic line SG9811-00409 (c-c'). Seismic build-ups are scattered in this location. Position of seismic lines is shown in Figure 3.9. SSC = seismic sequence C.
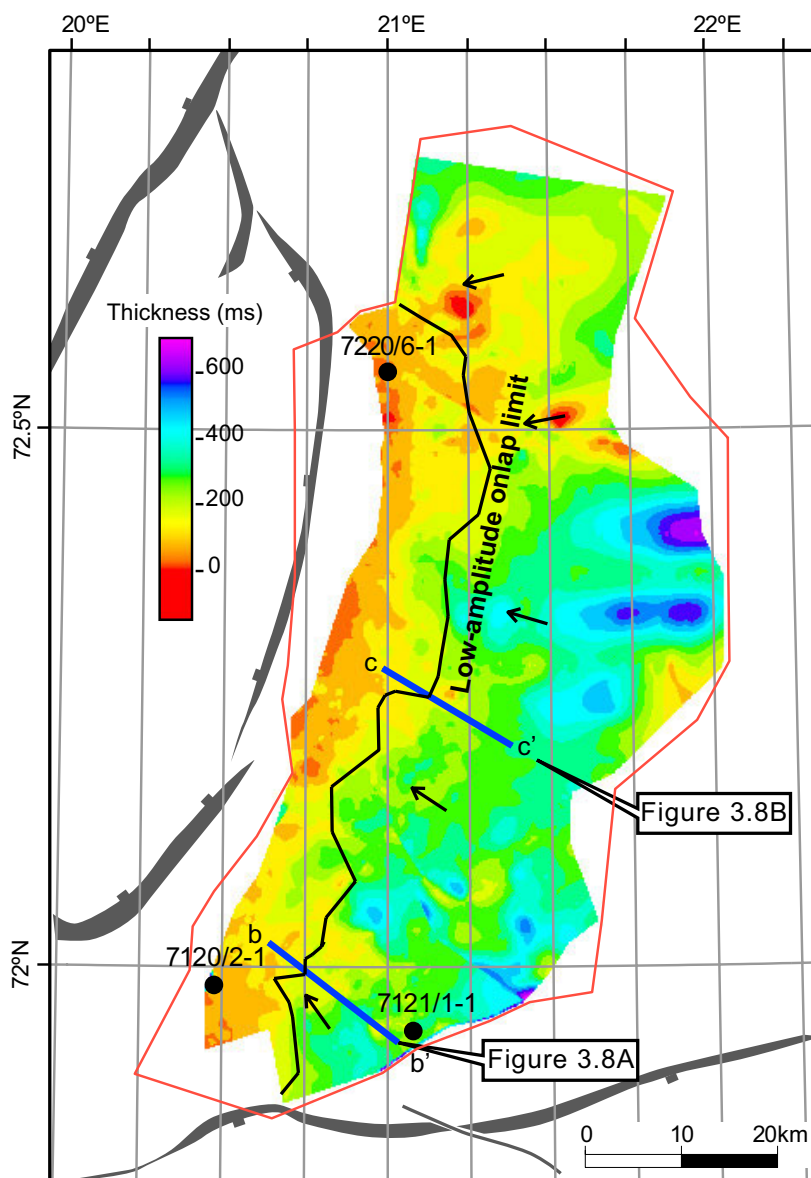
Figure 3.9 Time-thickness map of SSC, the unit covers all the studied area reaching 700 ms TWT. The maximum onlap limit of the High Amplitude band (see Figures 3.8A and 3.8B) is shown as a black continuous line.

4. *Seismic Sequence D (SSD) – Kasimovian (~307.2 – 303.4 Ma)*

Seismic Sequence D (SSD) is located between H4 and Horizon 5 (H5) (Figure 3.5). It is characterized by a set of reflectors of low- to medium- amplitude in the structural highs grading laterally to high-amplitude and well-bedded reflectors in the basins (Figures 3.10A and 3.10B). H4 truncates underlying reflectors and is onlapped by SSD internal seismic reflectors (Figure 3.10A). The spatial extent of this sequence is confined to the eastern part of the studied area and its time-thickness varies from 0 to 310 ms TWT (Figure 3.11B). The topographically depressed areas (sub-basins) –highlighted by dashed lines in the map of the Figure 3.11A– are controlled by faults and the pre-existing rift topography. The thickness of SSD increases significantly in those sub-basins.

The well 7121/1-1 penetrated the SSD interval and the lithofacies classification was performed from the cutting samples and sidewall core samples. The dominant lithofacies,

corresponding to this sequence, consists of dolomitic limestones with anhydrite beds; some argillaceous material, chert and silt. The anhydrite beds range between 1 m and 20 m of thickness (Alsgaard et al., 1987); their vertical distribution along the well path is shown in the Figure 3.10A. These sedimentary deposits indicate a marginal marine and restricted evaporitic environment of deposition. Biostratigraphic data assigns a Kasimovian age to the corresponding SSD interval (Alsgaard et al., 1987).

Integration of the seismic character and lithological data suggest depositional environments of marginal marine sabkhas in the topographical highs and hyper-saline lagoons in the fault-controlled depressions for SSD (Figure 3.14B). Similar depositional environments have been described in the Finnmark Platform during the Gzhelian (Bugge et al., 1995).
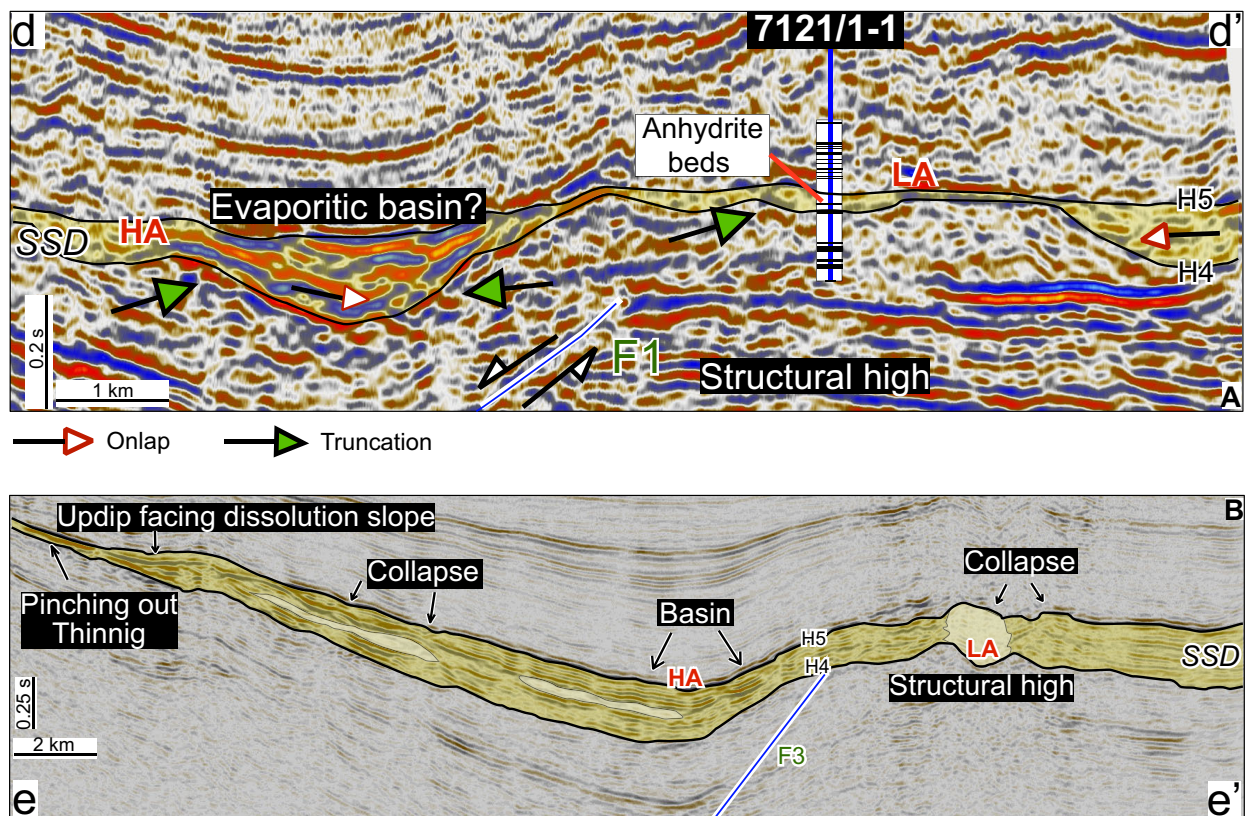
Figure 3.10 Seismic profile showing the SSD geometries. (A) Part of seismic profile SG8737-102 (d-d') showing the inferred evaporitic basin with HA reflections. The LA reflections are predominant in the structural high. Intercalation of anhydrite (black) and dolomite (white) along the path of well 7121/1-1 is shown. (B) Seismic line NH8414-107 (e-e') shows the predominance of high amplitude zone in the basin and low- to medium- amplitude towards the structural highs. The updip dissolution slope and collapse structures related with evaporites dissolution are also shown. SSD = seismic sequence D. LA = low amplitude. HA = high amplitude. White arrows represent onlap. Green arrows represent truncation. Position of seismic lines is shown in Figure 3.11.
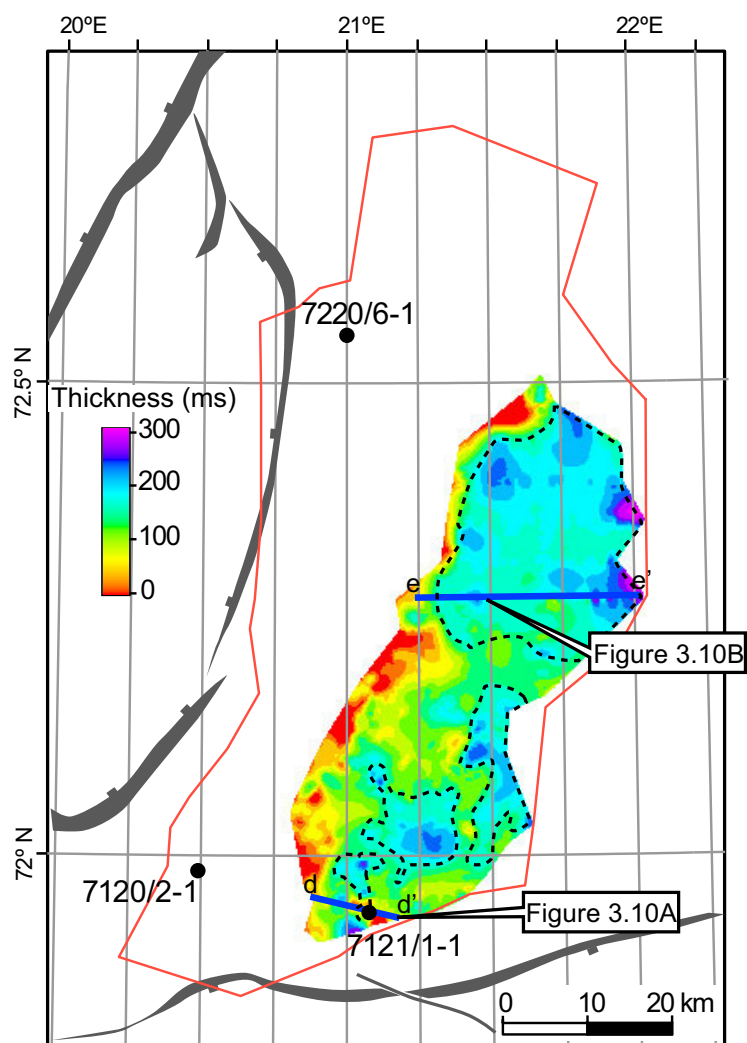
Figure 3.11 Time-thickness map of SSD showing that the unit is delimited to the east of the studied area. It attains a time-thickness of 310 ms TWT. The increase of thicknesses inside the black-dashed polygons is interpreted as large accumulation of sediments in fault controlled sub-basins with higher rates of subsidence.

5.   *Seismic Sequence E (SSE) – late Moscovian to late Asselian*

Seismic Sequence E (SSE) is bounded by H4 and H5 at the base and horizon 6 (H6) at the top (Figure 3.5). The top of SSE (H6) correlates with the Ørn formation of the Gipsdalen group in the wells 7220/6-1, 7120/2-1 and 7121/1-1 (Figure 3.4). The sequence comprises low- to medium- amplitude reflectors (Figure 3.12B and 3.12C). Time-thickness of the SSE varies from 0 to 460 ms TWT and its spatial extent covers mostly all the studied area, except the easternmost part, where poor quality of the available data hampered a detailed observation/analysis (Figure 3.13A). Mound-shape features of 30–140 ms TWT are observed in the dipslope of the hanging wall; they have a chaotic internal structure and their basal part shows bi-directional downlap reflections (Figure 3.12A and 3.12B), continuous seismic reflectors surround the mounds. To the east, in the lowermost part of the hanging wall, retrogradational stacking patterns occur. Aggradational stacking patterns are observed in the footwall (Figure 3.12A and 3.12B). The mound-shape features, retrogradational and aggradational stacking patterns are organized in elongated fringes oriented in NE-SW

direction and can be followed for several kilometers in the studied area (Figure 3.13A, 3.13B and 3.14C).
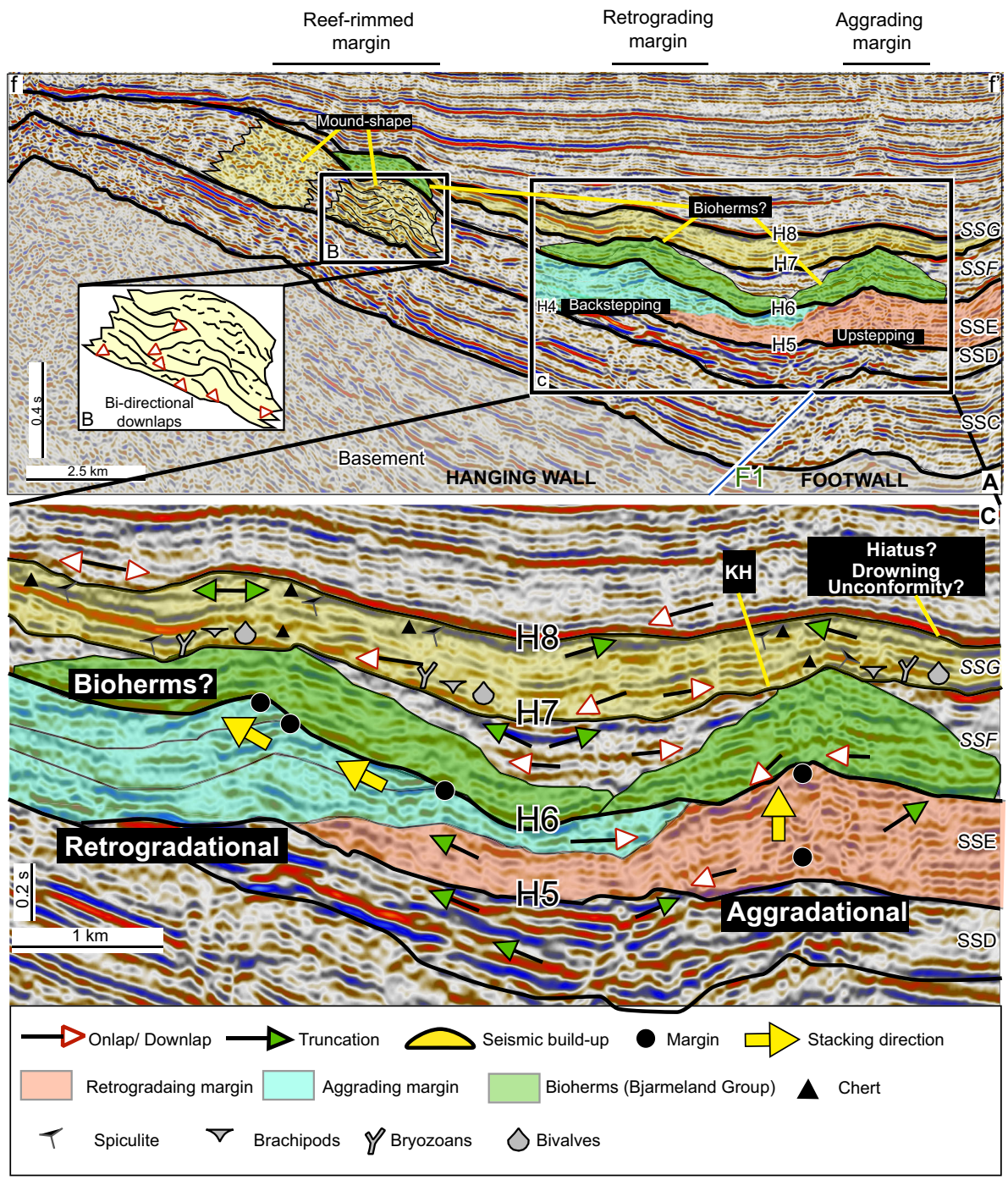
Figure 3.12 (A) Seismic line SG9309-405 (for location of seismic line, see figure 3.13A) with interpretation of SSE, SSF, and SSG. Note the geometries of the mound-shape features, retrogradational- and aggradational-stacking patterns interpreted as reef-rimmed, retrograding and aggrading margins respectively during the deposition of the SSE. (B) Enlargement of the mound-shape features depicts their internal configuration with bi-directional downlaps and chaotic reflections. (C) Enlargement in the SSE, SSF, and SSG with main reflector terminations. In the SSE the interpreted retrogradational and aggradational stacking patterns are shown. The retrograding and aggrading margins are marked with black dots and their trajectory is marked with yellow arrows. It is important to note that the units may be post-depositionally deformed and altered by diagenetic processes. In the SSF, the mound-shaped features have been interpreted as bioherm complexes of the Bjarmeland Group as observed in well 7121/1-1 (see text for details). The SSG onlaps the underlying SSF and the build-up features are not longer visible. The SSF is characterized by deeper-water sedimentary facies with abundant chert, abundant fossils specially spiculites.

The mound-shape features have been interpreted as stacked build-ups that form a rimmed margin. The retrogradational stacking patterns show two apparent phases of backstepping of about 100–150 ms TWT each (Figure 3.12B new), which may represent the retrogradation of an isolated platform that was not able to keep pace with the increasing base level. The aggradational stacking patterns, in the footwall, instead may correspond to the development of an isolated platform/atoll, which kept pace of the increasing base level (Figure 3.12B).

The lithofacies associated to SSE were described in the well 7121/1-1 by Alsgaard et al. (1987); they found dolomitized limestones and interbedded condensed intervals of argillaceous, silty and anhydritic deposits. Available well data from adjacent areas to the Loppa High shows that for the Ørn Formation shallow marine carbonates dominate on the platforms and interbedded carbonates and evaporites dominated in the distal ramps and basins (Larssen et al., 2002). The described biota are typical of warm-water environments and characterized by the presence of fusulinids and calcareous algae (Larssen et al., 2002; Larssen et al., 2005). The base of the Ørn formation is dated as late Moscovian in the well 7120/2-1 (Lindstrom, 2003).

The build-ups were not drilled by any well in the Loppa High but correlative sampled build-ups from the nearby Finnmark Platform, showed to be composed of abundant stacked *Palaeoaplysina*-phylloid algae together with other fauna such as brachiopods, bryozoans, bivalves, encrusting foraminifera, echinoids, gastropods suggesting deposition below wave-base in tropical waters (Bugge et al., 1995; Stemmerik et al., 1995; Ehrenberg et al., 1998a; Larssen et al., 2002; Larssen et al., 2005). Larger polygonal build-ups in the outer ramp settings have been described in the Loppa High (Elvebakk et al., 2002) (Figure 3.14C).

Overall, SSE suggests deposition in a variety of marine carbonate environments ranging from subtidal to open marine during arid to semi-arid climatic conditions.

6. *Seismic Sequence F (SSF) – mid-Sakmarian to late Artinskian*

Seismic Sequence F (SSF) is bounded by H6 and horizon 7 (H7). The whole SSF correlates with the Bjarmeland Group in the well 7121/1-1 (Figure 3.4). This sequence covers all the studied area and its time-thickness ranges from 0 to 330 ms TWT (Figure 3.13C). The internal seismic character ranges from semi-transparent to continuous reflectors with low- to medium- amplitude values. The lower SSF reflectors exhibit downlap and onlap terminations onto H6 (Figure 3.12B and 3.12C). Large mound-shape features of up to 200 ms TWT thick are frequent and appear on top of preexistent mounds of sequence SSE. The uppermost reflectors are
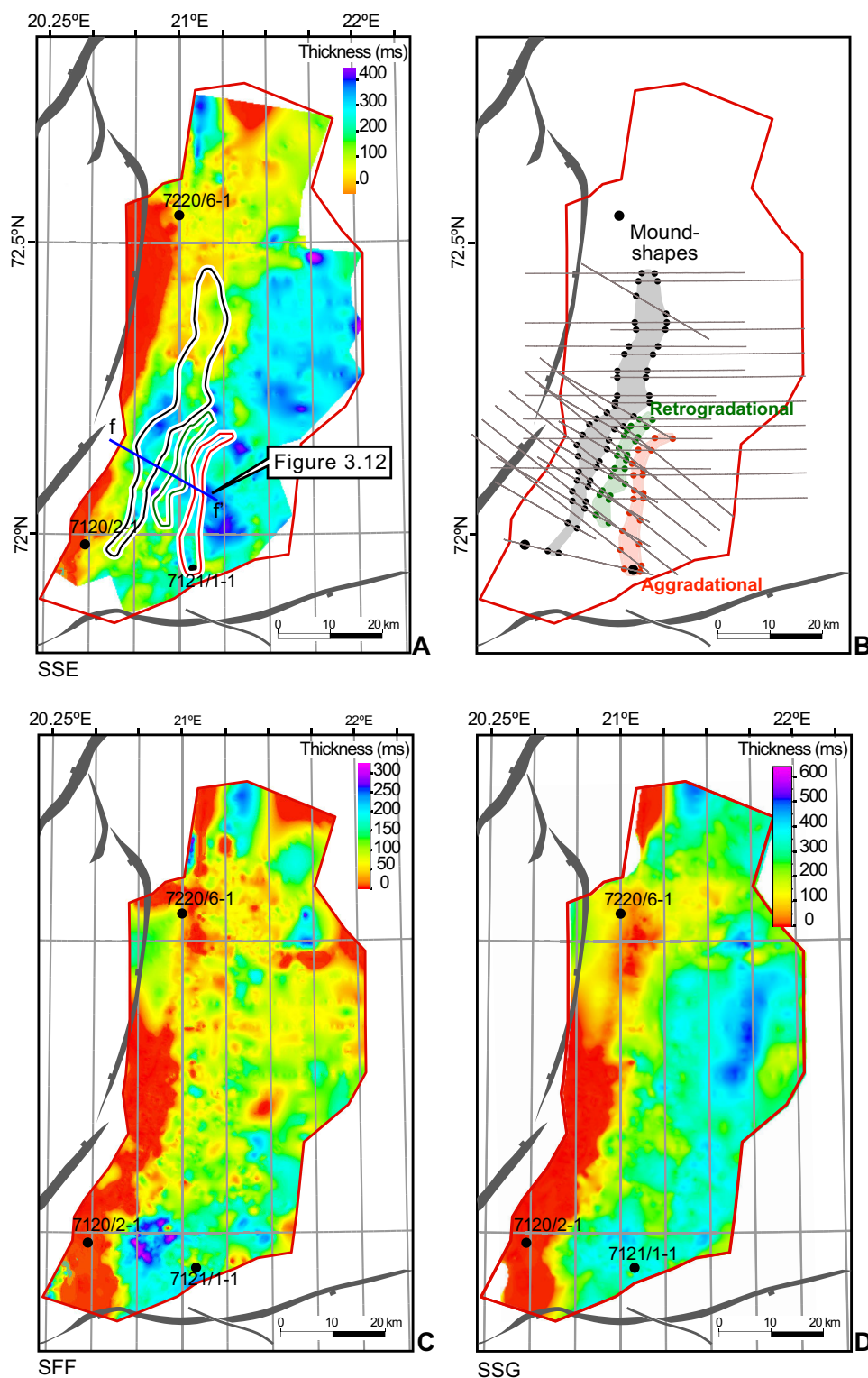
Figure 3.13 (A) Time-thickness map of SSE. The unit is traceable in all the studied area, except in areas with poor seismic resolution to the east (blank), and it reaches a time-thickness of 460 ms TWT. The spatial distribution of the reef-rimmed margin, retrogradational- and aggradational- margins are denoted with black, green and red polygons respectively. (B) Map showing the distribution of the seismic lines used to interpret the different stacking patterns. Each point represents the interception of the stacking patterns with the seismic lines. (C) Time-thickness map of SSF. The unit is thinner than the SSE and reaches time-thicknesses of 330 ms. TWT.

truncated by the seismic horizon H7 (Figure 3.12B and 3.12C). The lithofacies from well 7121/1-1 shows that the SSF is dominated by pure limestones with few argillaceous/silty and minor sands intervals (Alsgaard et al., 1987). Bryozoans and *tubiphytes* fragments are the dominant biota. They form bioherm complexes rigidified by early marine cement (Alsgaard et al., 1987). Fragments of foraminifera, brachiopods, bivalves, crinoids are also present, even if in lesser abundance (Alsgaard et al., 1987).

SSF probably deposited in deep waters below the storm wave-base (Alsgaard et al., 1987; Blendinger et al., 1997; Stemmerik et al., 1999). Such facies characterize the mid-Sakmarian–Artinskian Polarrev formations (Figure 3.3). The bioherm facies interfinger with bryozoan-crinoid rich wackestones of the Ulv Formation (Figure 3.3), which represent deposition in deep shelf environments below storm wave base, and also with the Isbjørn Formation made of crinoids-bryozoan rich packstones and grainstones indicating inner shelf environments (Larssen et al., 2002; Larssen et al., 2005) (Stemmerik et al., 1999).

According to the chronostratigraphic chart from Larssen et. al (2002, 2005), in the Loppa High the Bjarmeland Group may have deposited during the mid-late Sakmarian to the late Artinskian. In the Finnmark Platform, fusulinids biostratigraphy indicate an mid-Sakmarian to late Artinskian age (Ehrenberg et al., 2000). Onshore in the outcrops of Bjørnøya, the youngest formation (Hambergfjellet Formation) of the Bjarmeland group's equivalent is dated as late Artinskian (e.g., Nakrem, 1991). However in the geological completion report of well 7121/1-1 (Alsgaard et al., 1987) and the Norwegian Petroleum Directory (www.npd.no) the age of the lower bioherm facies (Polarrev Formation) is documented as late Gzhelian - early Asselian by biostratigraphic analysis.

7. Seismic Sequence G (SSG) – late Permian

Seismic Sequence G (SSG) is bounded by H7 and horizon 8 (H8) (Figure 3.5). The SSG correlates with the Tempelfjorden Group in the well 7121/1-1. H8 is defined in the well 7121/1-1 by a sharp peak in gamma ray values (Figure 3.4). The entire SSG is onlapping on the underlying H7 (Figure 3.5). Internally, the SSG is characterized by parallel to sub-parallel seismic reflectors of medium amplitude values that onlap and downlap the lower boundary bidirectionally (Figures 3.12A and 3.12C). The unit thickens gradually towards the eastern flank of the Loppa High reaching locally up to 500 ms TWT (Figure 3.13D).

The sedimentary deposits that characterize this sequence in well 7121/1-1 can be subdivided in two main units. The lower unit is composed of a siltstone layer rich in bryozoan, brachiopod, ostracods, crinoids, bivalves and sponge spicules fragments overlaid by a spicule-rich dolomitized limestone. The upper unit is composed of a sandy siltstone layer overlaid by a spicule-rich dolomitized limestone. The two units contains important amount of massive chert. The SSG represents deposition in a deeper environment with cooler waters compared to the environments where the underlying carbonate units formed (SSE-SSF) (Steel and Worsley, 1984; Bugge et al., 1995; Larssen et al., 2002; Samuelsberg et al., 2003; Larssen et al., 2005). Outcrop analogues of the group exist in the Bjørnøya Island and Spitsbergen in Svalbard (Steel and Worsley, 1984; Bugge et al., 1995; Larssen et al., 2002; Larssen et al., 2005). An age of Kungurian to Kazanian has been assigned to the Tempelfjorden Group in the shallow cores of the Finnmark platform (e.g., Bugge et al., 1995; Larssen et al., 2005). For the exploration wells in the Barents Sea a mid- to late- Permian age is assigned without further zonation (Alsgaard et al., 1987; Larssen et al., 2002; Larssen et al., 2005). Directly above the SSG, the sedimentary deposits are composed of shales, claystones and siltstones with increased amount of calcareous particles at the base representing a transition from marginal marine to open marine environments (Alsgaard et al.,

1987). These sedimentary deposits belong to the Havert Formation of the Sassendalen Group and are assigned an Induan age (Griesbachian) (Mørk et al., 1999) (www. npd.no).

3.5 Discussion

The development of the upper Paleozoic sedimentary deposits in the Loppa High show similar stratigraphy, facies evolution and biotic content to time-equivalent deposits of the adjacent areas in the Barents Sea, Bjørnøya, North and East Greenland, Svalbard, Sverdrup Basin in Arctic Canada and the Timan Pechora Basin (e.g., Steel and Worsley, 1984; Beauchamp, 1993; Stemmerik and Larssen, 1993; Stemmerik et al., 1995; Beauchamp and Desrochers, 1997; Stemmerik, 1997; Stemmerik et al., 1998; Stemmerik, 2000; Worsley et al., 2001). However, local tectonic processes have exercised a major control in shaping the Loppa High depositional sequences.

The Loppa High basin was established during the late Devonian-middle Carboniferous extensional period that affected the southwestern of the Barents Sea during the North Atlantic rifting (Stemmerik et al., 1991; Gudlaugsson et al., 1998; Stemmerik, 2000). The North Atlantic margin of the Pangaea was characterized by the development of half-graben structures. Whereas, the western part was subject to continental deposition, the eastern part was dominated by carbonate deposition (e.g., Bugge et al., 1995); the climate was warm and humid and these conditions prevailed until the Serpukhovian (e.g., Stemmerik, 2000).

In the Loppa High, the first deposited sediments belonging to the SSA (Figure 3.3) are of early Viséan to early Serpukhovian age (Lindstrom, 2003). This sequence as imaged from seismic data, is dissected into several sedimentary wedges of different thicknesses and lengths (Figures 3.6B and 3.6C). Similar wedge geometries, associated with the infilling of local half-graben structures and assigned to the Billefjorden Group, are also observed offshore in the central Bjarmeland Platform and the Nordkapp Basin (Larssen et al., 2002; Larssen et al., 2005) and in outcrops of the North and East Greenland, Spitsbergen and Bjørnøya (e. g., Gjelberg, 1981; Steel and Worsley, 1984; Stemmerik et al., 1991; Gudlaugsson et al., 1998; Stemmerik, 2000). However, our seismic interpretation of the SSA differs from previous interpretations of Larssen et al. (2002, 2005) and Bjørkesett (2009) in which the first seismic sequence in the Loppa High that correlated with the entire Billefjorden Group is interpreted as having a constant thickness (see Figure 5 in Larssen et al (2005)).

The sediments found in the well 7120/2-1, composed of red-colored continental breccias, conglomerates and volcanoclastics, have formed wedges by progressively filling the Carboniferous half-grabens created during the rifting. These sedimentary deposits differs somewhat from the typical continental deposits of the Billefjorden Group observed in Greenland, Spitsbergen, Bjørnøya and offshore areas of the Barents Sea. Therefore Larssen et al. (2002, 2005) assigned the sedimentary deposits of well 7120/2-1 only tentatively to the Billefjorden Group. The main differences consist in the red-colored sediments and the presence of volcanic clasts. In our opinion, the differences are due to a local control on the geographical position (east of the Caledonian mountains) and tectonic setting of the Loppa High. One of the explanation we propose for the red-colored sediments is that the may derive from the erosion of Caledonian mountain belts to the west of the Loppa High during the middle Devonian to early Carboniferous. Smelror et al. (2009) stated that the hinterlands west of the Barents Sea were gradually eroded from the middle Devonian to early Carboniferous transporting sediments to the western Barents Sea basins.

Since the type of volcanic rocks (ignimbrites) encountered in the core of well 7120/2-1 are described as volcanic debris (Gjelberg et al., 1985), we therefore hypothesize that they may also derive from the Caledonian mountains rather than deposited by nearby extension-

related syn-depositional volcanism. Hartz et al. (2002) found out that the volcanic rocks found in the Devonian Solund Basin in western Norway were Silurian in age and probably formed during the pre-collisional volcanism in the Scandinavian Caledonides. The authors suggest that the rocks reached the Solund Basin via landslides rather than deposited by syn-depositional volcanism as previously proposed. We therefore suggest that the sedimentary deposits of the SSA can be formally assigned to the Billefjorden Group.

During the Serpukhovian, the Barents Shelf experienced an uplift phase (Stemmerik et al., 1991; Stemmerik et al., 1998; Worsley, 2008). The uplift has been recorded in the Loppa High and is represented in the seismic lines by truncation of reflectors at the top of SSA (H2) (Figure 3.7B). Following the uplift, continental sedimentation dominated by conglomerates continued and gradually interfingered with marginal marine sediments dominated by shallow marine sandstones, marine siltstones and some carbonates (Stemmerik et al., 1999; Larssen et al., 2005) during the deposition of SSB (Figure 3.3). The SSB leveled out the paleotopography inherited from the underlying SSA. Stemmerik et al. (1999) suggest that the Loppa High was an easterly dipping platform area from the late Bashkirian to Moscovian. In our study, we have recognized seismic features such offlapping hanging wall derived fans in the hanging wall dipslope of the Loppa High indicating tectonic rotation during the deposition of the SSB (Figure 3.7B). Our observations suggest that by late Serpukhovian the hanging wall dipslope of the Loppa High started to rotate clockwise and an easterly dipping ramp established itself in the area (Figure 3.7B). The main controls in the resulting geometries of SSA and SSB are likely the tectonic movements caused by the extensional regime from the Viséan to the Serpukhovian and the rifting phase during the early Bashkirian respectively (Figures 3.3A and 3.3D). From the late Bashkirian the tectonic activity had gradually ceased and the deposition of the SSC was controlled by an increasing sea level and regional basin subsidence (Figures 3.3C and 3.3D). The SSC records the first marine transgression in the Loppa High from the late Bashkirian to early Moscovian characterized by the gradual change from continental to marine deposition (Stemmerik et al., 1998; Larssen et al., 2002; Larssen et al., 2005). In the SSC, the wedge geometries observed in the underlying SSA and SSB are no longer visible in the seismic lines; the thickness of the SSC increases gradually towards the east (Figures 3.8A and 3.8B). We suggest that the presence of parallel high-amplitude reflectors onlapped by low-amplitude reflectors in the SSC (Figures 3.8A and 3.8B) reflects the seismic response of the intercalation of siliciclastic and carbonate sediments overlaid by pure carbonate sediments (see 'Results and Interpretation' section). The observed seismic mounds may represent the first settlement of isolated organic build-ups in the hanging wall dip slope of the Loppa High. The observed mounds in the Loppa High may be compared to the stacked phylloid algal mounds of the upper Moscovian successions in the Bjørnøya outcrops, described by Stemmerik et al. (1998).

At the Serpukhovian-Bashkirian boundary a change from warm and humid to warm and arid climate took place in the Southern Norwegian Barents Sea (Stemmerik and Worsley, 2005b). We suggest that the SSD, which deposited during the Kasimovian, shows the seismic expression of evaporitic subbasins formed during this arid period and probably during sea level lowstands accompanied by tectonic pulse rotation of the hanging wall. Indeed, the sea level curve of Haq and Schutter (2008) shows at least three low stands cycles for the Kasimovian period (Figure 3.3C). If our interpretation of the SSD will be confirmed by well data, then the question regarding the age of the first appearance of massive evaporitic deposits in the Loppa High will be opened. Stemmerik et al (1999) reports the presence of a shallow evaporitic basin on the eastern flank of the Loppa High during the Gzhelian time. Biostratigraphic data from well 7121/1-1 (Alsgaard et al., 1987) assigns a Kasimovian age (~307.2 - 303.4 Ma) for the core material from 4525 to 4681 m, which corresponds to the

SSD interval (Figure 3.10A). Due to the characteristic observed in the sedimentary deposits (see 'Results and Interpretation' section) and the seismic facies, the SSD can be compared with the interval I interpreted in the Loppa High, Bjarmeland Platform and Nordkapp Basin by Gérard and Buhrig (1990), which comprises a regressive sequence characterized by massive salt deposition and thickening of the unit in the basinal areas.

The presence of high amplitude reflectors in the westward of well 7121/1-1 (Figure 3.10A) and the low amplitude and patchy reflectors in the structural high could represent the lateral change from stratified carbonates-evaporite cycles in the basins to irregular anhydrite-filled areas in sabkha environments of the structural highs and margins (Figures 3.10A and 3.10B). The high amplitude reflectors may also represent the acoustic impedance contrast between layers of carbonates and evaporites and the encasing units of SSD (SSC and SSE) that eventually may contain some clastic sediments. This effect has been recognized in seismic sections of the carbonate/evaporite succession of the Zechstein basin in the southern North Sea (Jenyon, 1988).

The observed updip facing slope in Figure 3.10B has been interpreted as the seismic expression of the slope formed by dissolution and removal of the evaporites. The evaporite dissolution occurred in the most proximal areas and caused the SSD unit to retreat. Jenyon (1988) has described similar updip slope geometries in the Zechstein basin of the southern North Sea. Concave features observed at the top of the SSD may be associated with evaporite-related collapse structures (Figure 3.10B). Rafaelsen et al. (2008) (Rafaelsen et al., 2008) interpreted similar features as collapses related to evaporite dissolution in the Upper Paleozoic sedimentary deposits from the Finnmark Platform. Sayago et al. (2012) inferred the presence of an extensive karstic terrain (associated with sinkholes and caves) in the western crest of the Loppa High and related it with the dissolution of carbonates and evaporites during periods of prolonged subaerial exposures.

According to all the available data for the SSD, we suggest a new evaporitic phase in the chronostratigraphic scheme presented for Larssen et al. (2002, 2005) during the Kasimovian period (Figure 3.3B).

From late Bashkirian until late Asselian the Loppa High experienced a decrease in tectonic activity and regional basin subsidence (Figure 3.3D)(Stemmerik and Worsley, 1989; Stemmerik et al., 1991; Stemmerik et al., 1999). During the same period a gradual increase in sea level is reported in the sea-level curve of Haq et al (2008) and the warm and arid climatic conditions persisted until the Asselian time (e.g., Stemmerik et al., 1999). By the late Kasimovian all the Arctic area was flooded and the central part of the north Pangaean shelf was characterized by carbonate platforms separated by deeper water basins (Stemmerik and Worsley, 2000). This period was characterized by an icehouse earth and high-frequency and high-amplitude sea-level fluctuations (Wright, 1992; Sohregan and Giles, 1999). The SSE reflects the establishment of the carbonate-dominated deposition in the Loppa High. The presence of three types of depositional styles in the SSE seems to be related with the structural position, of each developing margin, in the half-graben of the Loppa High. The interpreted rimmed margin (Figure 3.12A) in middle ramp settings is likely to have the same composition of the cored mid-Gzhelian–upper Asselian build-ups of the Finnmark platform, formed by *Palaeoaplysina*-phylloid algae and linked with arid shoreline environments (Bugge et al., 1995). The underlying topography and syn-depositional faulting most probably controlled the build-ups that are located on tectonic highs (Elvebakk et al., 2002). The presence of coeval retrogradational and aggradational stacking patterns may reflect the tectonic control on the depositional trends in the hanging wall and footwall respectively on either side of the main fault of the half-graben (Figure 3.12A and 3.12C). The retrogradational stacking patterns may reflect the retrogradation of a developing platform-margin in response to rapid subsidence in the hanging wall basin. The aggradational stacking

patterns may reflect the keep-up response of the platform-margin in the footwall, which may have experienced lower subsidence than the hanging wall. The tectonic control in the development of sedimentary successions in extensional half-graben settings has been observed and discussed by several authors in different sites (e.g., Bosence et al., 1998; Cross et al., 1998; Purser et al., 1998; Purser and Bosence, 1998; Brachert et al., 2002; Ruiz-Ortiz et al., 2004; Bosence, 2005).

In the early Sakmarian a major flooding event is recognized across the central Pangaean shelf (e.g., Stemmerik and Worsley, 2005a). This event was accompanied by a change in hydrographic regime and a change to a cooler climate (e.g., Stemmerik et al., 1999). This event was recognized both, in seismic data by Samuelsberg et al. (2003) at the base of their seismic sequence 4 in the Finnmark Platform and in well data and cores from the Barents Shelf (e.g., Larssen et al., 2002; Larssen et al., 2005). Furthermore during this period the evaporitic deposition in the basins and exposure-bounded cyclic deposition in the shelf areas ended (e.g., Ehrenberg et al., 1998a; Stemmerik, 2000; Stemmerik and Worsley, 2005a). The global changes occurring in the early Sakmarian are recorded also in the Loppa High during the deposition of the SSF. The reflector terminations with onlaps and downlaps over H6 indicate the progressive flooding over the Loppa High (Figure 3.12 C), whereas the presence of cool-water biota reflects the climatic change. The mound-shape features, observed in the SSF, ontop pre-existent topography of the SSE (Figures 3.12 A and 3.12C) are likely composed by bryozoans and *tubiphytes* resembling the bioherm complex encountered in well 7121/1-1.

Stemmerik et al. (1999) based on seismic (partially our same dataset) and well data from the well 7120/2-1 in the Loppa High suggest the growth of stratigraphically younger isolated 'keep-up' mounds towards the western updip proximal areas; to the east in the distal areas, close to the shelf margin and over structural highs, extensive stacked build-ups complexes formed by bryozoan, *tubiphytes* and echinoderms are described. All of the large build-ups structures seem to have risen during the early Sakmarian flooding, however isolated mound-shape structures were already observed in the SSC.

In general, the build-ups observed in the SSE and SSF correlates and confirm the observations of several authors regarding the development of build-up complexes in the Loppa High. Gérard and Buhrig (1990) recognized from the seismic data extensive ridges of composite stacked buildups formed during the Carboniferous–Permian and resulted in the rimming of the Barents shelf. The underlying topography and syn-depositional faulting controlled the location of the build-up complexes (Elvebakk et al., 2002; Samuelsberg et al., 2003). In the late Sakmarian–Artinskian an uplift of the shelf margins and structural highs across the central Pangaea shelf took place (Worsley et al., 2001; Stemmerik and Worsley, 2005a). This uplift event likely affected also the Loppa High as suggested by Stemmerik et al. (1999) and may have exposed and truncated the underlying carbonates, triggering the first karstic episodes in the crest of the Loppa High (Figure 3.14 C).

Although in the Loppa High there is an uncertainty in the age of the SSF in well 7121/1-1 several authors have assigned an upper Sakmarian–Artinskian age (lowermost Kungurian?) to the sedimentary successions equivalent to the Bjarmeland Group in North Greenland and Sverdrup Basin (Stemmerik et al., 1996; Beauchamp et al., 2001). In the offshore wells of the Finnmark Platform a mid-Sakmarian to late Artinskian age is assigned to the group (Ehrenberg et al., 2000). We suggest that the SSF ranges from mid-Sakmarian to late Artinskian in age, taking into consideration the development of the Bjarmeland Group in the Barents Sea (Figure 3.3A) (e.g., Larssen et al., 2002; Larssen et al., 2005; Stemmerik and Worsley, 2005b).

The chronostratigraphic scheme from Larssen et al. (2002, 2005) describes a hiatus spanning the whole Kungurian, which separates the Bjarmeland Group from the overlying

Tempelfjorden Group (Figure 3.3A). In the seismic data, the limit between the SSF (Bjarmeland Group) and the overlying SSG (Tempelfjorden Group) is marked by an unconformity defined by reflectors truncation at the top of the SSF and onlap terminations above it (Figure 3.12C), which may be the seismic expression of the Kungurian hiatus. The establishment of the SSG reflects a significant change in the sedimentary deposition in the Loppa High. The gradual increase of siliceous spiculites, cherts, fine-grained sedimentation and decrease in carbonate deposition found in the well 7121/1-1 has been also observed in the wells of the Hammerfest Basin, Bjarmeland Platform and Finnmark Platform (Ehrenberg et al., 1998a; Larssen et al., 2002; Samuelsberg et al., 2003; Larssen et al., 2005). The base of the SSG correlates with the top of the unit L-8 of Ehrenberg et al. (1998), which has been interpreted as a drowning unconformity *sensu* Schlager (1989), based on the rapid termination of the carbonate sedimentation and a long period of non-deposition. Stemmerik et al. (1996) suggest that the latest Kungurian-Kazanian sequence in the western Barents Sea (equivalent to the Tempelfjorden Group in the Loppa High and our SSG) is separated from the underlying sediments by a subaerial exposure surface in the platform areas. We consider that the limit between SSF and SSG may be a combination of subaerial exposure in the uplifted zones and coeval drowning in the subsiding areas. For example, Prosser (1993) has described this phenomenon in several examples of half-graben rotating fault blocks.

The change in biota and type of sedimentation between SSF and SSG has been associated with an increasing climatic cooling and/or changes in oceanic circulation patterns that introduced cooler waters in the previously warm-water bathed shelves of the arctic areas during the late Permian (e.g., Beauchamp, 1994; Beauchamp and Desrochers, 1997; Ehrenberg et al., 1998a; Beauchamp and Baud, 2002). The upper boundary of the SSG correlates with the top of unit L-9 of Ehrenberg et al. (1998). The authors have considered this boundary also as a drowning unconformity based on the abrupt termination of siliciclastic biogenic production, a change towards siliciclastic-dominated sedimentation and the overlying donwlapping stratal geometries. However, because the poor paleontological control at the top of L-9, the same authors does not rule out the possibility of a subaerial exposure surface representing a major hiatus between the late Permian and the overlying Triassic sediments. In the figure 3.5B the updip portion from sequences SSC to SSG shows truncation most likely occurred during the prolonged Permian-Triassic unconformity.

Paleogeographic evolution of the Loppa High

The reconstructed paleogeography from the Loppa High is summarized in four key stages of evolution:

• From the Viséan to middle Moscovian (Figure 3.14A) the map shows the different sedimentary depositional environment reflected in the analysis from SSA, SSB and SSC. The sea gradually transgressed the most proximal environments characterized by alluvial, fluvial and probably lacustrine deposits. Marine deposits with some organic build-ups were laid down as the transgression advanced from the east.

• The Kasimovian was a time of restricted environmental conditions as inferred from the analysis of SSD (Figure 3.14B). Warm and arid climate, sea level-stand and tectonic uplift have contributed to the isolation of different areas triggering the accumulation of evaporites in shallow and deep environments.

•   In the Gzhelian-late Artinskian (early Kungurian?) period occurred the deposition of SSE and SSF (Figure 3.14C). This period was characterized by biogenic carbonate deposition. The late Moscovian to late Asselian warm-water carbonates formed contemporaneous margins with different depositional styles. Tectonic controls in extensional half-graben settings were likely responsible of the resulting geometries. The mid-Sakmarian to late Artinskian cool-water carbonates formed stacked build-ups ontop pre-existing structural highs and in distal basinal areas. The late Sakmarian–Artinskian uplift may have exposed the carbonates units triggering the first karstic episodes in the Loppa High.

•   In the late Permian (Kungurian to the Urzhumian) the deposition of the SSG took place (Figure 3.14D). This time was characterized by colder climates, gradual deepening and the change towards silica-dominated biogenic production dominated by sponge spicules. Fine-grained siliciclastics, silicified skeletal limestones and chert dominated the sedimentary deposits. Exposure of the carbonates at the western crest of the Loppa High has produced a wide karsted terrain at the top of the sedimentary units.

VISEAN - MIDDLE MOSCOVIAN

Main Uplift Axis

Basin Filling

Siliciclastic Influx

AOE

A

KASIMOVIAN

Exposed shelf

Main Uplift Axis

Coastal /Sabkha

Marine carbonate /evaporites

?

?

?

Deep evaporite sub-basins

I

GZHELIAN - LATE ARTINSKIAN

IR/Platform   MR   OR

Rimmed margin

Retrograding margin

Aggrading margin

Intramargins seaway

B

0   10   20 km

C

LATE PERMIAN

Basin

Exposed shelf

I
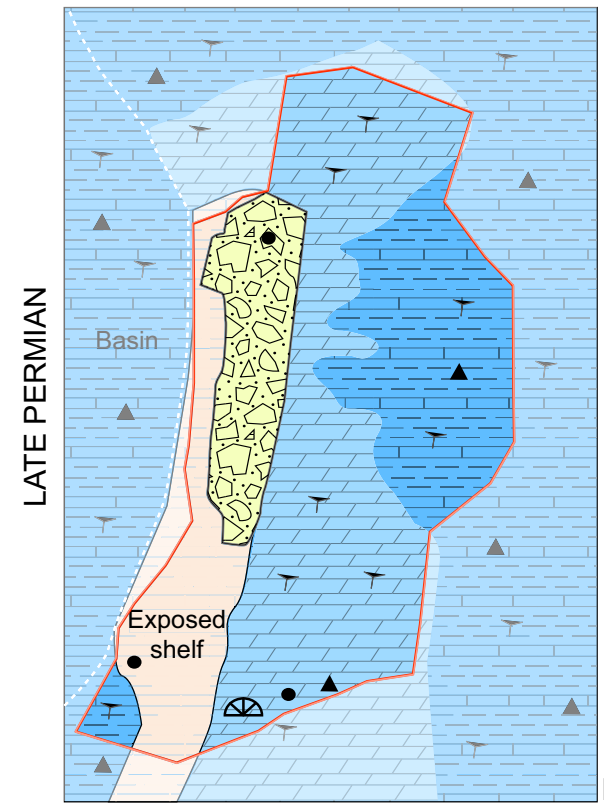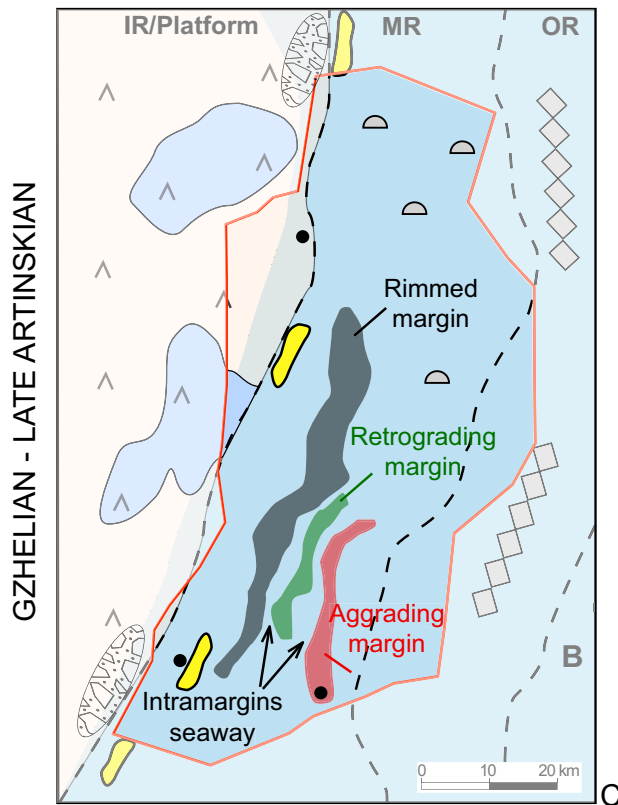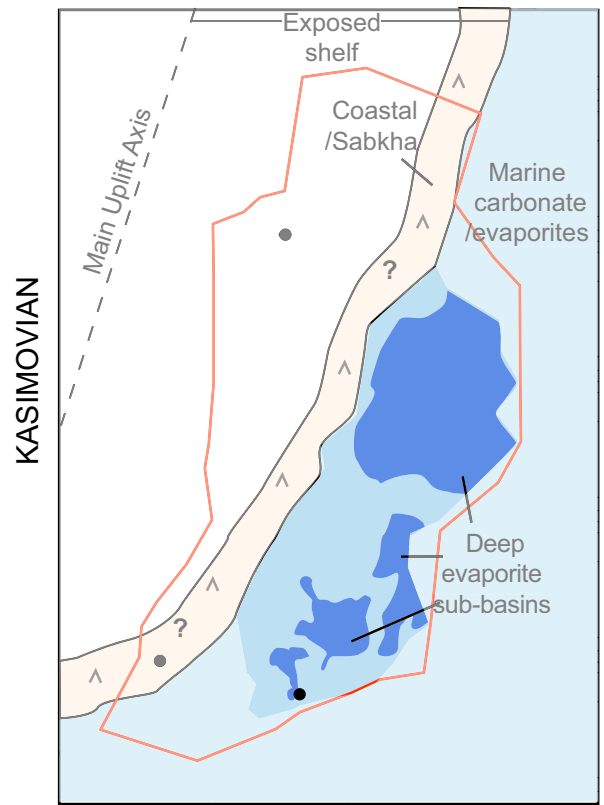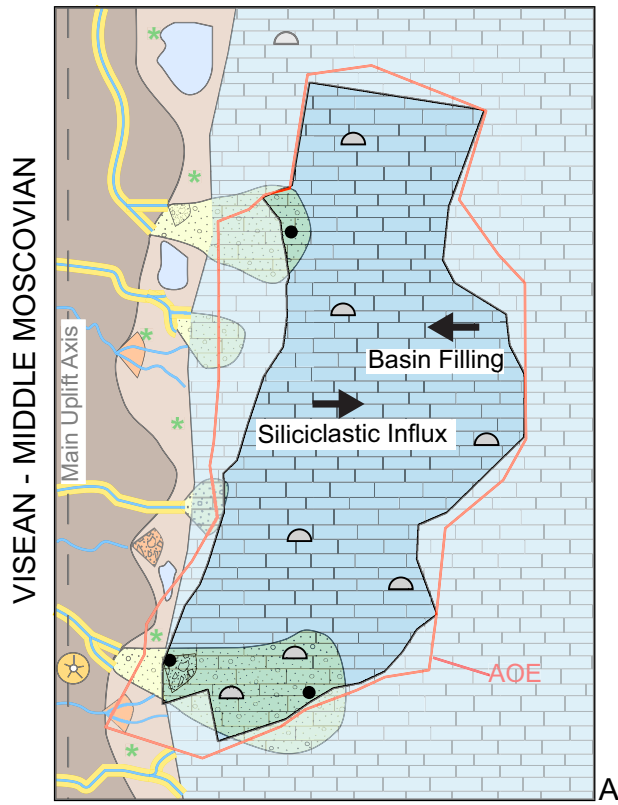
Figure 3.14: (A) Palaeogeographic reconstruction from Viséan to middle Moscovian represented by sequences SSA, SSB and SSC. The development of the sequences starts with continental sedimentation dominated by alluvial fans, braided rivers with presence of volcanoclastics in the SSA, overlie by marginal marine sedimentation dominated by subaqueous debris flows of alluvial- and delta- fans of SSB, turning upwards to mixed siliciclastic–carbonate sedimentation of the SSC as result of the first marine transgression in the Loppa High. (B) Palaeogeographic reconstruction within the Kasimovian with a sea-level lowstand and exposure of the shelf represented in SSD. A coastal environment with marginal-marine sabkha is interpreted at the shoreline position and in the uplifted basinal highs. The fault-controlled subbasins may have formed hyper-saline environments with thick accumulation of evaporites. (C) Palaeogeographic reconstruction from the Gzhelian–late Artinskian representing the development of the SSE and SSF. The establishment of three contemporaneous margins in middle ramp settings (reef-rimmed, backstepped, aggraded) is inferred from the seismic geometries and well data (see text). The coeval asymmetric patterns reflect the tectonic control in extensional half-graben settings. (D) Palaeogeographic reconstruction from the late Permian represented by the SSG. Two different sectors are represented in the map; the light blue area corresponds to the environments dominated by carbonates deposition and spicules. The dark blue represent the environments with predominant deposition of cherty carbonates and fine-grained deposits as well with spicule fauna. The extent of the karstified areas as mapped by Sayago et al. (2012) is represented in the map.

3.6 Conclusions

The integration of 2D/3D seismic data combined with well and core data have supported the seismic stratigraphic analysis of the upper Paleozoic sedimentary units in the half-graben of the Loppa High. A total of seven seismic sequences (SSA to SSG), separated by seismic discontinuities, have been interpreted and they represent third- to second-order sedimentary cycles. The time-thickness maps (isochrones) for each sequence were constructed and allowed depicting the changes in the geometries and depocenters trough time and space. The geometries of the seismic sequences together with the sedimentary facies permitted reconstructing the paleogeography of each key stage of development during the late Paleozoic in the Loppa High.

The Loppa High is a half-graben structure formed during the late Paleozoic extensional period that affected the northern margin of Pangaea. Continuous rotation of the Loppa High hanging wall led to the development of wedge-shaped depositional sequences. Our results suggest that tectonic rotation and uplift are the principal controls in the overall 3-D morphology of the seismic sequences in the Loppa High. Global sea-level oscillations and climate changes have modified the biotic evolution and were responsible of the small-scale features inside each sequence. The sedimentation type varies from clastic-dominated (SSA and SSB) to mixed siliciclastic-carbonates (SSC), to evaporites-dominated (SSD), to carbonated-dominated (SSE and SSF). A final phase of drowning and demise of the carbonates factories is characterized by the presence of siliceous spiculites, cherts and fine-grained sedimentation (SSG). The seismic sequences were identified and mapped by observing the geometrical configuration of reflections and their bounding discontinuities; they comprise second- and third-order stratigraphic cycles according to the available age-control.

Detailed review of the available age-control along with the seismic geometries allowed questioning the age of the first evaporitic deposits in the Loppa High. Furthermore, the interpretation of synchronous rimmed-, retrograding- and aggrading- margins for the same sequence reveal the tectonic control in the development of the sedimentary sequences in the Loppa High.

This study complements previous works related with the tectono-sedimentary evolution of the western Barents Sea, and represents the first detailed seismic stratigraphic

analysis with particular focus in the sedimentary succession ranging from early Carboniferous to late Permian in the Loppa High half-graben structure.

4

FACIES AND SEISMIC ANALYSIS FROM THE LATE CARBONIFEROUS–EARLY PERMIAN FINNMARK CARBONATE PLATFORM (SOUTHERN NORWEGIAN BARENTS SEA): A NEW ASSESSMENT OF THE CARBONATE FACTORIES AND DEPOSITIONAL GEOMETRIES

Di Lucia M., Sayago J., Frijia G., Mutti M., Cotti A., Sitta A.

Submitted to the <u>American Association of Petroleum Geologist</u>, *AAPG Bulletin*

Abstract

The late Palaeozoic carbonate platform of the Finnmark Platform in the Norwegian Barents Sea is a system developed under shifting paleoclimatic and paleoceanographic conditions. Detailed core analysis from the explorations wells 7128/4-1 and 7128/6-1, combined with 2D seismic sections and previous studies in the area have allowed a re-evaluation of the depositional scenarios of the main lithostratigraphic units (Ørn and Isbjørn Formations). Nine lithofacies associations have been described and interpreted in terms of their depositional environments. During the mid-Sakmarian two major changes are observed between the Ørn and Isbjørn Formations: (1) the variation in the type of the carbonate factories and (2) the change in platform morphology. The changes in the types carbonate factories were controlled by a number of factors and are expressed by changes in biota, facies associations and depositional geometries. The morphological variation has been associated with a change from a distally steepened ramp to a homoclinal ramp. Our results may help to improve the assessment of future evaluations in the Finnmark Platform area, in terms of reservoir properties, which are strictly associated with the depositional styles and their post-depositional modifications.

4.1 Introduction

The growth history of a carbonate depositional system, its facies heterogeneity and external architecture, strictly depend on the interaction of numerous biological, chemical and physical factors, acting at different temporal and spatial scales (Read, 1985; Tucker, 1990; James, 1997; Wright and Burchette, 1996, 1998; Pomar, 2001; Mutti and Hallock, 2003; Schlager, 2003; Bosence, 2005; Pomar and Kendall, 2007). Decades of research on modern and ancient examples have highlighted how sensitive the carbonate platforms are and how difficult is to interpret their evolution considering all the above-mentioned factors. This is particularly true for the deeply buried depositional systems for which temporal and spatial scales are less constrained and the primary features are often strongly altered by the diagenetic/structural overprint. A comprehensive understanding of how carbonate platforms develop and change across consecutive phases of their growing history, represents a crucial

achievement when economical interests linked to hydrocarbon originate, since carbonate rocks host more than half of the global hydrocarbon productive reserves. In the last three decades, numerous studies led to a significant step forward in the understanding of the Arctic regional geology, associated with the increasing offshore exploration in the area (Stemmerik and Worsley, 1989; Cecchi, 1993; Lønøy, 1988; Beauchamp and Desrochers, 1997; Ehrenberg et al., 1998a; Stemmerik and Worsley, 2005; Worsley, 2006; Larssen et al., 2005; Colpaert et al., 2007; Rafaelsen et al., 2008). One of the upper Paleozoic sedimentary successions attracting most of the interests of the oil industry is represented by the Finnmark Platform, a buried depositional system of the southern Norwegian Barents Sea (Figure 4.1A), developing as part of the Arctic epicontinental shelf (Bugge et al., 1995; Stemmerik, 2000; Larssen et al., 2002; Worsley, 2006) and dominated by carbonate deposition (for ~27.5 Ma) during the late Carboniferous–early Permian (Gzhelian-Artinskian) (Stemmerik, 1997; Ehrenberg et al., 1998a; Larssen et al., 2002). Among the upper Paleozoic deposits of this area, the stratigraphic interval corresponding to the Gipsdalen Group is considered as having a high reservoir potential (Ehrenberg, 2004; Stemmerik and Worsley, 2005 and references therein) and has been lately object of renewed interest for E&P purposes to assess future possible plays. At the same time, the late Paleozoic Finnmark Platform represents a notable example of how the interplay of simultaneous mechanisms of diverse nature, can influence the long-term and large-scale depositional evolution of a carbonate system.

The depositional geometries of the Finnmark Platform carbonates were influenced by the preexistent NE-SW fault-controlled rift topography of the underlying Billefjorden Group –Mississippian   clastic sediments– affected by the Devonian-Serpukhovian Atlantic rift (Stemmerik, 2000; Worsley, 2006). Moreover, during the late Carboniferous-early Permian, the Arctic shelf development and its sediment accumulation patterns were influenced by the following major climatic-oceanographic changes: i) the northward drifting of the Eurasian plate, from tropical (~20°) to temperate (~45°) latitudes, with a rate of about 2-3 mm/y (Scotese and McKerrow, 1990; Scotese and Langford, 1995; Golonka and Ford, 2000;) and persistent dry climatic conditions (Stemmerik, 2000). ii) The presence of the Gondwanan icecaps, whose expansions and retreats phases controlled the cyclicity and magnitude of the sea-level fluctuations (Stemmerik, 2008 and references therein). iii) The stepwise closure of the Eastern European gateway connecting the Arctic regions with the warmer tropical Paleo-Tethys, influencing successive oceanic circulation patterns (Reid et al., 2007 and references therein).

On the Finnmark Platform, the most remarkable sedimentary expression of such paleoclimatic and paleoceanographic changes took place during the middle Sakmarian and records a major change in carbonate factories (Steel and Worsley, 1984; Stemmerik, 1997; Ehrenberg et al., 1998a; Larssen et al., 2002). Exploration wells and shallow cores within the proximal Finnmark domain, reveal a shift in carbonate production style and accumulation between two major (2nd order) depositional phases of platform development, represented by the photozoan-dominated (*sensu* James, 1997) sequences of the Gipsdalen Group (Ørn Formation) and the overlying heterozoan carbonates (Stemmerik, 1997; Ehrenberg et al., 1998a; Larssen et al., 2002) of the Bjarmeland Group (Isbjørn Formation).

Although several core- and seismic-based studies have been published so far it is still not fully clear how the Finnmark Platform evolved in terms of change in geometry and how the
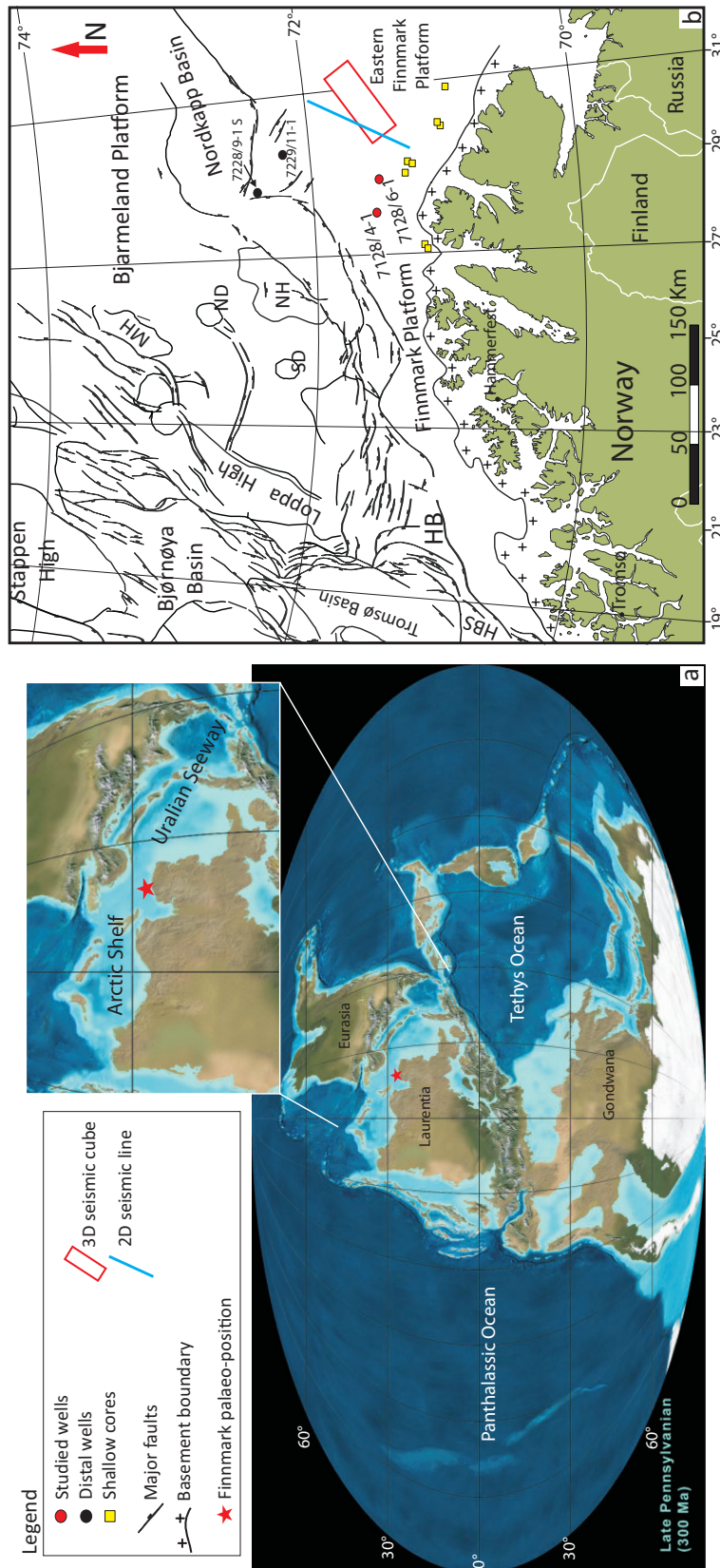
Figure 4.1. a) Late Pennsylvanian (Ghzelian stage, 300 Ma) palaeoceanographic map (from http://cpgeosystems.com/globaltext2.html) and paleo-position of the Finnmark Platform domain within the Arctic epicontinental shelf. b) Structural/depositional domains of the Norwegian Barents Sea. The Finnmark Platform, object of this study, is bordered by the Norwegian land to the south and by the Nordkapp Basin to the north. The map shows the position of the four exploration wells reaching the Paleozoic strata and the three shallow cores mentioned in the text. The position of the selected 2D seismic line ST9715-213 across the NE-SW platform profile (Figure 4.8) is shown, together with the 3D cube ST9802. HB: Hammerfest Basin; HBS: Harstad Basin;NH: Norsel High; SD: Samson Dome; ND Nordvang Dome. Modified after Samuelsberg et al. (2003).

above-mentioned early Permian scenario influenced changes in sediment accumulation type. Therefore, for this study, we present a detailed core analysis across the Asselian-Artinskian Ørn and Isbjørn Formations of the wells 7128/6-1 and 7128/4-1 (Figure 4.1B). Additionally, our study is supported by 2D seismic interpretation across the profile of the eastern Finnmark domain, to better assess the impact that the abovementioned mechanisms had on the long-term platform evolution and to extend the understanding of its large-scale depositional geometries.

4.2 Geological evolution and lithostratigraphy

During the Late Paleozoic, the Arctic shelf lied in the northern margin of the Laurentia super continent (Figure 4.1A). It was extended from the Arctic Canada across the North Greenland, Svalbard and the Barents Sea, to the Arctic Russia (Beauchamp and Desrochers, 1997, Larssen et al., 2002; Stemmerik and Worsley, 2005; Worsley, 2006). In particular, the late Paleozoic structural style of the Barents Sea domain derives from Caledonian (NE–SW oriented), and in less extent Baikalian (NW–SE oriented) orogenic lineaments affecting the Pre-Devonian basement (Gabrielsen, 1990; Gudlausson et al., 1998; Samuelsberg et al., 2003). The late Devonian–early Carboniferous separation of the North America from the Fennoscandian craton resulted in a rift-controlled paleo-topography and development of extensional tectono-stratigraphic provinces dominated by wide shelves (Finnmark and Bjarmeland Platforms), relatively deep basins (Hammerfest, Nordkapp, Bjørnøya, Tromsø Basins), and isolated structural features (Loppa and Stappen highs) (Larssen et al., 2002) (Figure 4.1B).

At present, the late Paleozoic Finnmark Platform is a buried monocline (gradient of ~2° at the top Permian level, Ehrenberg, 2004) grading northward to the rift-controlled Nordkapp (NE side) and Hammerfest (NW side) basins (Figure 4.1B). To the south, the Finnmark Platform is delimited by the Norwegian land (the Fennoscandian craton) and truncated by an angular unconformity. To the west, the Ringvassøy-Loppa fault complex delineates it, whereas to the east, it grades towards the Timan-Pechora Basin (Gudlaugsson et al., 1998; Larssen et al., 2002)

The sedimentary record of the Finnmark Platform starts from the early Carboniferous. After Larssen et al. (2002), its late Paleozoic stratigraphic evolution has been associated to four distinct depositional phases, corresponding to four lithostratigraphic units: the Billefjorden, Gipsdalen, Bjarmeland and Tempelfjorden Groups (Figure 4.2). Starting from the early Carboniferous (early Viséan), the rift-related basement morphologies of the Finnmark area have been gradually filled by continental to marginal marine siliciclastic of the Billefjorden Group (Soldogg, Tettegras and Blaererot formations, Figure 4.2), deposited under tropical-humid climatic conditions as testified by the common presence of coaly horizons (Larssen et al., 2002). A regional middle Serpukhovian–earliest Bashkirian uplift-related unconformity, associated with reactivation of the underlying structural lineaments of the basement, separates the Billefjorden Group deposits from the overlying early Bashkirian–early Sakmarian Gipsdalen Group. The onset of the Gipsdalen Group deposition is characterized by a shift in the tectonic style, with a progressive reduction of the tectonic activity and increasing subsidence (Gudlaugsson et al., 1998; Larssen et al., 2002; Worsley, 2006). Moreover, in this phase took place a significative paleoclimatic transition from tropical humid to overall semi-arid to arid conditions, (Stemmerik et al., 2000; Worsley, 2006) testified by a gradual increase of shallow and basinal evaporitic deposits. Moreover, the Gipsdalen Group was deposited under high- frequency (100 k.y.) and amplitude (> 50 m)

glacio-eustatic sea-level fluctuations reflecting the Gondwanan icecaps activity (Stemmerik et al. 2008, and references therein; Koch and Frank, 2011). The group
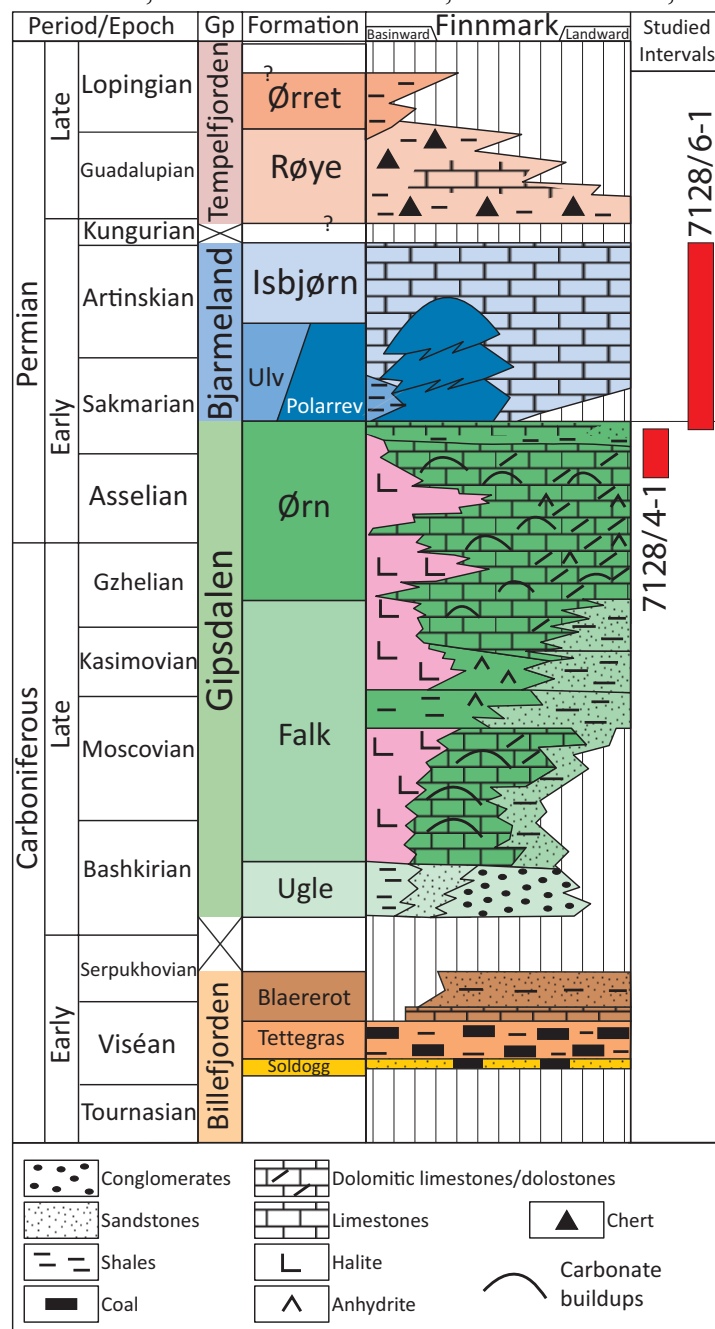
Figure 4.2 Upper Palaeozoic lithostratigraphic units of the Southern Norwegian Barents Sea and their relationship across the Finnmark Platform profile (Modified after Larssen et al., 2005). The stratigraphic position of the studied interval of the Gipsdalen Group (Ørn Formation) and the Bjarmeland Group (Isbjørn Formation) from the wells 7128/6-1 and 7128/4-1 is shown.

comprises three formations reflecting distinct sub-phases of the Finnmark Platform evolution. The basal interval is associated with the deposition of continental siliciclastics of the Ugle Formation, followed by a widely recognized Bashkirian–Moscovian transgression associated with tectonic subsidence that led to the deposition of the Falk Formation. The latter marks a stepwise shift to mixed continental to shallow marine siliciclastic and carbonates, and deeper subtidal evaporites (Figure 4.2) (Larssen et al., 2005). Starting from the Gzhelian, the proximal areas of the Finnmark domain were mostly dominated by peritidal to subtidal photozoan limestones/dolostones and minor sabkha evaporites of the Ørn Formation, with periodic occurrence of transgressive heterozoan carbonates. Silty mudstones, gypsum and halite were deposited in the basinal areas (Figure 4.2) (Larssen et al., 2005; Stemmerik, 2008). The early Sakmarian marks an important regional transition associated with a major

melting phase of the Gondwanan ice (Stemmerik, 2008; Koch and Frank, 2011). This led to the termination of the glacio-eustacy and marked the depositional transition between the Gipsdalen Group and the overlying transgressive Bjarmeland Group, entirely dominated by heterozoan carbonates.

The Bjarmeland Group is characterized by three laterally transitional formations (Figure 4.2). The shallowest platform environments show crinoidal-bryozoan carbonates of the Isbjørn Formation whereas the deeper distal shelf areas hosted muddy carbonates and shales of the Ulv Formation (Larssen et al., 2002). Outer environments were also site of deposition of large buildups complexes of the Polarrev Formation, dominated by bryozoan-*Tubiphytes* and microbial-stromatactis boundstones (Blendinger et al., 1997; Stemmerik, 1997).

From the early Kungurian?–Tatarian?, further northward drifting and cooling, associated with drowning and termination of the temperate carbonate factory on the shelves areas of the Barents Sea, led to the deposition of the outer platform silica- and clastic-dominated Tempelfjorden Group (Figure 4.2) (Stemmerik, 1997; Beauchamp and Desrochers, 1997; Ehrenberg et al., 1998a; Ehrenberg et al., 2001), composed by the Røye Formation and the Ørret Formation, the latter absent on most of the Finnmark Platform (Larssen et al., 2002).

4.3 Material and methods

4.3.1 Stratigraphic dataset and methods

For this study, we described the late Asselian-late Artinskian stratigraphic cored intervals from the wells 7128/6-1 and 7128/4-1, both placed in the central-eastern area of the Finnmark Platform domain at a distance of 26.1 km from each other (Figure 4.1B). The standard core description has been performed at cm- to dm-scale and followed by the semi-quantitative microfacies analysis on 154 thin sections, mainly focused on the identification of the carbonate/clastic textures, biological content and sedimentary structures. The well depth is given in measured depth (MD) below kelly bushing.

The most complete upper Paleozoic stratigraphic archive from the subsurface of the Norwegian Barents Sea has been recovered (472.4 m of cores/901 m of drilled interval) from the exploration well 7128/6-1 (Conoco, 1991). It represents the type section for the Ørn (215.3 m-thick), the overlying Isbjørn (89.4 m-thick) and Røye formations (117.4 m-thick). The 51.7 m-thick sequence recovered from the exploration well 7128/4-1 (Statoil, 1993), covers the late Asselian-early Sakmarian uppermost interval of the Ørn Formation. A precise stratigraphic correlation between the 7128/4-1 and 7128/6-1 sequences is ensured by the integration of facies analysis, gamma ray log trends and correlative seismic stratigraphic horizons (Figure 4.3) (Ehrenberg et al., 1998a; Larssen et al., 2002; Colpaert et al., 2007).

Across the entire late Carboniferous-Permian interval of the well 7128/6-1, Ehrenberg et al. (1998a) defined two second-order and seven third-order depositional sequences (S-1 to S-7) according to the terminology of Goldhammer et al. (1991) bounded by major sequence boundaries (SB) and maximum flooding surfaces (MFS) (Figure 4.3). Nine lithostratigraphic units (L1-L9) have also been defined on the basis of major vertical facies changes. Units L1-L7 are ascribable to the Gipsdalen Group, whereas the units L8 unit L9 respectively to the Bjarmeland and Tempelfjorden Groups (Figure 4.3). Fusulinid-based biostratigraphy across the well 7128/6-1 suggests a late Gzhelian-early Sakmarian age for the Ørn Formation and a late
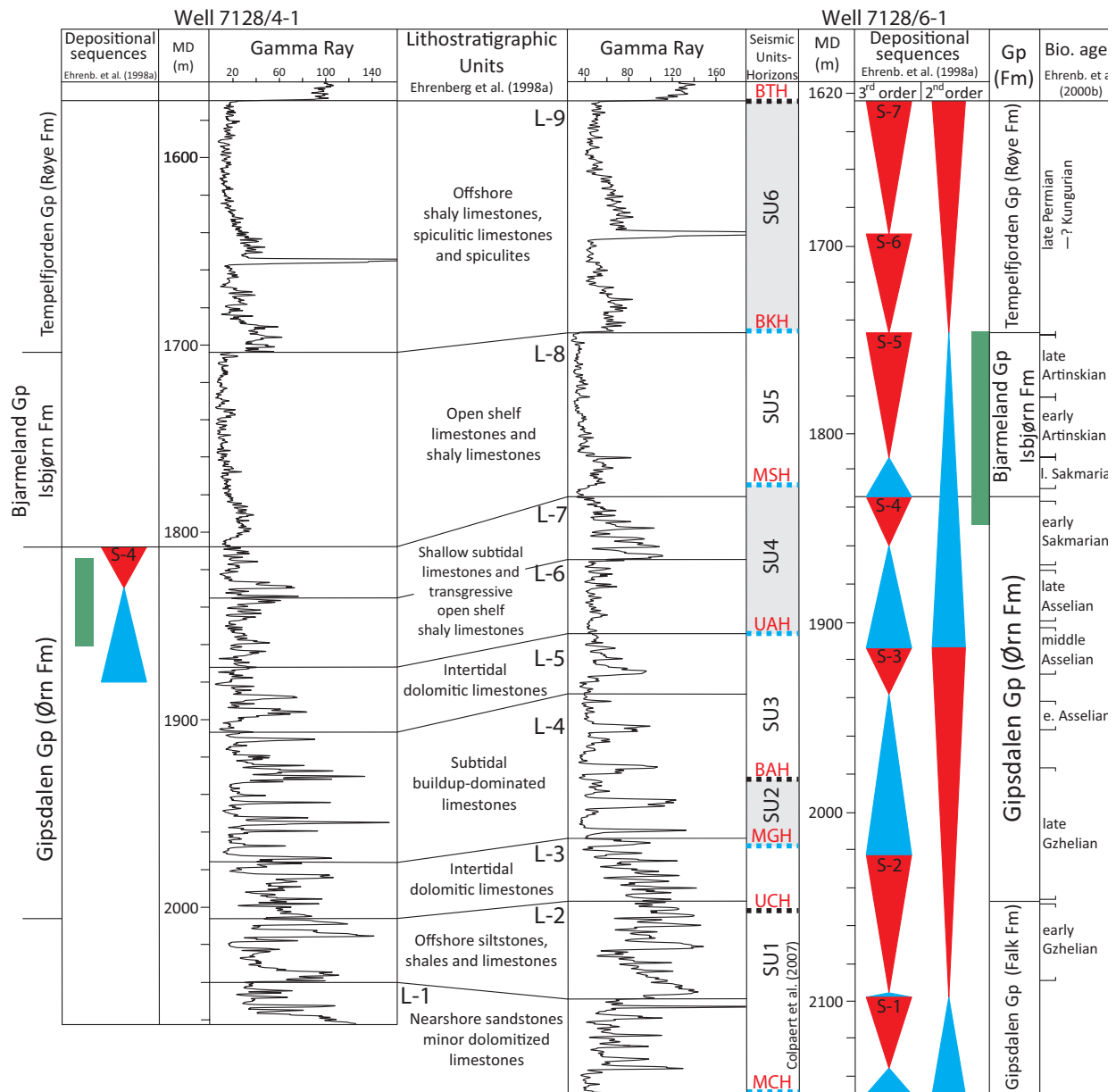
Figure 4.3 Stratigraphic correlation between the wells 7128/6-1 and 7128/4-1 across the Gipsdalen, Bjarmeland and Tempelfjorden Groups. The scheme is based on the integration of GR profiles, 2nd and 3rd order (S-1–S-7) depositional sequences and lithostratigraphic units (L1–L-9) (Ehrenberg et al., 1998a), fusulinid-based biostratigraphy (Ehrenberg et al., 2000b). Seismic horizons (dashed lines) and related seismic units (SU1–SU6) across the well 7128/6-1 from Colpaert et al. (2007) are shown. MCH: middle Carboniferous Horizon UCH: upper Carboniferous Horizon, MGH: middle Gzhelian Horizon, BAH: base Asselian Horizon, UAH: upper Asselian Horizon, MSH: middle Sakmarian Horizon, BKH: base Kungurian Horizon, BKH: base Tatarian Horizon. The blue-colored horizons are the ones considered for this study (MCH, MGH, UAH, MSH, and BKH). Dark green segments correspond to the intervals investigated for this study.

68

69

Figure 4.4 Logs showing the main lithological, stratigraphic and sedimentological features of the studied Asselian–Artinskian intervals from the wells 7128/4-1 (log 1) and 7128/6-1 (logs 2 and 3). For an easier reading of the figure, the stratigraphic relationship between the logs is also shown in the yellowish quadrangle. Refer to the text for the explanation of the lithofacies associations (LA). Textures/lithologies: c: clay; m/e: mudstone/evaporite; w: wackestone; fs: fine sandstone; p: packstone; g: grainstone; b: boundstone.

Sakmarian-late Artinskian age for the Isbjørn Formation (Ehrenberg et al., 2000b and references therein).

The studied segment from the well 7128/6-1 has a thickness of 104.6 meters (1850-1745.4 m). It covers the topmost part of the Ørn Formation (15.3 m) and the entire overlying Isbjørn Formation (89.4 m) (Figures 4.3 and 4.4). The Ørn Formation segment (1850-1834.7 m) corresponds to the early Sakmarian uppermost portion of the sequence S-4 of Ehrenberg et al. (1998a) (upper part of the lithostratigraphic unit L-7, Figure 4.3). The Isbjørn Formation segment (1834.7-1746 m) covers the entire late Sakmarian-late Artinskian third-order sequence S-5 of Ehrenberg et al. (1998a) (lithostratigraphic unit L-8). The sequence deepens upward, with the Maximum Flooding Surface (MFS) placed at 1813 m, and then it shallows up until the boundary with the Tempelfjorden Group (Figures 4.3 and 4.4).

The studied interval (1865.7-1814 m) of the well 7128/4-1 covers most of the third-order depositional sequence S-4 of Ehrenberg et al. (1998a) (lithostratigraphic units L6-L7). The sequence marks a deepening-up trend with a MFS at 1837.7 m, followed by shallowing up to the end of the cored interval (Figures 4.3 and 4.4). For a better understanding of the depositional-sedimentological features of the Finnmark areas, we also used other available Paleozoic stratigraphic data, including cores from the exploration wells 7228/9-1S (Norsk Hydro, 1989) and 7229/11-1 (Shell, 1993), located in a more distal position, and the shallow cores 7128/12-U-01, 7129/10-U-01 and 7030/03-U-01 (IKU Petroleum Research, 1987-1988) drilled in a landward position of the studied wells, closer to the Norwegian coast (Figure 4.1B).

4.3.2 Seismic dataset and stratigraphy

The 2D seismic line 213 from the survey ST9715 has been used for seismic interpretation (Figure 4.1B). The line is 97 km-long and oriented NE-SW covering a proximal-distal transect of the eastern Finnmark Platform. The frequency values of the 2D line range from 20 to 50 Hz, with a dominant frequency of 25 Hz. The internal velocities of the carbonate interval range from 4000 to 6000 m/s, therefore the vertical seismic resolution fluctuates between 40 to 60 m (according to the dominant frequency). Seismic vertical scales are given in two-way travel time TWT (in seconds). The seismic-well tie was done by creating synthetic seismograms that allowed identification of main reflectors in the wells 7128/4-1 and 7128/6-1. Reflector continuity and key stratal terminations have been considered to identify and mark the selected seismic and to develop a seismic sequence stratigraphic model along the 2D line (Figure 4.10B, C). Different seismic attributes (i.e. frequency band filter, variance, gradient magnitude) were applied to highlight the stratal terminations and eventual major structural discontinuities. To facilitate comparisons with previous works based on the same dataset, we followed for the interpreted seismic horizons the nomenclature adopted by Colpaert et al. (2007). The middle Carboniferous Horizon (MCH) marks the boundary between the Billefjorden and the Gipsdalen Groups (Figure 4.3) and reflects the middle Serpukhovian–earliest Bashkirian major uplift and erosional event. The reflector can be well recognized across the platform since it shows evident reflectors truncation of the underlying clastic reflectors (Figure 4.10B, C). MCH delimitates the base of

the seismic unit SU1 of Colpaert et al. (2007) (Figure 4.3). Upwards, the middle Gzhelian Horizon (MGH) has been traced. It correlates with the top of the depositional sequences S-2 of Ehrenberg et al. (1998a), thus matches the third-order sequence boundary following the Gzhelian highstand and the onset of the Ørn Formation. MGH marks the top of the seismic unit SU1 of Colpaert et al. (2007) (Figure 4.3). Following upwards, the upper Asselian Horizon (UAH) has been selected. It correlates with the sequence boundary at the top of the depositional sequence S-3 (Figure 4.3) and represents the top reflector of the seismic units SU3 of Colpaert et al. (2007). Upwards, the middle Sakmarian Horizon (MSH) has been marked and corresponds to the boundary between the Ørn and the Isbjørn Formation (Gipsdalen Group-Bjarmeland Group) (Figure 4.3). It correlates with the third-order sequence boundary at the top of the depositional sequence S-4 and marks the top of the seismic unit SU4. Evident onlap terminations above MSH in the marginal areas reflect the early transgressive character of the Isbjørn Formation on the platform (Figure 4.10B, C). The last selected reflector corresponds to the Base Kungurian Horizon (BKH) marking the top of the Bjarmeland Group. It correlates with the third-order sequence S-5 of Ehrenberg et al. (1998a) and marks the top of the seismic unit SU5 (Figure 4.3).

4.4 Results and interpretation

The studied cores are dominated by carbonates (limestones and subordinate dolostones), with minor occurrence of calcareous sandstones, calcareous shales and evaporites (Figure 4.4). Core description and microfacies analysis allowed defining nine lithofacies associations (LA1–LA9), mainly based on lithology, textures, skeletal/non-skeletal components and sedimentary structures. The facies nomenclature follows at large the first description of the two wells given by Ehrenberg et al. (1998a), as well as other facies studies performed in adjacent coeval depositional Arctic domains, as the Svalbard and Sverdrup areas (Beauchamp and Desrochers, 1997; Hüneke et al., 2001; Reid et al., 2007; Blomeier et al., 2009, 2011). Major erosive surfaces are always associated through the cores with distinct mm- to cm-thick silty-clayey partings. Due to lack of diagnostic sedimentary features, it is often complicated to assess if such surfaces are associated to phases of subaerial exposure and/or submarine erosion/non sedimentation. However, the vertical facies changes allowed detecting meter-scale (up to 8 m) subtidal to peritidal shallowing-up (SU) and deepening-up (DU) cycles, defined across the Ørn Formation segment of both the wells, as shown in Figure 4.4. Contrarily, across the Isbjørn Formation of the well 7128/6-1 results difficult to identify a precise stacking pattern and record of depositional cyclicity higher than the 3rd order of Ehrenberg et al. (1998). One reason could be that the Isbjørn Formation was mainly deposited within subtidal settings and under low frequency/amplitude sea level fluctuations. Moreover, the original record of depositional cycles given by facies variations (LA8–LA9) has been further obliterated by burial compaction.

4.4.1 Lithofacies Associations (LA)

Nodular Anhydrite (LA1)

This lithofacies is characterized by a mosaic of millimetric to centimetric roundish to elongated and wavy nodules of anhydrite, referable to the typical "chicken-wire" and "entherolitic" fabrics (Butler, 1970; Ciarapica et al, 1985; Warren, 2006, and references therein), in a mixed dolomitic and fine sandy to silty matrix (Figure 4.5A). In place the nodules are densely packed and surrounded by thin stylonodular seams as probable result of burial compaction. From hand lens observation no faunal content has been detected in the matrix. LA1 occurs as a 1.4 m-thick bed in the studied interval of the well 7128/4-1 (Figure 4.4). The lack of thin sections did not allow a petrographic description.. The LA1 is interpreted as associated to a supratidal sabkha-dominated depositional environment.

Dolomitic Mudstones (LA2)

It is characterized by partially to highly dolomitized mudstones to pure fine crystalline dolostone. Scattered millimetric to centimetric anhydrite nodules are visible (Figure 4.6A) and arranged parallel to the bedding. They show occasionally an "entherolitic-like" fabric and are at times associated with dolomitized mm-thick laminae. Some dm-thick horizons are completely barren and rarely alternated with a regular horizontal pattern of molds, possibly associated with dissolution cavities (fenestral-like). Sparse fine-grained sub-rounded quartz grains and isolated particles of organic material (microbial peloids?) are common, together with cm-sized chert nodules of diagenetic origin. Faunal content is rare and is made of thin-shelled ostracods and small encrusting foraminifera. This lithofacies caps at times the SU cycles of the 7128/4-1 core (at 1858.9, 1853.7 and 1840.5 m, Figure 4.4) and it occurs frequently across the middle Gzhelian and middle Asselian intervals of the well 7128/6-1, associated to the third-order SBs of the sequences S-2 and S-3 of Ehrenberg et al. (1998a) (Figure 4.3). LA3 is interpreted as deposited in a restricted intertidal to very shallow subtidal hypersaline environment, associated with marginal marine tidal flat/lagoonal settings.

Fine-grained calcareous Sandstones (LA3)

This microfacies (Figure 4.6B) consists of fine-grained, sub-angular to sub-rounded, moderately- to poor-packed and well-sorted quartzose sandstone, including a lesser amount (up to 30 %) of bioclastic fragments of diverse nature, at times completely recrystallized. The LA is almost devoid of the micritic/microsparitic component and the intergranular pore spaces are partially occluded by blocky calcite and minor anhydrite cement. The bioclastic content shows fragments of rugose corals, bryozoans and green algae; rare are small foraminifera, calcispheres and ostracods. Non-skeletal grains are represented by rare microbial peloids and muddy lithoclasts. LA3 has a limited occurrence within the studied Ørn Formation interval of both the wells. Two 1.5 and 1.1 m-thick beds have been recognized in the lower and upper part of the 7128/6-1 core (respectively at 1945.5 and 1937.2 m, Figure 4.4). A 0.7 m-thick bed occurs at the top of the core 7128/4-1 (1814.7 m, Figure 4.4) (the top of this bed is undefined due to lack of cores upwards). The bedding shows poor-marked parallel to planar cross-laminae, massive horizons and pseudo-bedding due to stylonodular seams of burial origin. LA3 is vertically alternated with bioclastic grainstones (see LA5) and has been interpreted as deposited in a sand flat/beach environment, ranging intertidal to

shallow subtidal settings, above the FWWB. According to Ehrenberg et al., (1998a), these fine-grained clastics record transport from the land during shoreline progradational phases. Successive washing and sorting by the waves and currents action helped the mixing with shoal/lagoonal-derived skeletals and the removal of the muddy component.

Bioclastic Wackestone-Packstones (LA4)

It is characterized by massive beds of wackestones to packstones showing moderate to high faunal diversity, in a micritic/microsparitic matrix, at times partially to highly dolomitized or clotted. The microfabric does not show any preferential orientation of the skeletal components, at times dissolved and replaced by fibrous and blocky cements.

Despite the highly variable relative abundance, the most abundant taxa are represented by small foraminifera and calcareous algae (Figure 4,6C, D). The foraminifera refer to globular encrusting and benthic forms as tuberitinids, globivalvulinids, apterinellids, as well as textulariids, tetrataxids (*Tetrataxis*) and bradyinids. The larger fusulinids are less frequent. The calcareous algae are mainly represented by epistamoporids (*Epimastopora* sp.) and minor beresellids. Common subordinate bioclastic variety includes fragments of rugose corals, *Palaeoaplysina*, incrustations of the microproblematica *Tubiphytes*, *Girvanella* and *Ellesmerella*, red algae (*Komia* sp.), bryozoans, crinoids, ostracods and rare calcispheres. Non-skeletal grains are represented by peloids and rare oncoids. Fine-grained quartz grains are common. This lithofacies occurs frequently in the Ørn Formation interval of both the cores (Figure 4.4).

LA4 is interpreted as deposited in subtidal (below the FWWB) and partially protected lagoonal settings as shown by the presence of mud and the associated high faunal diversity. Such environment was strictly interconnected with sand shoals (LA5) and skeletal buildups (LA6).

Bioclastic Grainstones (LA5)

It is made of fine to coarse grainstones that appear on core as poorly to highly cemented, either massive or showing slightly inclined bedding within few horizons. The microfacies is characterized by moderate to highly diversified biota, often fragmented and recrystallized. It is comparable with LA4 as relative abundance among the different taxa. It is mainly composed of smaller foraminifera (encrusting and small benthic forms), fragments of green algae (*Epimastopora* sp.), *Palaeoaplysina*, rugose corals and bryozoans, encrustations of *Tubiphytes*, *Girvanella* and *Ellesmerella*. Subordinate are red algae (*Komia* sp.), calcispheres, monoaxon sponge spicules and crinoidal fragments. Non-skeletal grains are represented by peloids and rare oncoids (Figure 4.6E, F). LA5 occurs frequently across the Ørn Formation of both the studied cores (Figure 4.4).

LA5 is interpreted as a shoal-dominated shallow subtidal environment, placed around the FWWB and dominated by high hydrodynamic regime that contributed to wash away the muddy component through a constant wave action. The clear similarity in the overall skeletal content, plus the frequent vertical transition between LA5, LA4 and the buildup facies of LA6, suggests a strong interaction between these three depositional inner ramp sub-domains. Therefore, we assume that the LA5 skeletal shallow banks represent here the reworking of both the muddy lagoonal textures and the biostrome debris.

Skeletal Boundstones (LA6)

It can be considered as a composite lithofacies association comprising dm- to m-thick boundstones, dominated by different categories of reef-builders. They are mainly made by *Palaeoaplysina* and rugose colonial corals, associated with minor phylloid algae (Figure 4.4). Rare are the bryozoans and tabulate corals colonies. LA6 occurs within both the sections and is named following Ehrenberg et al. (1998a).

Palaeoaplysina Boundstones (LA6a)

The facies is made of mm-thick slightly undulated plates of *Palaeoaplysina*, mostly horizontal and occasionally inclined up to 30°, forming a skeletal framework that baffles/traps sediments. The interstitial space (Figure 4.6B) is generally made of subtidal wackestone-packstones (LA4), at times dolomitized and occasionally alternated with bioclastic grainstones (LA5), suggesting variations of the hydrodynamic regime associated with the buildup growth. In some cases, the internal structures of *Palaeoaplysina* are often almost completely reset by diagenetic overprint related to meteoric leaching, insomuch that it is difficult to discriminate primary textures. *Palaeoaplysina* boundstones (Figures 4.5B, and 4.7A) reach a thickness of about two meters in the 7128/4-1 core. They do not occur within the studied segment of the well 7128/6-1 but are recurrent (and up to 6.7 m-thick) through the underlying Ghzelian-Asselian interval, making most of the lithostratigraphic unit L-4 of Ehrenberg et al. (1998a, Figure 4.3).

Palaeoaplysina was a major reef-builder and sediment-baffler organism of the upper Carboniferous-Lower Permian (Wahlman, 2002; Nakazawa et al., 2011). Its taxonomic affinity is still under debate and so far has been ascribed to sponges (Krotov, 1888; Flügel, 2004), stromatoporoids (Stuckenberg, 1895), hydrozoans (Davies, 1971) and green algae. The latest affinity (Vachard and Kabanov, 2007) considers *Palaeoaplysina* as Archaeolithophyllacean red algae.

Outcrop analogs of late Carboniferous-early Permian *Palaeoaplysina*-dominated buildups, have been widely described across the entire northern Pangaea margin (Skaug et al., 1982; Breuninger et al., 1989; Beauchamp and Desrochers, 1997; Stemmerik et al., 1994, 1999; Morin et al., 1994; Bugge et al., 1995; Hüneke et al., 2001; Wahlman, 2002; Stemmerik, 2003; Reid et al., 2007; Blomeier et al., 2011). These works describe such bio-constructions as having different size, morphology and subordinate faunal associations, depending on the interactions between depositional and tectono-stratigraphic settings in which they were growing (Wahlman, 2002; Stemmerik, 2003). This could suggest that the growth of *Palaeoaplysina* was not tied to specific environmental conditions. However, the composition of the subordinate faunal associations (mostly light-dependent) always limits the development to the shallow photic zone. In fact, it has been generally assumed that the growth of m-thick (up to 10 m) isolated patches and lenticular laterally-developed banks (up to 100s m-wide) was favored by the reduced accommodation within inner platform environments. In turn, stacked and thicker complexes could have been formed in deeper subtidal settings but always in the photic zone (see Wahlman, 2002 for a review). Has been also suggested that, although *Palaeoaplysina* communities did not "despise" agitated conditions (see also Breuninger et al., 1989 and Davies, 1989), they likely preferred more open subtidal settings of the inner/middle ramp areas to colonize the substrate (Hüneke et al. 2001).

Palaeoaplysina boundstones are interpreted here as forming isolated banks, growing within inner to middle ramp settings. The dominance of interstitial muddy textures (L4-like) suggests buildups development below the FWWB under moderate hydrodynamic settings, with periodic shallowing-up and enhanced water dynamism testified by the interstitial grainstones.

Occasionally, platy and cup-shaped recrystallized *Eugonophyllum* phylloid algal fragments (Udoteacean and Halimedacean algal affinity; see Forsythe et al., 2002 and reference therein) occupy interstitial cavities among the *Palaeoaplysina* plates, suggesting the presence of colonies in nearby areas. Phylloid algae are not common within the studied intervals but are frequently associated with *Palaeoaplysina* in the lower part of the unit L-4 of the well 7128/6-1, dominated by buildups (Figure 4.3). *Eugonophyllum* phylloid algae represent widespread tropical-subtropical reef-builder organisms across the Moscovian-Sakmarian time (Wahlman, 2002). In general, the size, morphology and associated fauna of such bio-constructions do not differ from the *Palaeoaplysina*-dominated ones. Therefore, their development has been frequently described within analogous or transitional environmental settings (Bugge et al., 1995; Ehrenberg et al., 1998a; Morin et al., 1994; Stemmerik et al., 1999; Hüneke et al., 2001; Wahlman, 2002; Stemmerik, 2003; Nagazawa et al., 2011). Among the two, the more fragile structure (faster growing mode) of the *Eugonophyllum* colonies could have made them preferring more quiet (more protected or deeper) environments to colonize the sea bottom (Morin et al., 1994 and references therein).

Coral/Bryozoan Boundstones (LA6b)

Coral boundstones are present in the Ørn Formation interval of both the studied sections. Differently from the *Palaeoaplysina*-phylloid algal boundstones, their occurrence across the Ghzelian-Asselian L-4 unit of the well 7128/6-1 is limited (Ehrenberg et al., 1998a; Larssen et al., 2002). In the studied intervals, they are arranged in massive cerioid (Figure 4.5C) or phaceloid (fasciculate structure of separated circular corallites, Figure 4.5D) colonies of rugose and rare tabulate (syringoporids) corals, reaching up to 1.6 meters. The inter-corallite spaces (Figure 4.6H) are mostly occupied by coarse-grained packstones-grainstones of LA4 and LA5, with a very variable fauna but prevalence of broken bio-eroded coral fragments, smaller encrusting foraminifera, *Tubiphytes*, *Girvanella, Ellesmerella*, bryozoan fragments and micropeloids. Sometimes, intra-corallite dissolution vugs are occluded by late chert and anhydrite cement fillings. In the studied intervals, the rugose coral colonies are commonly overlied by subtidal muddy facies (LA4 and LA7) and occupy the upper portion of the SU cycles. In fact, compared with the *Palaeoaplysina* boundstones, these small patches seemed to have undergone greater or at least more constant hydrodynamic regimes, responsible for a more efficient mud removal within interstitial cavities. Therefore, the coral boundstones are interpreted here as forming small scattered isolated patches of colonies thriving in a shallow subtidal inner ramp environment.

A 30 cm-thick Boundstone made up by a dendroid colony of cystoporid bryozoans occurs as a 30 cm-thick bed in the 7128/4-1 section (at 1847.8 m), embedded by partially dolomitized coarse packstones of the LA4. Isolated corallites of solitary rugose corals also occur within the bryozoan colony and the interstitial cavities are occasionally occupied by late anhydrite cement. The bryozoan boundstones are interpreted as small isolated colonies forming within the inner ramp environment, either isolated or possibly associated with the coral patch reefs.

Fusulinid Wackestone-Packstones (LA7)

This lithofacies is made of wackestone-packstones and sporadically packstone-grainstones with moderate faunal diversity and prevalence of fusulinids foraminifera (Figure 4.7C, D). The bedding ranges from massive to nodular (with increase of the fusulinid shelliness usually associated to horizons showing greater burial compaction) and some horizons show a preferred orientation of the biotic components, possibly related to transport

by subtidal current and/or storm. Subordinate skeletal content is often fragmented and shows common small benthic forams (mainly *Tetrataxis*), bryozoans and crinoids. Minor are *Palaeoaplysina*, rugose corals, *Tubiphytes* and brachiopods. Possible *Eugonophyllum* fragments, trilobites and monoaxon sponge spicules can be rarely observed (**plate 2 c, d**). The matrix is occasionally dolomitized and appears as micritic to microsparitic to calcisiltitic, including common silty-grained quartz and glauconite. This lithofacies occurs sporadically at the base of the SU cycles within both the studied cores (Figure 4.4). LA7 is interpreted as deposited in a subtidal open middle ramp environment, below the FWWB and transitional to the outer domains, as indicated by the subordinate faunal content.

Crinoidal-Bryozoan Grainstones (LA8)

The lithofacies shows massive beds of reworked, fine to coarse, bioclastic grainstones and sporadically rudstones with a low to moderate faunal diversity, dominated by fragments of bryozoans (mostly cystoporids) and crinoids (Figure 4.7E, F). Secondary skeletal content comprises variable proportions of brachiopods, fusulinids, siliceous sponges (entire and disarticulated in monoaxon spicules) and *Tubiphytes*. Rare small foraminifera, ostracods and trilobites fragments can be found, as well as sparse glauconitic mm-sized grains. High-amplitude stylolites and other pressure-solution features are frequently observed on core, together with sporadic centimetric to decimetric roundish chert nodules. This LA occurs in the upper part of the 7128/4-1 Ørn Formation (the interval between 1834 and 1821 m) and dominates, together with LA9, the overlying Isbjørn Formation of the 7128/6-1 core (Figure 4.4).

The LA8 grainstones were likely deposited in subtidal open marine settings, above and/or around the SWWB (distal middle ramp). The dominant fabric of reworked and disarticulated skeletals, point out toward areas characterized by open circulation, affected by currents and storms that contributed to accumulate mud-free bioclastic debris.

Crinoidal-Bryozoan silty Wackestone-Packstones (LA9)

This lithofacies is characterized by nodular bioclastic wackestone-packstones and rarely floatstones, bioturbated, mostly chaotically arranged, and dominated by disarticulated crinoids and bryozoans (Figures 4.5F and 4.7G, H). The matrix is micritic to calcisiltitic and becomes silty-clayey-rich within the most nodular intervals, showing irregular proportions of very fine sub-rounded quartz grains and less micas, plus mm- to cm-sized glauconitic grains. Subordinate faunal content is represented by variable proportions of brachiopods, monoaxon sponge spicules, molluskan fragments and rare *Tubiphytes* and fusulinid foraminifera. The nodular aspect of LA9 is given by the ubiquitous presence of burial diagenetic features. This process favored the accumulation of silty-clayey-dominated horizons following carbonate dissolution (Ehrenberg, 2004). This lithofacies association is gradually to sharply interbedded with LA8 in the upper part of the 7128/4-1 core and across the entire Isbjørn Formation of the 7128/6-1 core (Figure 4.4). LA9 represents the basinward transition of the LA8 grainstones and is interpreted as deposited within subtidal open marine outer ramp settings (below the SWWB). The chaotic fabric of some horizons might reflect reworking and accumulation under storm conditions within the proximal outer ramp areas, whereas in the more distal outer ramp, the size of the bioclastic fragments decreases and wackestones prevail on packstones.

4.4.2 Well sections description

4.4.2.1 Well 7128/4-1 section (Figure 4.4)

In the lower 12.7 meters (1865.7-1853 m), the sequence is dominated by a regular alternation of bioclastic grainstones (LA5), bioclastic wackestones-packstones (LA4) and foraminiferal wackestones (LA6), arranged in SU cycles and capped at the top by dolomitic mudstones (LA2). These facies are followed up to 1843 m, by bioclastic grainstones (LA5) and bioclastic wackestones-packstones (LA4) and are overlied at the cycles top by skeletal boundstones (LA6), dominated by *Palaeoaplysina* and colonial rugose corals. A 20 cm-thick bed of skeletal boundstones at 1847.8 m is represented by a colony of cystoporid bryozoans associated with isolated rugose corals.

From 1843 to 1834.6 m, bioclastic wackestones-packstones (LA4) are overlied by nodular anhydrite (LA1), whereas in the next SU cycle bioclastic grainstones (LA5) are alternated with foraminiferal wackestones (LA7). From 1834.6 m upwards, the sequence shows a DU trend. Skeletal boundstones (LA6), represented by 5-cm-thick colony of tabulate (syringoporids) corals, are followed by foraminiferal wackestones (LA7) and crinoidal-bryozoan nodular packstone-wackestones (LA9). Upwards the LA shallow-up again, from crinoidal-bryozoan grainstones (LA8) to bioclastic grainstones (LA5), passing through bioclastic wackestones-packstones (LA4) and a 1 m-thick bed of *Palaeoaplysina*-phylloid algae boundstones (LA6). From 1828.4 to 1820.4 a further DU-SU trend is recognizable. Nodular dark calcareous shales are followed upward by crinoidal-bryozoan silty wackestone-packstones (LA9), crinoidal-bryozoan grainstones (LA8) and bioclastic grainstones (LA5). The nodular dark shales of this cycle are associated with the 3rd order MFS of the sequence S-4 of Ehrenberg et al. (1998a) (Figures 4.3 and 4.4). The last cycle (1820.4-1814 m) is again dominated by bioclastic wackestones-packstones (LA4), shoaling-up to bioclastic grainstones (LA5) and alternated with two skeletal boundstones *Palaeoaplysina*-dominated beds (LA6), 2 m- and 1 m-thick respectively. At the top of the sequence, the cycle is capped by 70 cm of calcareous sandstones (LA3).

4.4.2.2 Well 7128/6-1 section (Figure 4.4)

The section starts with bioclastic packstones (LA4) followed by 1.5 meters of calcareous sandstones (LA3), that can be correlated with the sandstones bed at the top of the 7128/4-1 section (Ehrenberg et al., 1998a, Figure 4.4). The next two SU cycles are dominated by foraminiferal wackestones-packstones (LA7) and bioclastic grainstones (LA5), overlied at the cycles top by dm-thick skeletal boundstones (LA6) made of rugose colonial corals. The last two SU cycles of the Ørn Formation are dominated by bioclastic grainstones (LA4) with a 1.1 m-thick bed of calcareous sandstones (LA3) capping the first cycle top. The shift to the Isbjørn Formation (at 1834.7 m) is associated with an erosional surface at the top of the bioclastic grainstones (Figure 4.5E), followed by 5 cm of nodular silt that pass upward to massive crinoidal-bryozoan grainstones (LA8). This level corresponds to the 3rd order SB of the sequence S-4 of Ehrenberg et al. (1998a) (Figure 4.3). The presence of an early-middle Sakmarian stratigraphic hiatus marking the boundary between the Gipsdalen and Bjarmeland Groups is observed at regional scale, affecting with a slight different temporal occurrence structural highs and most of the proximal depositional areas (Stemmerik and Worsley, 2005 and references therein). However, the duration of such gap seems to reflect local settings. It is associated with karst features in Spitsbergen, Bjørnøya and North Greenland (Stemmerik et al., 1996, 1997; Worsley et al., 2001; Stemmerik and Worsley, 2005), whereas the corresponding erosional surfaces from the wells 7128/6-1 and 7129/10-U-02 (IKU shallow

core) of the Finnmark Platform (Figure 4.1B) are devoid of evidences of subaerial exposure (Bugge et al., 1995; Ehrenberg et al., 1998a) and may correspond to a relatively short period of non- deposition and submarine erosion prior to the following major transgression. As stated also by Groves and Wahlman (1997), the carbonate succession from the core 7128/6-1 was characterized by cyclic hiatuses, which are below the resolution of the fusulinid-based biostratigraphy.

The Isbjørn Formation interval (1834.7-1746 m) of the well 7128/6-1 is entirely dominated by an alternation of crinoidal-bryozoan grainstones (LA8) and subordinate nodular crinoidal-bryozoan wackestone-packstones (LA9). The first 4.5 meters overlying the Ørn Formation show massive grainstones (LA8). Upwards, the nodular LA9 prevails on LA8, showing an overall DU trend up to 1813 m. Here, a 70 cm-thick calcareous shaly wackestone bed marks the MFS of the sequence S-5 of Ehrenberg et al. (1998a) (Figure 4.4). Upwards, the section is dominated until the top by grainstones (LA8) in a SU trend, with sporadic occurrence of nodular wackestone-packstones (LA9). Within the topmost 20 cm of the section, nodular packstones show centimetric bioturbation cavities filled by microbreccia, in a matrix of greenish silt. The last 10 cm are brecciated and capped by an erosional contact with the overlying calcareous shales of the Tempelfjorden Group. The contact between the Bjarmeland and Tempelfjorden Group has been interpreted as a drowning unconformity across the whole Arctic region (Larssen et al., 2005).

Figure 4.5 Core pictures from the Asselian-Artinskian studied interval, related to some of the lithofacies associations (LA) described in the text. a) Densely packed mm to cm anhydrite nodules in a dolomitic/silty matrix (LA1) from the Ørn Formation interval of the well 7128/4-1 (1839.5 m). b) Particular of *Palaeoaplysina* boundstones (LA6a) from the Ørn Formation interval of the well 7128/4-1 (1818.4 m). Note the arrangement of the *Palaeoaplysina* plates (p) and the muddy matrix (m) occasionally trapped among them during successive phases of buildup development. Note also the typical protuberances of the *Palaeoaplysina* thallus (arrows), also shown on thin section in plate 3a. c) Particular of coral boundstones (LA6b) from the Ørn Formation interval of the well 7128/6-1 (1843.4 m). The colony of rugose corals shows a cerioid arrangement of the corallites, forming a massive skeleton. d) Rugose coral boundstones (LA6b) from the Ørn Formation interval of the well 7128/6-1 (1839.4 m). In this case the colony shows a phaceloid growth type of the corallites, surrounded by bioclastic grainstones of the lithofacies association LA5. e) Erosive surface marking the stratigraphic boundary between the Gipsdalen Group and the Bjarmeland Group in the well 7128/6-1 (1834.7 m). Shallow bioclastic grainstones (LA5) of the Ørn Formation, reflecting a Chloroforam sedimentation mode, are capped by an erosive surface and overlied by ~5 cm of nodular silt, passing upward to subtidal crinoidal-bryozoan grainstones (LA8) of the Isbjørn Formation, associated to a Bryonoderm sedimentation mode. See the text for further explanation. f) Outer ramp crinoidal-bryozoan silty wackestone-packstones (LA9) from the Isbjørn Formation interval of the well 7128/6-1 (1813.8 m). The pseudo-nodular aspect of this LA is mostly due to the dissolution of the calcareous component during burial compaction, associated with high silt/clay content.
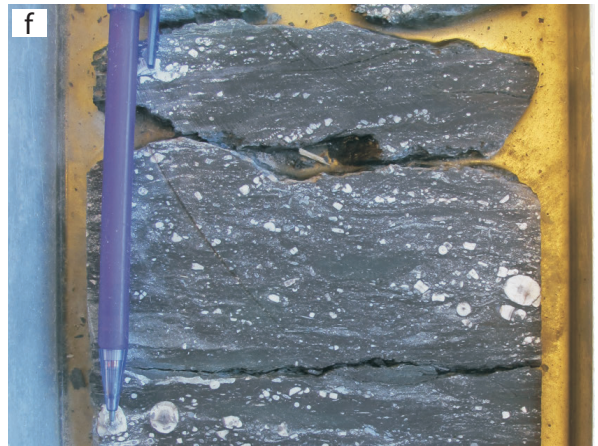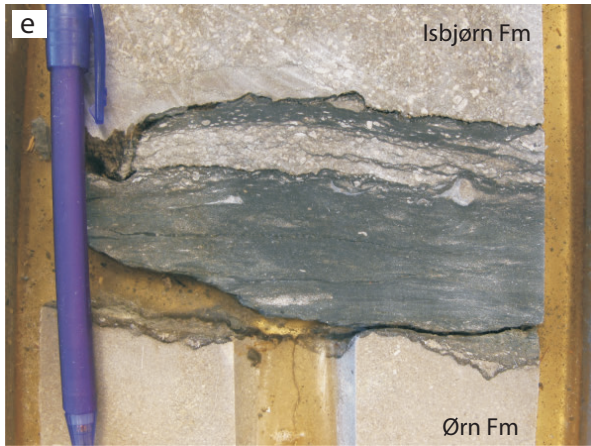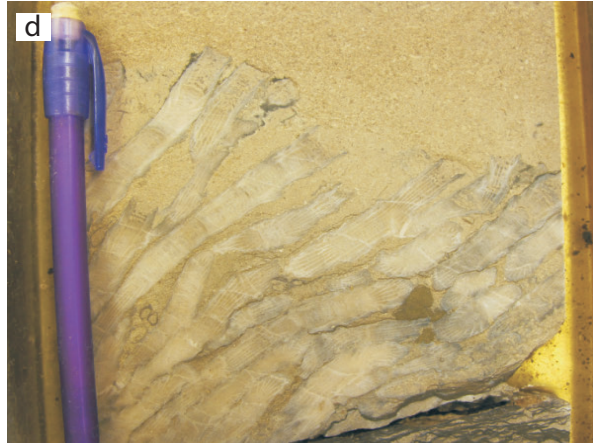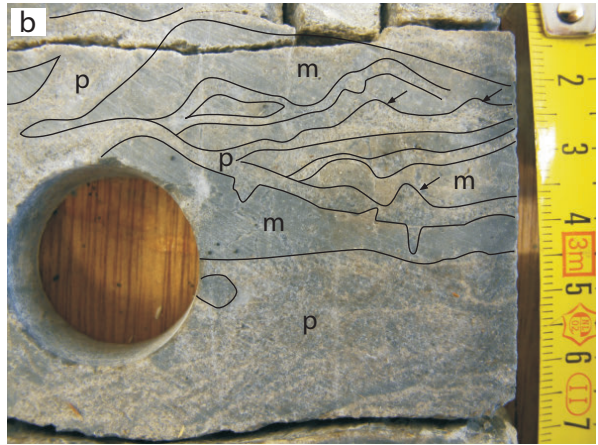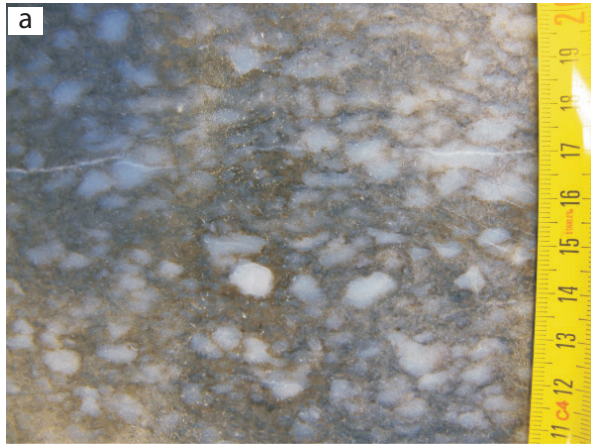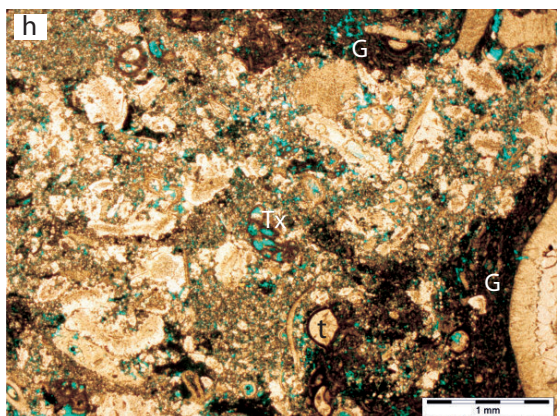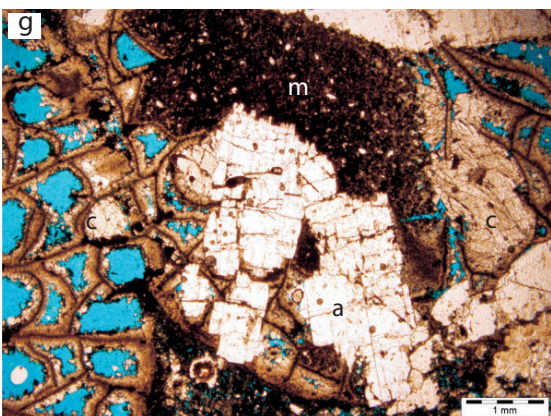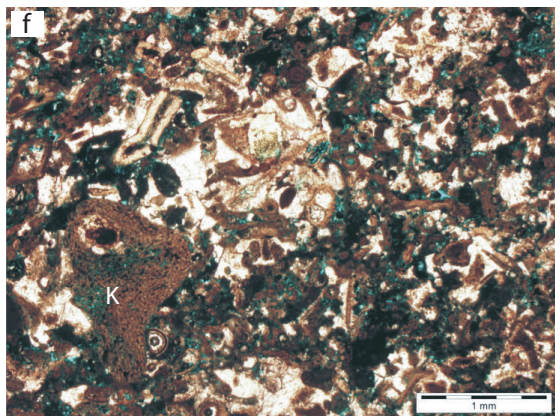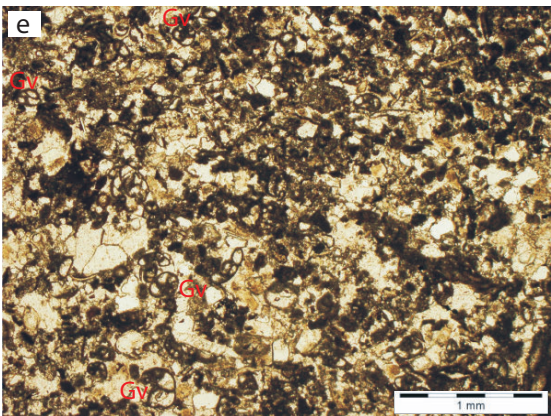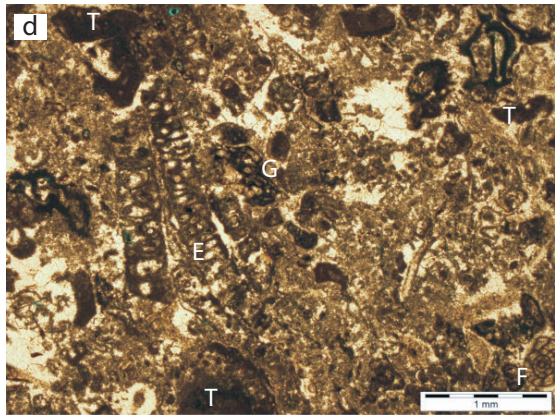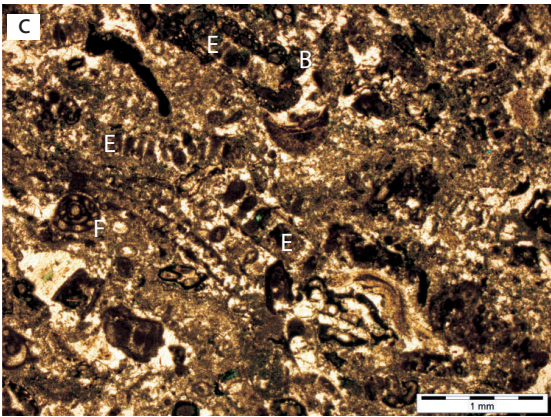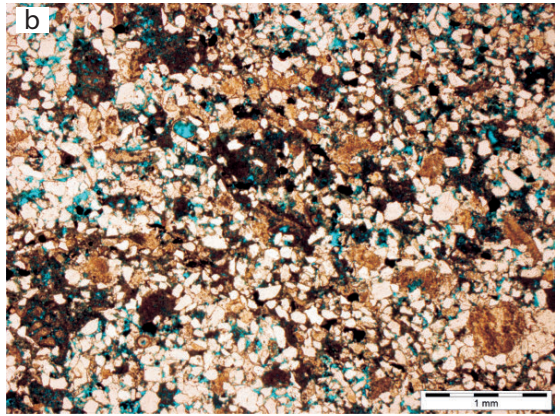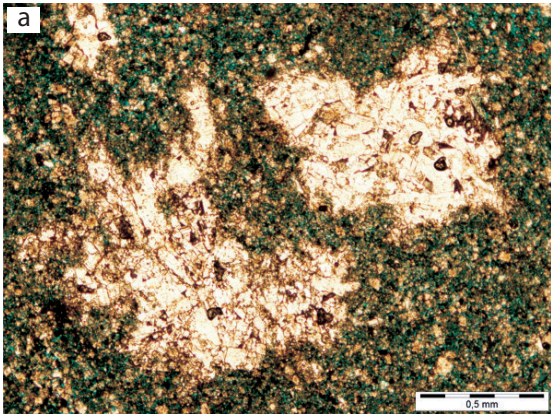
Figure 4.6 a) Dolomitized mudstones (LA2) from the Ørn Formation interval of the well 7128/4-1 (1853 m). The microfacies shows mm-sized cavities possibly related to intertidal fenestrae, filled by anhydrite cement in a fine dolomitic/micritic matrix, with high intercrystalline porosity. b) Fine quartzose-calcareous sandstones (LA3) from the Ørn Formation interval of the well 7128/4-1 (1814 m). The carbonate content is characterized by skeletal fragments (up to 30 %) and less blocky calcitic spar. The microfacies shows a well developed interparticle porosity. c-d) Bioclastic wackestone-packestones (LA4) from the Ørn Formation interval of the well 7128/4-1 (1815 and 1842 m respectively) showing calcareous algae (*Epistomora sp.*, E), benthic foraminifera (F) encrustations of bryozoans (B), *Tubiphytes* (T) and possible *Girvanella* (G). e) Bioclastic grainstones (LA5) from the Ørn Formation interval of the well 7128/4-1 (1865 m) dominated by globivalvulinid foraminifera (Gv) and peloids, plus undifferentiated recrystallized skeletal fragments and encrusting forms. f) Bioclastic grainstones (LA5) from the well 7128/6-1 (1837.75 m) dominated by red algae (*Komia sp.*) (K), bryozoan fragments and peloids. Note also the well developed interparticle porosity. g) Rugose coral boundstones (LA6b) from the Ørn Formation interval of the well 7128/4-1 (1849.25 m). The picture shows a micropeloidal matrix (m) and different generations of calcitic (c) and anhydrite (a) cements, partially filling intergranular and intragranular pores. Note the high intraparticle porosity within the corallites. h) Bioclastic packstones (with dolomitized matrix) occupying the interstitial space of the coral boundstones (LA6b), from the Ørn Formation interval of the well 7128/4-1 (1849.25 m). It is shows coral and crinoid fragments plus undifferentiated skeletals, often encrusted by Girvanella (G); *Tetrataxis* (Tx) and *Tuberitina* (t) foraminifera can be recognized. Note also the high interparticle porosity.

Figure 4.7 a-b) *Palaeoaplysina* boundstones (a) (LA6a) and interstitial matrix (b) (LA4) from the Ørn Formation interval of the well 7128/4-1 (1818 m). The thallus morphology of *Palaeoaplysina* shows the typical protuberances (p) and the upward-branching tubes (t) of the canal system mostly filled by the interstitial matrix. The latter is made by bioclastic packstones from LA4, showing small benthic foraminifera (F), fine fragments cystoporid bryozoans (B), ostracods (O) and possible *Tubiphytes* (T), plus undifferentiated recrystallized skeletals. c-d) Foraminiferal packstones (LA7) from the Ørn Formation interval of the well 7128/4-1 (1837 m). The microfacies is dominated by fusulinid foraminifera (F), with fragments of crinoids (C) and *Rugose* corals (R), less small benthic forams. In photo (d) the microfacies reflects a probable more distal position. It shows scattered fusulinids (F) and *Tetrataxis* (Tx) forams, crinoid (C) and trilobite (Tr) fragments, plus other undifferentiated shells. The matrix is partially dolomitized, including common sparse quartz grains (Ørn Formation interval of the well 7128/4-1, 1864 m). e) Crinoidal-bryozoan grainstones (LA8) from the Ørn Formation interval of the well 7128/4-1 (1824 m). The microfacies is chaotic and dominated by fragments of crinoids (C) and bryozoans (B). It shows moderate interparticle-intraparticle porosity when pores are not occluded by syntaxial overgrowth of calcitic cement. f) Crinoidal-bryozoan grainstones (LA8) from the Isbjørn Formation interval of the well 7128/6-1 (1809.75 m). It is characterized by fragments of crinoids (C), bryozoans (B) and *Tubiphytes* (T). The microfacies is very similar to the one observed within the Ørn Formation (photo e) but in this case, as all across the Isbjørn Formation interval, the porosity is very low, due to complete occlusion by syntaxial and blocky cements. g-h) Crinoidal-bryozoan silty wackestone-packstones (LA9) from the Ørn Formation interval of the well 7128/4-1 (1825 m). The microfacies shows chaotically arranged fragments of crinoids (C) and bryozoans (B) in a nodular calcisiltitic matrix with abundant quartz grains. In the more distal wackestones (photo h) the
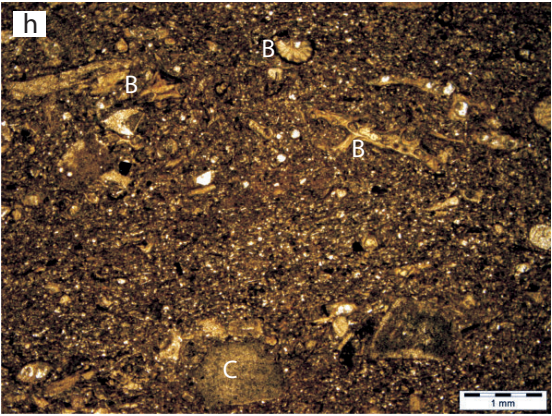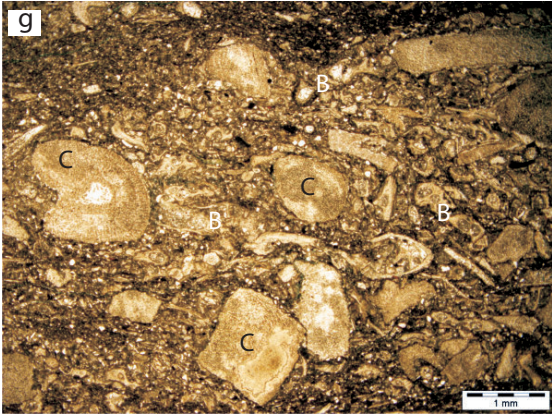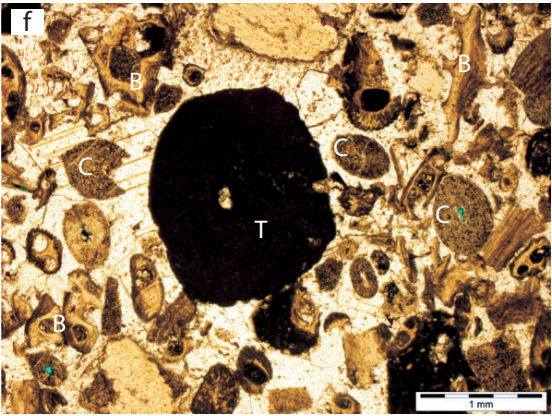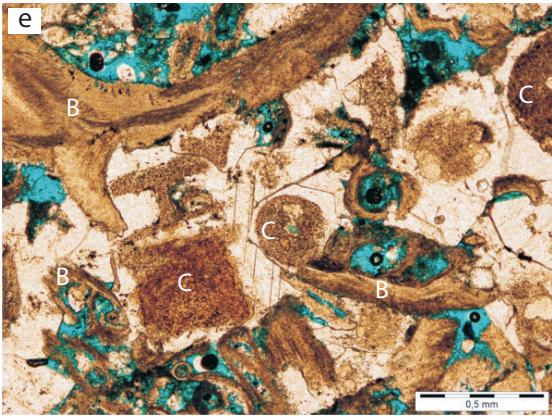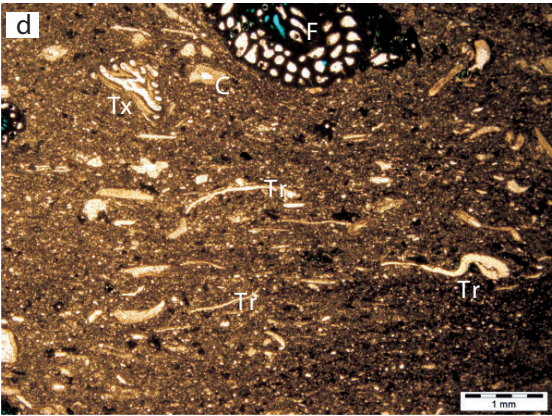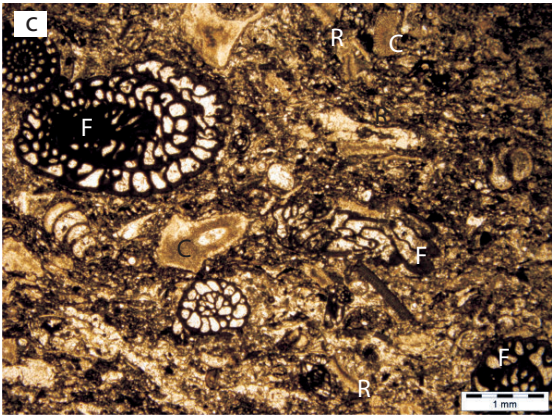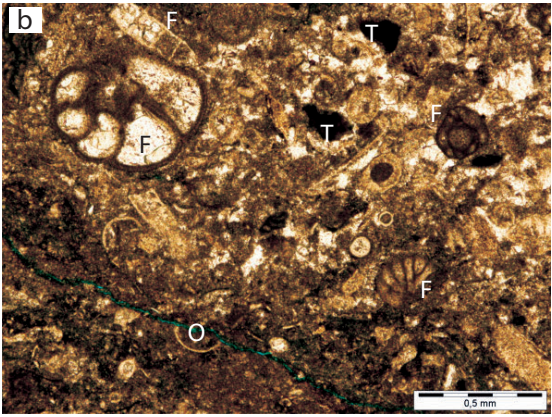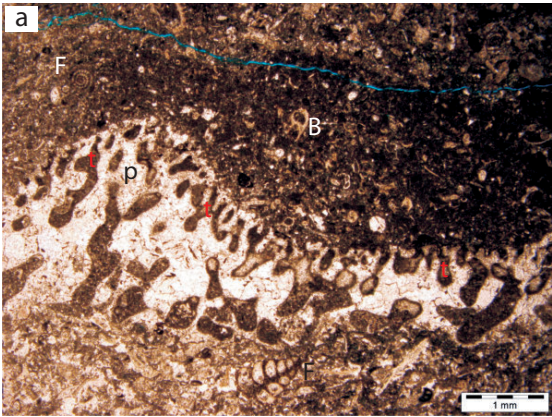
4.4.3 Carbonate factories and depositional paleoenvironments

Following previous classifications (Lees and Buller, 1972; Nelson, 1988a, b), Beauchamp (1994) introduced a specific nomenclature for the Paleozoic biotic/abiotic associations referring to Chloroforam, Bryonoderm-extended, Bryonoderm and Hyalosponge sedimentation modes that consider temperature-controlled sediment distribution based on paleolatitude and paleobathymetry variations (see also Beauchamp and Desrochers, 1997). In view of the close affinity with the faunal associations found in this study, the Chloroforam, Bryonoderm-extended and Bryonoderm modes will be used instead of the general warm-, mixed and cool-water modes respectively.

According to our microfacies analysis, the Asselian-early Sakmarian marine interval of the Ørn Formation carbonates records inner to outer ramp domains (Figure 4.8A) where Chloroforam assemblages are replaced, downward in the water column, by Bryonoderm-extended and then Bryonoderm fauna. Diversified associations dominated by small benthic foraminifera, green algae and encrusting communities, thrived in the shallowest inner ramp areas, characterized by intertidal sabkha/tidal flats, subtidal partially protected lagoons, shallow sandbars and m-thick buildup patches dominated by *Palaeoaplysina* and rugose corals. From the middle ramp downward, light-dependent communities are stepwise replaced by a mixed, Bryonoderm-extended fauna. Here, fusulinids and minor *Palaeoaplysina*, rugose and tabulate corals, were associated with typical heterozoan taxa as bryozoans and crinoids (LA7). Finally, the outer ramp domains were dominated by the growth of heterozoan Bryonoderm communities (bryozoans, crinoids, brachiopods).

Comparable vertical facies trends have been also assessed across the Ørn Formation of the proximal shallow cores 7030/03-U-01 and 7129/10-U-02 (Bugge et al., 1995 and Ehrenberg et al., 2000b). In addition, similar variation of the facies patterns with water depth (from photozoan to heterozoan) have been assessed from many other Arctic neritic domains of the Arctic shelf (Kleilen, 1992; Morin et al. 1994; Beauchamp and Desrochers, 1997; Hüneke et al., 2001; Reid et al., 2007; Blomeier et al., 2011), with small chronological discrepancies depending on slightly different paleo-position and local tectono/stratigraphic settings.

The sedimentary record of the most distal and deepest environments of the Finnmark domain during the deposition of the Ørn Formation is given by cores from the wells 7228/9-1S and 7229/11-1 (Figure 4.1, black circles). They are characterized by transgressive silty nodular mudstones alternated with lowstand subtidal evaporitic sequences. The evaporites are associated with intervals of increased restricted conditions and isolation of the Nordkapp Basin (Larssen et al., 2002; Rafaelsen et al., 2008; Stemmerik, 2008) and possibly correlate, in the well 7128/6-1, with the lithostratigraphic units L-3 and L-5, dominated by dolomitic mudstones and marked by the major sequence boundaries S-2 and S-3 (Figure 4.3) (Ehrenberg et al., 1998a; Colpaert et al., 2007).

Starting from the middle Sakmarian, the deposition of the Bjarmeland Group marks a significative change in the sediment accumulation type. The studied cores (Figure 4.4) across the Isbjørn Formation reveal that the Finnmark became site of deposition of pure heterozoan facies in the proximal areas, reflecting a landward transition of the fully Bryonoderm sedimentation mode. According to our facies analysis and previous interpretations of the core 7128/6-1 (Ehrenberg et al., 1998a), the schematic facies model of Figure 4.8B shows a general ramp profile where inner-middle ramp storm influenced areas were occupied by crinoidal-bryozoans grainstones (LA8), shifting below the SWWB to the mud-dominated nodular textures of the LA9. The coeval interval (sequence S-5) from the shallow cores 7129/10-U-02 and 7128/12-U-01 is thinner (~45
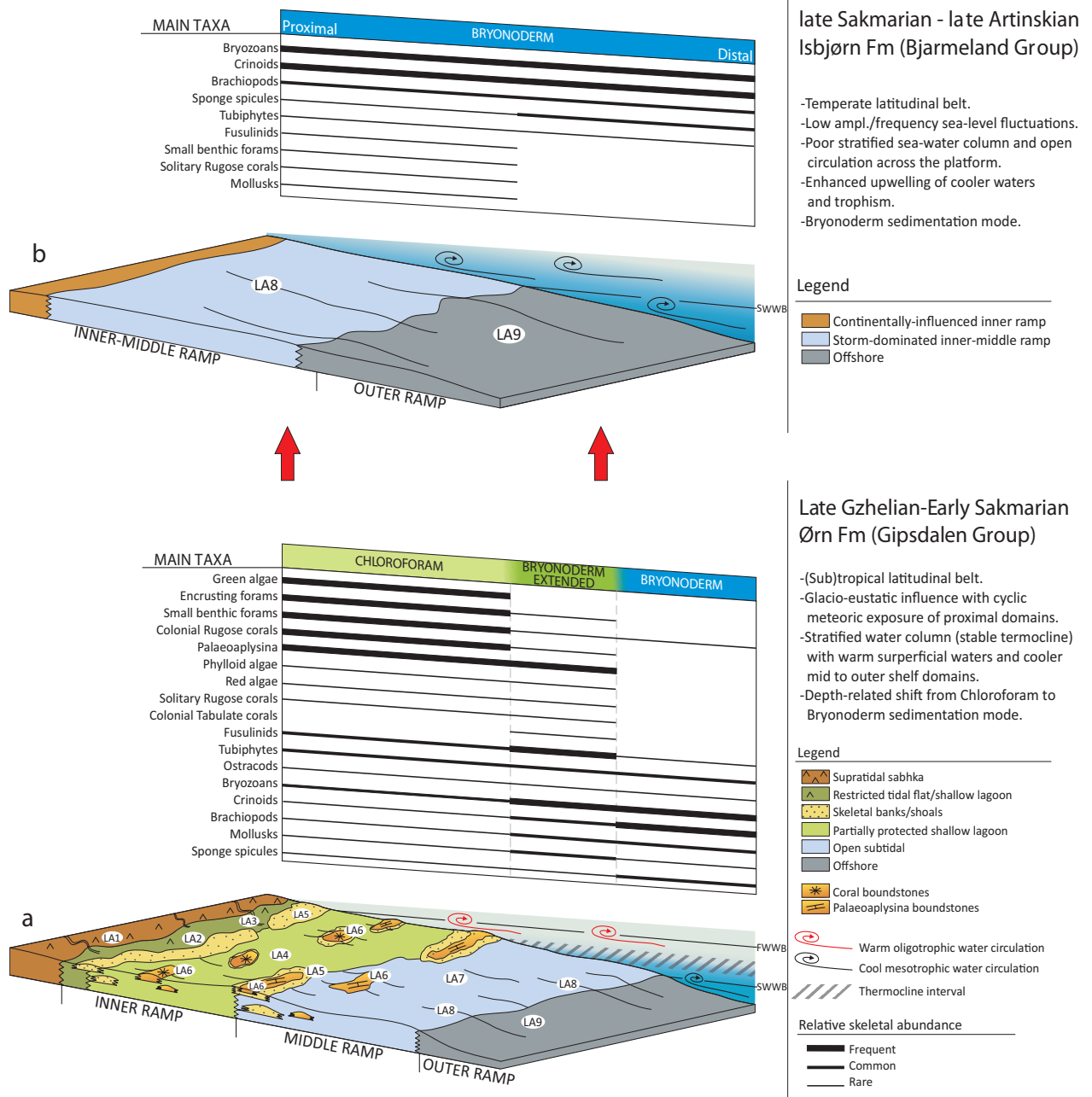
Figure 4.8 Schematic depositional models derived from the Asselian-Artinskian intervals of the wells 7128/6-1 and 7128/4-1, during the deposition of (a) the Ørn Formation (Gipsdalen Group) and (b) the Isbjørn Formation (Bjarmeland Group). The models show the assessed platform sub-environments, the spatial distribution of the Lithofacies Associations (LA1-LA9) and the relative abundance of the major skeletal components across the Finnmark profile according with the suggested shift in carbonate sedimentation modes, driven by major changes in the coeval palaeoceanographic/palaeoclimatic settings (see text for explanation). See figure 4.4 for the legend regarding the LA.

m vs. 89.4 m in the well 7128/6-1) and dominated by the LA8 grainstones, suggesting shallower conditions, less accommodation and presence of stratigraphic hiatuses due to lack of biozones (fusulinid zone 20) (Bugge et al., 1995; Ehrenberg et al., 2000). Seaward, cores from the well 7229/11-1 show that the outer ramp domains were, at the same moment, site of deposition of hundreds of meter-thick stacked buildups made up by bryozoans and *Tubiphytes* assemblages of the Polarrev Formation (Blendinger et al., 1997; Stemmerik,

1997; Larssen et al., 2002), forming an evident and mostly continuous ridge easily detectable on seismic (Figure 4.10). Deeper silty mudstones of the Ulv Formation were deposited around the buildup belt and further basinward.

4.5 Discussion

4.5.1 Factors affecting the shift in carbonate factories

Photozoan vs. heterozoan modern sediments distribution essentially varies with respect to sea-water temperature and depth, latitude and circulation patterns (Lees and Buller 1972; James 1997; Mutti and Hallock, 2003) that in turn, also regulate the trophic sources distribution by upwelling. The evolution of the Finnmark Platform, as part of the huge shallow Arctic epicontinental shelf, was affected by northward drifting of the Eurasian plate with a rate of 2-3 mm/year (e.g., Scotese and McKerrow, 1990). During the deposition of the Ørn Formation (Gzhelian–Sakmarian time) the Barents Sea domain was still lying within the (sub-) tropical belt (20°–30°) and was associated with high frequency (100 k.y.) and amplitude (>50 m) glacio-eustatic sea-level variations (Stemmerik, 2008). Moreover, the coeval paleogeographic scenario suggests open current circulation patterns due to the NW-SE connections between the Panthalassa and the Paleo-Tethys Oceans, through the Uralian seaway (Figure 4.1A) (Reid et al., 2007; Blomeier et al., 2009).

On the base of these assumptions and considering the sedimentary records of the Sverdrup Basin, the Svalbard archipelago and Easter European Platform, Reid et al. (2007) have assumed that the late Carboniferous-earliest Permian sedimentation patterns across the Arctic domain were influenced by prevalent circulation of wind-driven oligotrophic superficial warm-waters, from both the Tethys and Panthalassa Oceans. Therefore, they suggested the presence of a stratified water column and a stable thermocline during the Moscovian-Sakmarian time, to explain the coeval widespread development of shallow photozoan biota (associated with supra/intertidal evaporites in the most restricted areas) and deeper heterozoan mesotrophic associations. Such hypothesis is fully supported by our paleoenvironmental interpretations (Figure 4.8A) that consider (sub-) tropical settings and a depth-related transition in carbonate factories across the Ørn Formation sedimentary record of the Finnmark Platform.

From the late Sakmarian, the onset of a Bryonoderm sedimentation mode was established on the Finnmark Platform and across the Arctic province (Stemmerik, 1997). Such significant modification in the depositional style has been commonly associated to the effect of: i) an early Sakmarian flooding event associated with a major melting phase of the Gondwanan icecaps (Stemmerik, 1997; Stemmerik et al., 2008 and references therein); ii) the generalized cooling due to further northward drifting of the Arctic shelf up to the temperate latitudinal belt (Stemmerik, 1997); iii) the stepwise closure of the Uralian corridor connecting the tropical Tethyan waters with the Arctic seas (Fokin et al., 2001; Reid et al., 2007 and references therein).

The interplay of such mechanisms led to a new climatic-oceanographic Arctic scenario, characterized by temperate and more seasonal climatic conditions associated with a low frequency/amplitude of the sea-level cyclicity and a generalized subtidal open marine storm-affected sedimentation. Such circumstances possibly contributed to weaken the water masses stratification, resulting in a disruption of the thermocline and consequent upwelling and influx of panthalassic nutrient-rich cool waters across the entire Arctic shelf (Beauchamp and Baud, 2002; Reid et al., 2007). The result was the ultimate turnover in favor of heterozoan assemblages that from the late Sakmarian invaded also the more proximal and shallow environments until the Kungurian time.

Besides cooling and upwelling-driven mesotrophic conditions, enhanced nutrients delivery through siliciclastic continental run-off could have been another important factor for the intensification of the trophic levels and consequential instauration of a full Bryonoderm carbonate factory, especially with regard to land-attached carbonate depositional systems as the Finnmark Platform, where clastic input is an ordinary aspect. In the studied sections, but also in the coeval intervals of the shallow cores and in the underlying Gzhelian Ørn Formation (well 7128/6-1), a discrete amount of scattered quartz grains is always present (Bugge et al., 1995; Ehrenberg et al., 1998a); but a considerable relative increase of quartz-dominated very fine sand and silt is observed in the bryozoan-crinoidal wackestone-packstones (LA9) of the Ørn and the Isbjørn Formation. The clastic component within these intervals could likely reflect phases of increased land-derived siliciclastic supply associated with coastline retrogradation (Ehrenberg et al., 2000) and successive reworking due open circulation. However, in our case the observed increasing rate of insoluble detritic load could reflect burial compaction, whose sedimentary features (stylolites and nodular seams) represent a typical aspect of lithofacies association LA9.

4.5.2 The Finnmark Platform large-scale geometries

The Finnmark area is affected by the late Devonian-middle Carboniferous inherited extensional trend (reactivated following the Caledonian structures), striking NE-SW and marking the overall boundary with the Nordkapp Basin (Faleide et al., 1984; Gudlaugsson et al., 1998). Prior to the deposition of the Ørn Formation, syn-rift structural highs were eroded and the depressions partially filled by clastics of the Billefjorden and lower Gipsdalen Group (Ugle and Falk Formation). Therefore, following the Moscovian transgression, the onset of the Ørn Formation carbonates on the Finnmark Platform took place in quite diverse and subsiding neritic settings reflecting local physiography, along with the previous-mentioned climatic and oceanographic changes. This makes challenging to define how the large scale depositional profile of the platform evolved following the biological shift between the Gipsdalen and Bjarmeland Group, and how to classify this system according with the current geometric classifications that vary from rimmed shelves and homoclinal ramps, plus a wide number transitional profiles (Pomar, 2001; Williams et al., 2011). Such complexity is also revealed by the different previous hypotheses about the platform profile development across the Gipsdalen-Bjarmeland transition, made on the base of seismic- and/or core analyses. For example, Nilsen et al. (1993) considered a major shift from a ramp during the deposition of the Gipsdalen Group to a rimmed shelf with marginal buildups during the Bjarmeland Group, whereas Ehrenberg et al., (1998a) supposed for the Finnmark a distally steepened ramp profile with a marginal buildup trend also during the deposition of the Gipsdalen Group.

Colpaert et al. (2007) stated there was a shift from a prograding carbonate platform/slope system with marginal buildup complexes and barriers during the Gipsdalen Group deposition, to a more restricted heterozoan platform with stacked buildup complexes on the slope during the Bjarmeland Group. Finally, Rafaelsen et al. (2008) suggested that the Finnmark was a "northerly dipping distally steepened ramp with buildups" from the mid-Carboniferous throughout the Permian, with detached intra-basinal platforms (structural high on well site 7229/11-1) that became attached to the ramp during the deposition of the transgressive Bjarmeland Group.

A point that is generally accepted is the presence of an arched-like platform margin active during the deposition of the Gipsdalen Group, revealed by seismic profiles and partially controlled by the inherited NW-SE lineaments. The E-W trend of the margin and its approximate position across the platform (Figure 4.9A) is given by considering the southern depositional limit of the Gzhelian-Asselian lowstand evaporitic sequences of the Nordkapp

Basin, pinching out on the margin itself (Gérard and Buhrig, 1990; Bruce & Toomey 1993; Gudlaugsson et al., 1998; Ehrenberg et al., 1998a; Colpaert et al., 2007). Similarly, the overall distribution of the late Sakmarian–Artinskian heterozoan buildup complexes of the Polarrev Formation (Bjarmeland Group) has been seismically mapped within the Finnmark domain (Gudlaugsson et al., 1998; Ehrenberg et al., 1998a). Their southern limit is mostly placed slightly basinward of the Gzhelian–Asselian basinal evaporites and follow nearly the same lineaments along the platform (Figure 4.9B).

Therefore, the main keys to delineate a reliable development of the Finnmark Platform depositional profile through time, together with the information from the facies analyses, could be given by considering i): the location of the buildups across the platform, their forming-biota and shape variation across the Gipsdalen and Bjarmeland Groups; ii) the position of the margin and its evolution in terms of depth and morphology. These points have certainly a strong implication on assessing the geometry of the Finnmark Platform because, according with the classical models of the carbonate sedimentology, a shallow marginal barrier would point to a flat-topped platform whereas an offshore deeper margin to a distally steepened ramp profile (Read, 1985; Pomar, 2001 and references therein).

Previous and current cores analyses from the wells 7128/6-1, 7128/4-1 and the shallow cores (Bugge et al., 1995; Ehrenberg et al., 1998a; Ehrenberg et al. 2000b) have assessed that during the deposition of the Ørn Formation (Gzhelian-Asselian) the proximal platform areas were characterized by presence of proximal scattered (up to 6 m) bio-constructions dominated by *Palaeoaplysina*-phylloid algae and subordinate corals. These bodies likely had a tabular and laterally extended (>100 m-wide) morphology, highlighted by multi-attribute analyses in the proximal areas of the 3D cube ST9802 (Figure 4.1B for location). Cyclic subaerial exposures bounding the buildup bodies in the proximal domains suggest the reduced accommodation space as the main factors limiting their vertical growth, favoring in turn their lateral expansion (Stemmerik et al., 1999; Colpaert et al., 2007).

On the other hand, seismic-scale mounded features within the Ørn Formation interval have been observed and interpreted as buildups along the marginal domains of the platform and structural highs (Samuelsberg et al., 2003; Colpaert et al., 2007; Rafaelsen et al., 2008). However, a precise assessment of such buildups is strongly limited by the lack of cored sequences through the observed mounded features. An example of potential seismic marginal buildups developing during the Gipsdalen Group has been shown in the distal part of the 3D seismic cube ST9802. In these areas, Colpaert et al. (2007) developed a seismic sequence stratigraphic model integrating multi-attribute analysis and inverted impedance data. They interpreted Asselian seismic scale mounded structures as transgressive/highstand polygonal buildup complexes (top SU2, Base Asselian Horizon), as well as km-long complex (top SU3, below the UAH) associated to a platform barrier. Hence, according to their interpretation, starting from the early Asselian (SU2-SU3 seismic units) the system evolved as a rimmed platform with a prograding margin and a slope (up to 400 m-high), on which the lowstand basinal evaporites pinched out. Subsequently, on top of the mid Sakmarian Horizon (MSH), the transgressive sequence corresponding to the lower part of the Bjarmeland Group (Figure 4.3) led to retrogradation of the margin and development of a restricted heterozoan platform with stacked bryozoan-*Tubiphytes* buildup complexes on the slope. The 2D seismic sequence stratigraphic interpretation of the marginal platform area (Figure 10B) from the studied line shows, similarly to Colpaert et al. (2007), a carbonate system prograding during highstand phases the of the third-order depositional sequences S-3 and S-4, bounded by MGH, UAH and MSH. Seismic scale mounded buildup-like morphologies can be also recognized on the margin and the slope areas between MGH and UAH.

With the available data it is not possible to assess the nature of the biotic associations making up the marginal buildups during the deposition of the Ørn Formation, which would mainly

depend on the dominant paleoecologic settings favoring certain reef-builders more than others. It has been suggested so far that also the marginal and distal/deeper buildup assemblages were dominated by *Palaeoaplysina* and phylloid algae associations, similar to the outcropping stacked complex observed in the Kapp Dunér Formation in Bjørnøya (Lønøy, 1988; Stemmerik et al., 1994; Stemmerik and Worsley, 2005). However, according with the facies study proposed here, during the deposition of the Ørn Formation the Finnmark offshore environments were characterized by heterozoan assemblages (Figure 4.8) and therefore we cannot exclude that deep bryozoan-*Tubiphytes* buildups/mounds developed on the Finnmark platform also during the Gzhelian-Asselian time, prior to the formation of the facies-equivalent and much thicker (Colpaert et al., 2007; Rafaelsen et al., 2008) overlying complexes of the Bjarmeland Group (described in the distal well 7229/11-1). This possibility is further supported by the light-dependent nature of the *Palaeoaplysina*-phylloid algae buildups and their frequent associated fauna, commonly thriving in the shallowest platform domains (inner to middle ramps). Similarly, a depth-related change in biotic buildups composition at tropical-subtropical latitudes, from the shallow *Palaeoaplysina*-phylloid algae to the deeper bryozoan-dominated buildups has been observed during the Asselian-Sakmarian of the Sverdrup Basin (Beauchamp, 1993; Beauchamp and Desrochers, 1997) and during the early Carboniferous (Moscovian) of the north Greenland (Stemmerik, 2003). In the second area, buildups dominated by bryozoans and associated heterozoan fauna have been placed around the lower limit of the photic zone.

Hence, on the base of these assumptions and from the large-scale view of the studied seismic line (Figure 4.10A), the Finnmark Platform geometry of the eastern areas during the deposition of the Ørn Formation can be assimilated to a wide (>100 km) distally steepened ramp (Figure 4.10A). We suggest that the carbonate system was gently grading toward the offshore domains where a subtidal margin/slope system (below the SWWB) was associated with the development of seismic scale heterozoan-dominated buildups during transgressive–highstand phases (Figure 4.10C), favored by accommodation rates (due to the coupled effect of eustacy and subsidence rates) greater than in the most proximal platform areas. Hence, it can be assumed that during the deposition of the Ørn Formation, while the shallowest ramp domains were dominated by peritidal m-scale cycles capped by subaerial exposures with possible formation of structurally-controlled lowstand evaporitic deposits within structural saddles (Samuelsberg et al., 2003), the distal depositional areas were mostly sites of subtidal cyclicity and more open circulation. Similarly, Stemmerik (2008) affirms that on the Finnmark domain and during the deposition of the Ørn Formation: "most deposition seems to have taken place in deeper-water, mid- and outer-shelf environments". In fact, contrarily to what is observed in the proximal domains, the stacked nature of the distal buildups forming seismically recognizable features should clearly point to the presence of a greater available space during transgressive and highstand phases.

With the deposition of the Bjarmeland Group and the instauration of the Bryonoderm sedimentation mode, heterozoan buildups developed almost across the whole ramp. In the most proximal domains, the presence of heterozoan bio-constructions below the seismic resolution cannot be excluded. However, they have not been observed, nor in the cored intervals of the well 7128/6-1 (Figure 4.3) neither in the coeval shallow cores (Ehrenberg et al. 2000b). In the distal shelf areas close to the margin, composition and shape of the heterozoan buildup complexes of the Polarrev Formation are well known from the well 7229/11-1 (Blendinger et al., 1997; Stemmerik, 1997) and from detailed 3D seismic interpretations (Rafaelsen et al. 2008; Colpaert et al. 2007). They are dominated by bryozoan-*Tubiphytes* framestones and stromatactis mud-wackestones forming mounds and ridges of 350–1500 m-wide, more than 27 km-long and up to 325 m-high. Their approximate trend along the Finnmark Platform is shown in Figure 4.9.

The seismic interpretation of the line 213, also supported by the interpretation of Colpaert et al. (2007) shows that the heterozoan buildups complexes of the Polarrev Formation developed between MSH and BKH in a slightly distal position with respect to the offshore margin of the underlying prograding distally steepened ramp (see Figure 4.9). Onlap reflectors on top of MSH are associated with the major transgressive Sakmarian depositional phase of the Bjarmeland Group, causing the stepwise reduction of the preexistent slope gradient (Figure 4.10B, C). Therefore, we suggest that the shift to the Bjarmeland Group possibly led to the instauration of a heterozoan homoclinal ramp, devoid of a clear subtidal margin/slope system and gently grading toward the Nordkapp Basin. Huge heterozoan buildup complexes developed in the outer ramp growing on the seafloor and along topographic/structural reliefs as isolated mounds and polygonal ridges, supported by optimal ecological conditions, coupled with the ongoing tectonic subsidence and eustatic sea-level rise. In fact, after the Sakmarian major flooding and according with the current paleoceanographic/paleoclimatic scenario, the increased accommodation, lowering of the seawater temperatures and enhanced trophic levels created the best conditions for the heterozoan biota to create the observed mounded belt across the offshore late Sakmarian-late Asselian Finnmark environments (Figure 4.10B, C). As shown by the studied seismic line and other available seismic interpretations (Samuelsberg et al., 2003; Colpaert et al., 2007; Rafaelsen et al., 2008), the Bjarmeland transgressive interval on top of the MSH draped the Ørn Formation derived-morphologies resulting in the persistence of an overall ramp profile landward of the marginal areas. Later, following the late Sakmarian MFS, the ramp morphologies possibly became further smoothed due to the progradational cover of the shallowest grainy facies of the Isbjørn Formation above the buildup complexes, as also observed in the cored sequences of the well 7229/11-1 (Blendinger et al., 1998).

4.5.3 Implication for hydrocarbon prospectivity

The here described interplay between climatic/oceanographic factors across the Upper Carboniferous-Lower Permian and the resulting major biotic turnover and large-scale geometries strongly influenced the depositional history of the Finnmark Platform with major influences on the development of potential Paleozoic plays in the areas. Core-based reservoir models and diagenetic studies (Ehrenberg et al., 1998b; Stemmerik, 1999) from the well 7128/6-1 indicate the Ørn Formation as characterized by many high (primary and secondary) porosity intervals, given by a combination of different favorable factors as dolomitization and meteoric leaching of the metastable aragonitic skeletals, associated with high amplitude/frequency sea-level fluctuations. Such features led considering the Chloroforam shallow domains and the *Palaeoaplysina*-phylloid buildups of the Gipsdalen Group as the best potential reservoirs of the Barents Sea area (Stemmerik, 1999; Stemmerik and Worsley, 2005). On the other hand, the subtidal Isbjørn Formation carbonates and buildup complexes show very low porosities and are considered non-prospective, due to the overall stable mineralogy of its biotic components (low-Mg calcite) and the common presence of silty-clayey horizons favoring dissolution and calcite cementation through stylolites. Therefore, assuming the platform profile as a distally steepened ramp rather than a flat-topped platform during the deposition of the Ørn Formation will have important implications on assessing the lateral extension of the areas affected by subaerial exposure and more prone to develop secondary porosity, and therefore more prospective in terms of potential reservoir interval. This represents a key point to take in account when planning future exploration in the eastern Finnmark domains and in other buried land-attached Paleozoic carbonate depositional systems along the Arctic epicontinental shelf.
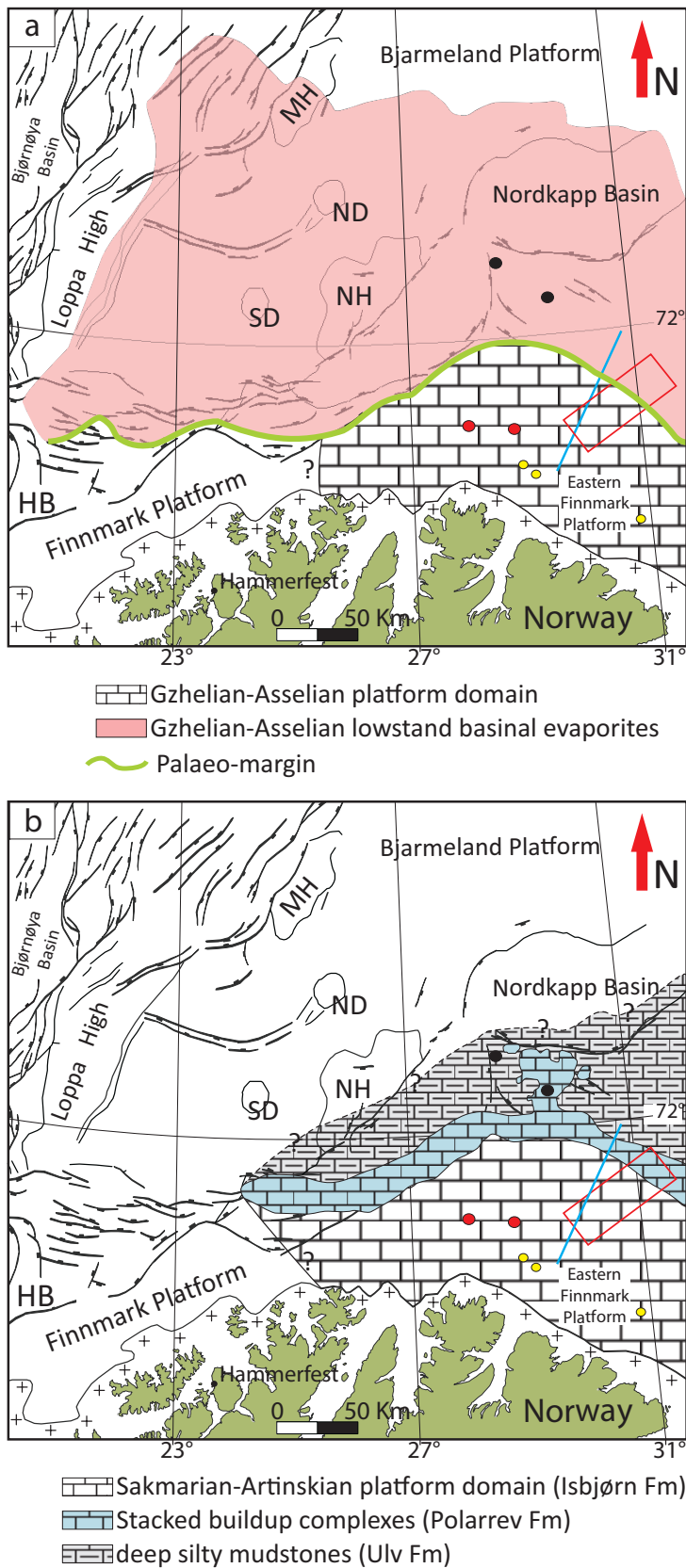
Figure 4.9. a) Gzhelian-Asselian large-scale facies map showing the limit of the subtidal evaporites of the Nordkapp Basin (anhydrite and halite sequences cored from the wells 7228/9-1 S and 7229/11-1). The southern limit (in red) marks the approximate position of the palaeo-margin at the Finnmark Platform/Nordkapp Basin transition. B) Sakmarian–Artinskian large scale facies map of the Finnmark domain showing the seismically-interpreted large-scale distribution of the Sakmarian-Artinskian stacked heterozoan buildup complexes. Modified after Gudlaugsson et al. (1998).

91
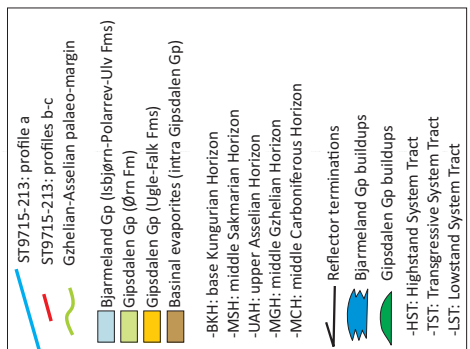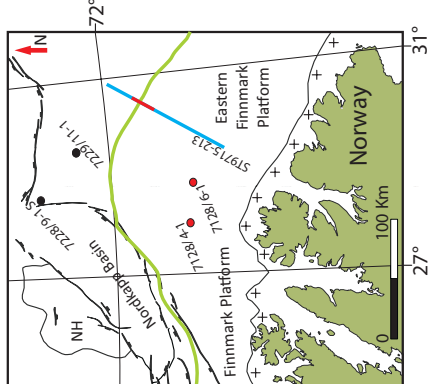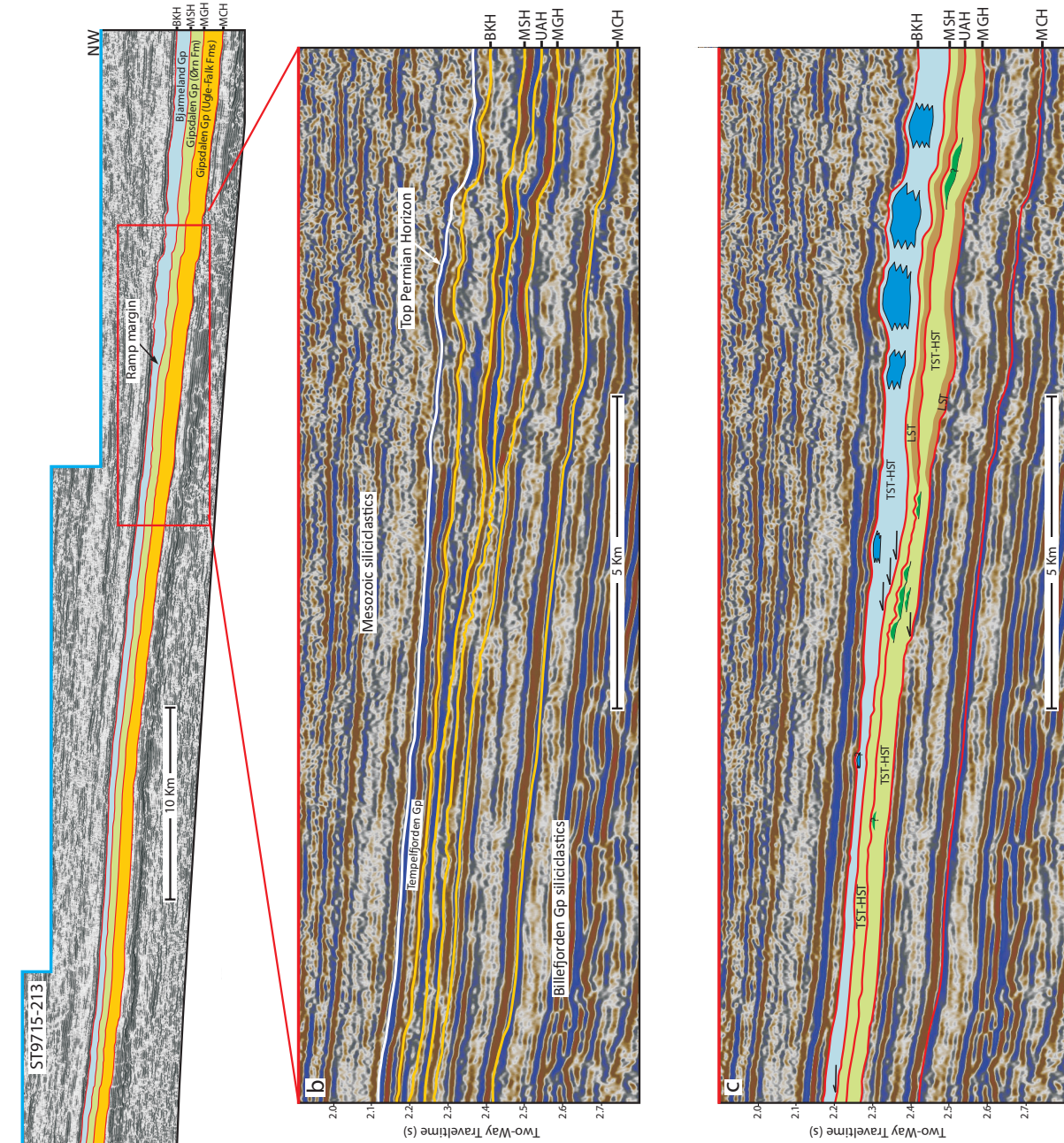
Figure 4.10. Seismic interpretation of the 2D line ST9715-213. a) Large scale view of the seismic line across the SE-NW profile of the eastern Finnmark Platform and the seismic intervals corresponding to the entire Gipsdalen Group and Bjarmeland Group. The line covers approximately 97 km in length. b) Seismic profile showing the five selected horizons discussed in the text (in yellow) and the top Permian horizon (in white), across the marginal platform area. c) Seismic sequence stratigraphic model derived from profile b, showing the Finnmark platform evolution of the marginal geometries across the Gipsdalen and Bjarmeland Group transition. Note the change from a distally steepened ramp (Ørn Formation) to homoclinal (Bjarmeland Group) profile. See text for the detailed discussion.

4.6 Conclusions

- Facies analysis of the uppermost Ørn Formation (Gipsdalen Group) from the cores 7128/6-1 and 7128/4-1 of the Finnmark Platform domain reveals that during Asselian-early Sakmarian time the shallowest inner ramp depositional environments were dominated by a Chloroforam sedimentation mode and photozoan biota (as small benthic foraminifera, green algae, encrusting organisms, *Palaeoaplysina* and rugose corals forming buildup patches) Such communities were stepwise replaced toward the deeper and distal outer ramp environments by mixed Bryonoderm-extended (fusulinids, bryozoan, crinoids, *Palaeoaplysina*) and then heterozoan Bryonoderm assemblages (bryozoans, crinoids, brachiopods). According with the coeval paleoceanographic-paleoclimatic scenario across the Arctic domain during the deposition of the Ørn Formation (sub-/tropical latitudes of deposition, open connection and current circulation with the Tethyan tropical realm), we support, for this depth-related transition in carbonate factories, the hypothesis of the presence of a stratified water column and a stable thermocline, separating the photozoan biota thriving in shallow and warm waters from the heterozoan associations, well adapted to deeper and cooler mesotrophic waters.

- The shift from the Ørn (Gipsdalen Group) to the Isbjørn Formation (Bjarmeland Group) across the well 7128/6-1 reveals the full instauration of the Bryonoderm sedimentation mode on the Finnmark Platform starting from the middle-late Sakmarian. Transgressive heterozoan facies dominated by crinoids, bryozoans and brachiopods invaded also the proximal shallow shelf areas (before occupied by photozoan communities) favoring the installation of an open storm-dominated ramp. Such modifications of the Finnmark Platform depositional style in favor of the heterozoan communities were driven by the evolution of climatic-oceanographic Arctic scenario (melting phases of the Gondwanan icecaps, cooling due to drifting to temperate latitudes, closure of the connections with the Tethyan realm) that led to the disruption of the thermocline with consequent influx of nutrient-rich cool waters across the Finnmark domain from the Panthalassic realm.

- Facies and paleoenvironmental analyses (supported by 3D seismic interpretations), suggest that during the deposition of the Ørn Formation (Gipsdalen Group), *Palaeoaplysina*, phylloid algae and rugose corals were responsible for the formation of m-scale buildup patches within the inner to middle ramp environments, whereas the still unexplored mounded seismic features observed offshore, along the subtidal margin/slope system of the distally steepened ramp, could have been formed by the heterozoan communities, following the observed depth-related shift from chloroforam to bryonoderm sedimentation mode. Following the middle Sakmarian transgression and the shift to a heterozoan homoclinal ramp profile, the observed bryozoan-*Tubiphytes* stacked buildup complexes developed along the outer ramp domains.

- On the base of our seismic interpretation across the eastern platform profile, coupled with the facies and paleoenvironmental analysis, we suggest that the eastern Finnmark large scale geometry changed from a distally steepened ramp to homoclinal ramp, following the ongoing climatic-oceanographic modifications and the consequent shift between the two major depositional phases represented by the Gipsdalen and the Bjarmeland Groups. According with the presence of high frequency/amplitude glacio-eustatic fluctuations, it can be assumed that during the deposition of the Gipsdalen Group the proximal ramp domains were cyclically subaerially exposed, whereas in the outer ramp a subtidal cyclicity was more persistent. At the same time, major phases of restriction and isolation of the Nordkapp basin led to the deposition of the observed subtidal evaporitic sequences pinching out on the distally-steepened ramp slope.

- Given the good reservoir properties of the Gzhelian–Sakmarian Gipsdalen Group within the Finnmark depositional domain and the whole Norwegian Barents Sea area, the assessment of changes in the platform depositional profile as described here, across the observed regional shifts in sedimentation modes, represents a fundamental point to consider for future exploration purposes, due to the impact it has on the reservoir properties.

5

GENERAL CONCLUSIONS

The upper Paleozoic sedimentary succession buried in the subsurface of the Barents Sea represents a case of mixed siliciclastic-carbonate sedimentation, which deposited in extensional settings during the North Atlantic rifting and experienced a coeval northward drift in paleolatitudinal position related with the northward movement of the northern margin of Pangaea. In this study, a multidisciplinary analysis based on the integration of conventional seismic interpretation, 3D multi-attribute seismic facies classification, seismic sequence stratigraphy, and core analysis allowed the investigation of the basin infill evolution in the Loppa High and Finnmark Platform areas with focus in the deposition of the upper Palaeozoic deposits.

First, the integration of core data, seismic interpretation, and seismic facies classification, allowed the characterization of a buried paleokarst terrain and other sedimentary unconformities among the upper Paleozoic sedimentary package of the Loppa High area. The Loppa High is one of several half-graben structures, which resulted from the North Atlantic rifting during the late Paleozoic. The core data, obtained from a well (7220/6-1) located at the crest of the Loppa High structure, showed breccia-dominated deposits that were interpreted to have formed by cave developments followed by cave collapses in an evolving karst system. The 3D multi-attribute seismic facies classification permitted both the identification and the estimation of the volume occupied by the seismic facies related with the breccia deposits as well as the observation of several sedimentary unconformities within the studied interval. The spatial extent of the breccia-dominated deposits, of approximately 12 km in width, 46 km in length, and reaching thicknesses of up to 150 m, suggests that such deposits show evidence of an extensive coalesced collapsed paleocave system. The cave forming processes were interpreted as being produced by dissolution of evaporitic rocks additionally to carbonates rocks, as observed within the outcrop analogues of the Billefjorden Trough (central Spitsbergen area).

Second, the late Paleozoic palaeogeography, for key time intervals, in the Loppa High area was reconstructed by means of a detailed seismic sequence stratigraphic analysis combined with core analysis from two additional wells (7120/2-1 and 7121/1-1). From the Viséan to the middle Moscovian the Loppa High was dominated by continental deposition characterized by alluvial, fluvial, and probably lacustrine deposits that were gradually replaced by marine deposits, dominated by carbonates, as the sea transgressed on the Loppa High from the east. The subsequent Kasimovian period was characterized by the accumulation of evaporites in both shallow and deep environments. During the Gzhelian to the late Artinskian biogenic carbonate deposition dominated. Overall, two main phases are recognized: (1) from the late Moscovian to the late Asselian, the warm-water carbonate factories governed the biotic associations and formed coeval depositional margins with different depositional styles in both the hanging wall and footwall of the half-graben; (2) from the mid-Sakmarian to the late Artinskian, cool-water carbonates dominated biotic associations and developed stacked build-ups either ontop pre-existing structural highs or within distal basinal areas. Finally, in the late Permian, from the Kungurian to the Urzhumian, the biogenic production changed to the siliciclastic domain including fine-grained siliciclastics, silicified skeletal limestones, and abundant chert with abundance of sponge spicules. The data integration and interpretation suggest that the overall 3D morphology of the seismic sequences in the Loppa High were mainly controlled by tectonic rotation and uplift of the half-graben, although smaller-scale variability within each sequence, reflected by the changes of biotic assemblages as well as the

facies dynamics, were probably controlled by global sea-level oscillations and climatic changes.

Third, the Finnmark platform area, located around 200 km to the east of the Loppa High area, was investigated using core analysis of two exploration wells (7128/4-1 and 7128/6-1) as well as the interpretation of a key 2D seismic section located along the depositional profile. Facies analysis of the uppermost Ørn Formation of the Gipsdalen Group revealed that during the Asselian to the early Sakmarian the shallowest inner ramp depositional environments were dominated by a Chloroforam sedimentation and photozoan biota, including small benthic foraminifera, green algae, encrusting organisms, *Palaeoaplysina*, and rugose corals forming buildup patches. Mixed Bryonoderm-extended assemblages, dominated by bryozoans, crinoids and brachiopods, characterizing deeper and distal outer ramp environments, gradually replaced them. We interpreted this synchronous transition of carbonate factories as reflecting a stratified water column and a stable thermocline, separating the photozoan biota thriving in shallow and warm waters from the heterozoan biota in deeper and cooler mesotrophic waters. The geometrical change in platform morphology, observed along the depositional profile, in the boundary between the Ørn and Isbjørn formations, is suggested to represent a change from a distally steepened ramp to a homoclinal ramp. This geometrical change may reflect the establishment of a Bryonoderm sedimentation on the Finnmark Platform starting from the middle to late Sakmarian, which favored the formation of an open storm-dominated ramp. Given the good reservoir properties of the Gzhelian–Sakmarian sedimentary successions within the Finnmark depositional domain and the whole Norwegian Barents Sea area, the assessment of such changes in the platform depositional profile as described here, may represent a fundamental point to consider for future exploration purposes.

BIBLIOGRAPHY

Ahlborn, M., Stemmerik, L., and Kalst√∏, T.-K., 2014, 3D seismic analysis of karstified interbedded carbonates and evaporites, Lower Permian Gipsdalen Group, Loppa High, southwestern Barents Sea: Marine and Petroleum Geology, v. 56, no. 0, p. 16-33.

Alsgaard, P. C., El-Tablawy, M., Foss, K. O., Johannesen, J., Millen, R., and Moreton, D., 1987, Geological completion report - Well 7121/1-1: Esso Norge a.s.

Baaske, U. P., Mutti, M., Baioni, F., Bertozzi, G., and Naini, M. A., 2007, Using multi-attribute neural networks classification for seismic carbonate facies mapping: a workflow example from mid-Cretaceous Persian Gulf deposits, *in* Davies, R. J., Posamentier, H. W., Wood, L. J., and Cartwright, J. A., eds., Seismic Geomorphology: Application to Hydrocarbons Exploration and Production: London, Geological Society, Special Publication 277, p. 105-120.

Banchs, R. E., and Michelena, R. J., 2002, From 3D seismic atrributes to pseudo-well-log volumes using neural networks: Practical considerations: The Leading Edge, v. 21, no. 10, p. 996-1001.

Barnes, A. E., 1993, Instantaneous spectral bandwidth and dominant frequency with applications to seismic reflection data: Geophysics, v. 58, no. 3, p. 419-428.

Barnes, A. E., 2001, Seismic attributes in your facies: CSEG Recorder Canadian Society of Exploration Geophysicists, v. 26, no. 7.

Barnes, A. E., 2007, Redundant and useless seismic attributes: Geophysics, v. 72, no. 3, p. 33-38.

Beauchamp, B., 1993, Carboniferous and Permian reefs of the Sverdrup Basin, Canadian Arctic Islands, *in* Vorren, T. O., Bergsager, E., Dahl-Stamnes, Ø. A., Holter, E., Johansen, B., Lie, E., and Lund, T. B., eds., Arctic Geology and Petroleum Potential, Volume Norwegian Petroleum Society Special Publication 2: Amsterdam, Elsevier, p. 217-241.

Beauchamp, B., 1994, Permian climatic cooling in the Canadian Arctic: Geological Society of America Special Papers, v. 288, p. 229-246.

Beauchamp, B., and Desrochers, A., 1997, Permian warm- to very cold-water carbonates and chert in the Sverdrup Basin-Barents Sea area, northwestern Pangaea, *in* James, N. P., and Clarke, J. A. D., eds., Cool-water carbonates, Volume 56, Society of Economic Paleontologist and Mineralogist Special Publication 56, p. 349-364.

Beauchamp, B., Harrison, J., Utting, J., Brent, T. A., and Pinard, S., 2001, Carboniferous and Permian subsurface stratigraphy, Prince Patrick Island, Northwest Territories, Canadian Arctic, Geological Survey of Canada Bulletin.

Beauchamp, B., and Baud, A., 2002, Growth and demise of Permian biogenic chert along northwest Pangea: evidence for end-Permian collapse of thermohaline circulation: Palaeogeography, Palaeoclimatology, Palaeoecology, v. 184, no. 1-2, p. 37-63.

Bjørkesett, S. S., 2009, Late Paleozoic-Triassic evolution of the paleo-Loppa High, linked to tectonic events and depositional patterns [Master Thesis: University of Oslo, 1-103 p.

Blendinger, W., Bowlin, B., Zijp, F. R., Darke, G., and Ekroll, M., 1997, Carbonate buildup flank deposits: An example from the Permian (Barents Sea, northern Norway) challenges classical facies models: Sedimentary Geology, v. 112, no. 1-2, p. 89-103.

Blomeier, D., C. Scheibner, and H. Forke, 2009, Facies arrangement and cyclostratigraphic architecture of a shallow-marine, warm-water carbonate platform: the Late Carboniferous Ny Friesland Platform in eastern Spitsbergen (Pyefjellet Beds, Wordiekammen Formation, Gipsdalen Group), Facies, v. 55, p. 291–324.

Blomeier, D., D. Carmohn, H. Forke, and C. Scheibner, 2011, Environmental change in the Early Permian of Spitsbergen: from a warm-water carbonate platform (Gipshuken

Formation) to a temperate, mixed siliciclastic-carbonate ramp (Kapp Starostin Formation): Facies, v. 57, 493–523.

Bosence, D., Cross, N., and Hardy, S., 1998, Architecture and depositional sequences of Tertiary fault-block carbonate platforms; an analysis from outcrop (Miocene, Gulf of Suez) and computer modelling: Marine and Petroleum Geology v. 15, no. 3, p. 203-221

Bosence, D., 2005, A genetic classification of carbonate platforms based on their basinal and tectonic settings in the Cenozoic: Sedimentary Geology, v. 175, no. 1-4, p. 49-72.

Brachert, T. C., Krautworst, U. M. R., and Stueckrad, O. M., 2002, Tectono-climatic evolution of a Neogene intramontane basin (Late Miocene Carboneras subbasin, southeast Spain): revelations from basin mapping and biofacies analysis: Basin Research, v. 14, no. 4, p. 503-521.

Brown, A. R., 1996, Seismic attributes and their classification: The Leading Edge, v. 15, no. 10, p. 1090.

Breuninger, R. H., Canter, K. L., and P. E. Isaacson, 1989, Pennsylvanian–Permian Palaeoaplysina and algal buildups, Snaky Canyon Formation, East-Central Idaho, U.S.A., in H. H. J. Geldsetzer, N. P. James, and G. E. Tebbutt, eds., Reefs, Canada and Adjacent Areas: Canadian Society of Petroleum Geology, Memoir, 13, p. 631–637.

Bugge, T., and Fanavoll, S., 1995, The Svalis Dome, Barents Sea a geological playground for shallow stratigraphic drilling First Break, v. 13, p. 237-251.

Bugge, T., Mangerud, G., Elvebakk, G., Mørk, A., Nilsson, I., Fanavoll, S., and Vigran, J. O., 1995, The Upper Palaeozoic succession on the Finnmark Platform, Barents Sea: Norsk Geologisk Tidsskift, v. 75, p. 3-30.

Bugge, T., G. Elvebakk, S. Fanavoll, G. Mangerund, M. Smelror, H. M. Weiss, J. Gjelberg, S. E. Kristensen, and K. Nilsen, 2002, Shallow stratigraphic drilling applied in hydrocarbon exploration of the Nordkapp Basin, Barents Sea: Marine and Petroleum Geology, v. 19, p. 13–37.

Burchette, T. P., 1988, Tectonic control on carbonate platform facies distribution and sequence development: Miocene, Gulf of Suez: Sedimentary Geology, v. 59, no. 3–4, p. 179-204.

Butler, G.P., 1970, Holocene gypsum and anhydrite of the Abu Dhabi Sabkha, Trucial Coast: an alternative explanation of origin: Third Symposium on Salt, p. 120–152.

Canter, K. L., Stearns, D. B., Geesaman, R. C., and Wilson, J. L., 1993, Paleostructural and related paleokarst controls on reservoir development in the Lower Ordovician Ellenburger Group, Val Verde basin, in Fritz, R. D., Wilson, J. L., and Yurewicz, D. A., eds., Paleokarst related hydrocarbons reservoirs SEPM Core Workshop 18, p. 61-99.

Carr, M., Cooper, R., Smith, M., Taner, M. T., and Taylor, G., 2001, Instantaneous spectral bandwidth and dominant frequencywith applications to seismic reflection data: Rock Solid Images, http://www.rocksolidimages.com.

Carrillat, A., Hunt, D., Randen, T., Sonneland, L., and Elvebakk, G., 2005, Automated mapping of carbonate build-ups and paleokarst from the Norwegian Barents Sea using 3D seismic texture attributes, in Doré, A. G., and Vining, B. A., eds., Petroleum Geology: North-West Europe and Global Perspectives, Proceedings of the 6th Petroleum Geology Conference: London, Geological Society, p. 1595-1611.

Cecchi, M., 1993, Carbonate sequence stratigraphy: application to the determination of play-models in the Upper Paleozoic succession of the Barents Sea, offshore northern Norway, in Vorren, T. O., Bergsager, E., Dahl-Stamnes, Ø. A., Holter, E., Johansen,

B., Lie, E., and Lund, T. B., eds., Arctic Geology and Petroleum Potential, Volume Norwegian Petrol. Soc. Spec. Publ. No. 2: Amsterdam, Elsevier, p. 419-438.

Chen, Q., and Sidney, S., 1997, Seismic attribute technology for reservoir forecasting and monitoring: The Leading Edge, v. 16, no. 5, p. 445-448.

Chopra, S., and Marfurt, K. J., 2007, Attribute Expression of Carbonate Depositional Environments, *in* Chopra, S., Marfurt, K. J., and Hill, S. J., eds., Seismic Attributes for Prospect Identification and Reservoir Characterization, Volume 11: Tulsa, SEG Geophysical Developments Series.

Ciarapica, G., L. Passeri, and C. B. Schreiber, 1985, Una proposta di classificazione delle evaporiti solfatiche: Geologica Romana, v. 24, p. 219–232.

Coleou, T., Poupon, M., and Azbel, K., 2003, Interpreter's Corner---Unsupervised seismic facies classification: A review and comparison of techniques and implementation: The Leading Edge, v. 22, no. 10, p. 942-953.

Coléou, T., Poupon, M., and Azbel, K., 2003, Unsupervised seismic facies classification: A review and comparison of techniques and implementation: The Leading Edge, v. 22, no. 10, p. 942-953.

Colpaert, A., Pickard, N., Mienert, J., Henriksen, L. B., Rafaelsen, B., and Andreassen, K., 2007, 3D seismic analysis of an upper palaeozoic carbonate succession of the Eastern Finnmark Platform area, Norwegian Barents Sea: Sedimentary Geology, v. 197, no. 1-2, p. 79-98.

Corradi, A., Ruffo, P., Corrao, A., and Visentin, C., 2009, 3D hydrocarbon migration by percolation technique in an alternate sand-shale environment described by a seismic facies classified volume: Marine and Petroleum Geology, v. 26, no. 4, p. 495-503.

Cross, N., Purser, B. H., and Bosence, D., 1998, The tectono-sedimentary evolution of a rift margin carbonate platform: Abu Shaar, Gulf of Suez, Egypt, *in* Purser, B. H., and Bosence, D., eds., Sedimentary and tectonic evolution of rift basins—the Red Sea–Gulf of Aden: Amsterdam, Chapman Hall-Kluwers, p. 95-271.

Curl, R. L., 1986, Fractal dimensions and geometries of caves: Mathematical Geology, v. 18, p. 765-783.

Dallmann, W. K., 1999, Lithostratigraphic lexicon of Svalbard: review and recommendations for nomenclature use: Upper Palaeozoic to Quaternary bedrock, Norsk Polarinstitut.

Davies, G. R., 1971, A Permian hydrozoan mound Yukon Territory. Canadian Journal of Earth Sciences, v. 8, p. 973–988.

Davies, G. R., 1989, Lower Permian Palaeoaplysinid mound, northern Yukon, Canada, in H. H. J. Geldsetzer, N. P. James, and G. E. Tebbutt, eds, Reefs, Canada and Adjacent Areas: Canadian Society of Petroleum Geology, Memoir, 13, p. 638–642.

DeHass, R. J., and Jones, M. W., 1989, Cave levels of the Trenton-Black River formations in central southern Michigan, *in* Keith, B. D., ed., The Trenton Group (Upper Ordovician Series) of eastern North America, Volume 29, AAPG Studies in Geology, p. 237-266.

Dengo, C. A., and Røssland, K. G., 1992, Extensional tectonic history of the western Barents Sea, *in* Larsen, R. M., Brekke, H., T., L. B., and Talleraas, E., eds., Structural and Tectonic Modelling and its Application to Petroleum Geology, Volume 1: Amsterdam, Norwegian Petroleum Society Special Publication, p. 91-107.

Doré, A. G., 1991, The structuralfoundation and evolution of Mesozoic seaways between Europe and the Arctic: Palaeogeography, Palaeoclimatology, Palaeoecology, v. 87, no. 1-4, p. 441-492.

Edison, 2011, Reservoir evaluation of well 7220/6-1 of the Loppa High. Internal report.

Ehrenberg, S. N., Nielsen, E. B., Svånå, T. A., and Stemmerik, L., 1998a, Depositional evolution of the Finnmark carbonate platform, Barents Sea: results from wells 7128/6-1 and 7128/4-1: Norsk Geologisk Tidsskrift, v. 78, no. 3, p. 185-224.

Ehrenberg, S. N., Nielsen, E. B., Svånå, T. A., and Stemmerik, L., 1998b, Diagenesis and reservoir quality of the Finnmark carbonate platform, Barents Sea: results from wells 7128/6-1 and 7128/4-1: Norsk Geologisk Tidsskrift, v. 78, p. 225–252.

Ehrenberg, S. N., Pickard, N., Svånå, T. A., Nilsson, I., and Davydov, V. I., 2000, Sequence stratigraphy of the inner Finnmark carbonate platform (Carboniferous-Permian), Barents Sea - correlation between well 7128/6-1 and the shallow IKU cores: Norsk Geologisk Tidsskrift, v. 80, p. 129-162.

Ehrenberg, S. N., Pickard, N., Henriksen, L. B., Svånå, T. A., Gutteridge, P., and McDonald, D., 2001, A depositional and sequence stratigraphic model for cold-water, spiculitic strata based on the Kapp Starostin Formation (Permian) of Spitsbergen and equivalent deposits from the Barents Sea: AAPG Bulletin, v. 85, p. 2061–2087.

Eliassen, A., and Talbot, M. R., 2005, Solution-collapse breccias of the Minkinfjellet and Wordiekammen Formations, Central Spitsbergen, Svalbard: a large gypsum palaeokarst system: Sedimentology, v. 52, no. 4, p. 775-794.

Elvebakk, G., 2003, Upper Carboniferous-Lower Permian Gipsdalen Group karstified reservoir carbonates of the Loppa High, Barents Sea; reservoir potential and drilling challenges, p. 1-4.

Elvebakk, G., Hogstad, K., Hunt, D., Pajchel, K., Rafaelsen, B., and Robak, H., Upper Carboniferous-Lower Permian Gipsdalen Group karstified reservoir carbonates of the Loppa High, Barents Sea; reservoir potential and drilling challenges *in* Proceedings Conference on Petroleum exploration and production in environmentally sensitive areas, Ålesund, 2003.

Elvebakk, G., Hunt, D. W., and Stemmerik, L., 2002, From isolated buildups to buildup mosaics: 3D seismic sheds new light on Upper Carboniferous–Permian fault controlled carbonate buildups, Norwegian Barents Sea: Sedimentary Geology, v. 152, no. 1, p. 7-17.

Entzminger, D. J., and Loucks, R. G., 1992, Paleocave reservoirs in the Wristen Formation at Emerald field, Gaines-Yoakum counties, Texas, *in* Candelaria, M. P., and Reed, C. L., eds., Paleokarst, karst related diagenesis and reservoir development: examples from Ordovician–Devonian age strata of west Texas and the mid-continent: Permian Basin Section, SEPM Publication 92-33, p. 126-130.

Esteban, M., 1991, Paleokarst: Pratical applications, *in* V.P. Wright, M. Esteban, and P.L. Smart, eds., Palaeokarsts and palaeokarstic reservoirs: Postgraduate Research for Sedimentology, University of Reading, PRIS Contribution 152, p. 89-119.

Faleide, J. I., Gudlaugsson, S. T., and Jacquart, G., 1984, Evolution of the western Barents Sea: Marine and Petroleum Geology, v. 1, p. 123-150.

Farzadi, P., 2006, Seismic facies analysis based on 3D multi-attribute volume classification, Dariyan Formation, SE Persian Gulf: Journal of Petroleum Geology, v. 29, no. 2, p. 159-173.

Farzadi, P., and Hesthammer, J., 2007, Diagnosis of the Upper Cretaceous palaeokarst and turbidite systems from the Iranian Persian Gulf using volume-based multiple seismic attribute analysis and pattern recognition: Petroleum Geoscience, v. 13, no. 3, p. 227-240.

Feazel, C., 2010, Using Modern Cave Systems as Analogs for Paleokarst Reservoirs, AAPG Search and Discovery Article #50252.

Fisher, G., Hunt, D., Colpaert, A., Wall, B., and Henderson, J., Comprehensive Karst Delineation from 3D Seismic Data, *in* Proceedings AAPG GEO 2010 Middle East, Bahrain, 2010.

Flügel, E., 2004, Microfacies of Carbonate Rocks, analysis, interpretation and application, Springer-Verlag, Berlin Heidelberg, 976 p.

Fokin, P. A., Nikishin, A. M., and Ziegler P. A., 2001, Peri-Uralian and Peri- Palaeo-Tethyan Rift systems of the East European Craton, in P. A. Ziegler, W. Cavazza, A. H. F. Robertson, and S. Crasquin-Soleau, eds., Peri-Tethys Memoir 6: Peri-Tethyan Rift/Wrench Basins and Passive Margins: Memoires du Museum National d'Histoire Naturelle, 186, p. 347–368.

Ford, D., and Williams, P., 2007, Karst Hydrogeology and Geomorphology, Chichester, John Wiley & Sons, Karst Hydrogeology and Geomorphology, 578 p.:

Ford, D. C., 1988, Characteristics of dissolutional cave system in carbonate rocks, *in* James, N. P., and Choquette, P. W., eds., Paleokarst: Berlin, Springer-Verlag, p. 25-57.

Forsythe, G. T., Wood, R., and Dickson, J. A., 2002, Mass spawning in ancient reef communities: Evidence from Late Paleozoic Phylloid Algae: Palaios, v. 17, p. 615–621.

Fritz, R. D., Wilson, J. L., and Yurewicz, D. A., Paleokarst Related Hydrocarbon Reservoirs, New Orleans, 1993, Volume Core Workshop 18 Society of Economic Paleontologist and Mineralogist, p. 275.

Gabrielsen, R. H., 1984, Long-lived fault zones and their influence on the tectonic development of the southwestern Barents Sea: Journal of the Geological Society, v. 141, no. 4, p. 651-662.

Gabrielsen, R. H., and Faerseth, R. B., 1989, The inner shelf of North Cape, Norway and its implications for the Barents Shelf-Finnmark Caledonide boundary. A comment: Norsk Geologisk Tidsskift, v. 69, p. 57-62.

Gabrielsen, R. H., Færseth, R. B., Jensen, L. N., Kalheim, J. E., and Riis, F., 1990, Structural elements of the Norwegian Continental Shelf. Part 1: The Barents Sea Region: Norwegian Petroleum Directorate Bulletin 6, p. 33.

Gastaldi, C., Biguenet, J. P., and De Pazzis, L., 1997, Reservoir characterization from seismic attributes: An example from the Peciko Field (Indonesia): The Leading Edge, v. 16, no. 3, p. 263-266.

Gérard, J., and Buhrig, C., 1990, Seismic facies of the Permian section of the Barents Shelf: analysis and interpretation: Marine and Petroleum Geology v. 7, no. 3, p. 234-252.

Gjelberg, J., Bugge-Johansen, K., and Steel, R. J., 1985, Core description and interpretation (cores 12-19) of Carboniferous clastic sequence well 7120/2-1, Loppa High: Norsk Hydro.

Gjelberg, J. G., 1981, Upper Devonian (Famennian)-Middle Carboniferous succession of Bjornoya: Norsk Polarinstitutt Skrifter, v. 174, p. 1-67.

Goldhammer, R. K., Oswald, E. J., and Dunn, P. A., 1991, Hierarchy of stratigraphic forcing: example From Middle Pennsylvanian shelf carbonates of the Paradox basin, in E. K. Franseen, W. L. Watney, C. G. Kendall, and W. Ross, eds., eds., Sedimentary modeling: Computer Simulations and Methods for Improved Parameter Definition, Kansas Geological Survey Bulletin, v. 233, p. 361–413.

Golonka, J., and Ford, D., 2000, Pangean (Late Carboniferous–Middle Jurassic) paleoenvironment and lithofacies: Palaeogeography, Palaeoclimatology, Palaeoecology, v. 161, no. 1, p. 1-34.

Granger, D. E., Fabel, D., and Palmer, A., 2001, Pliocene-Pleistocene incision of the Green River, Kentucky, determined from radioactive decay of 26Al and 10Be in Mammoth Cave sediments.: Geological Society of America Bulletin, v. 113, no. 7, p. 36-825.

Groves, J. R., and Wahlman, G. P., 1997, Biostratigraphy and evolution of Late Carboniferous and Early Permian smaller foraminifers from the Barents Sea (offshore Arctic Norway): Journal of Paleontology, v. 71, p. 758–779.

Gudlaugsson, S. T., Faleide, J. I., Johansen, S. E., and Breivik, A. J., 1998, Late Palaeozoic structural development of the South-western Barents Sea: Marine and Petroleum Geology, v. 15, no. 1, p. 73-102.

Gunn, J., 2004, Encyclopedia of Caves and Karst Science, New York & London, Fitzroy Dearborn.

Haq, B. U., and Schutter, S. R., 2008, A chronology of Paleozoic sea-level changes: Science, v. 322, no. 5898, p. 64-68.

Hardage, B. A., Carr, D. L., Lancaster, D. E., J. L. Simmons, J., Elphick, R. Y., Pendleton, V. M., and Johns, R. A., 1996, 3-D seismic evidence of the effects of carbonate karst collapse on overlying clastic stratigraphy and reservoir compartmentalization: Geophysics, v. 61, no. 5, p. 1336-1350.

Hart, B. S., and Balch, R. S., 2000, Approaches to defining reservoir physical properties from 3-D seismic attributes with limited well control: An example from the Jurassic Smackover Formation, Alabama: Geophysics, v. 65, no. 2, p. 368-376.

Hartz, E. H., Martin, M. W., Andresen, A., and Andersen, T. B., 2002, Volcanic rocks in the Devonian Solund Basin, Western Norway: large landslides of Silurian (439 Ma) rhyolites: Journal of the Geological Society, v. 159, no. 2, p. 121-128.

Herrera, V. M., Russell, B., and Flores, A., 2006, Neural networks in reservoir characterization: The Leading Edge, v. 25, no. 4, p. 402-411.

Heubeck, C., Story, K., Sullivan, C., and Duff, S., 2004, An integrated reservoir study of the Liuhua 11-1 field using a high-resolution three-dimensional seismic data set, *in* Eberli, G. P., Masaferro, J. L., and Sarg, J. F., eds., Seismic imaging of carbonate reservoirs and systems: Tulsa, The American Association of Petroleum Geologists & Shell International Exploration and Production B.V.,AAPG Memoir 81, p. 149-168.

Hopley, D., 1982, Geomorphology of the Great Barrier Reef: Quaternary development of coral reefs, New York, John Wiley - Interscience, John Wiley - Interscience, 453 p.

Hotelling, H., 1933, Analysis of a complex of statistical variables into principal components: Journal of Educational Psychology, v. 24, p. 417-441.

Hüneke, H., Joachimski, M., Buggisch, W., and Lützner, H., 2001, Marine carbonate facies in response to climate and nutrient level: the Upper Carboniferous and Permian of Central Spitsbergen (Svalbard), Facies, v. 45, p. 93–136.

Hunt, D., Elvebakk, G., Rafaelsen, B., Pajchel, K., Hogstad, K., Robak, H., and Randen, T., Paleokarst Recognition & 3D Distribution - New Insights from the Upper Paleozoic, Loppa High, Barents Sea, *in* Proceedings EAGE 65th Conference & Exhibition, Stavanger, 2 - 5 June 2003.

James, N. P., and Choquette, P. W., 1984, Diagenesis 9 -. Limestones - The Meteoric Diagenetic Environment: Geoscience Canada, v. 11, no. 4, p. 162-194.

James, N. P., Coniglio, M., Aissaoui, D. M., and Purser, B. H., 1988, Facies and geologic history of an exposed Miocene rift-margin carbonate platform; Gulf of Suez, Egypt: Aapg Bulletin, v. 72, no. 5, p. 555-572.

James, N. P., 1997, The cool-water carbonate depositional realm, in N. P. James and J. A. D. Clarke, eds., Cool-water carbonates: SEPM Special Publication 56, p. 1–20.

Jenyon, M. K., 1988, Seismic response to an evaporite/carbonate association: Carbonates and Evaporites, v. 2, no. 2, p. 89-93.

Jolliffe, I. T., 2002, Principal Component Analysis, New York, Springer-Verlag ,487 p.:

Kerans, C., 1988, Karst-controlled reservoir heterogeneity in Ellenburger Group carbonates of West Texas: AAPG Bulletin, v. 72, no. 10, p. 1160-1183.

Keilen, H. B., 1992, Lower Permian sedimentary sequences in Central Spitsbergen, Svalbard, in K. Nakamura, ed., Investigations on the Upper Carboniferous-Upper Permian succession of West Spitsbergen: Department of Geology and Mineralogy, Faculty of Sciences, Hokkaido University, Japan, p. 127–134.

Koch, J. T., and Frank, T. D., 2011, The Pennsylvanian-Permian transition in the low-latitude carbonate record and the onset of major Gondwanan glaciation: Palaeogeography, Palaeoclimatology, Palaeoecology, v. 308, p. 362–372.

Krotov, P., 1888, Geological research on the western slope of Urals of Solikamsk and Cherdynsk, Trudy Geologicheskago Komiteta, St-Petersburg, 6, p. 297–534 (in Russian).

Larssen, G., Elvebakk, G., Henriksen, E., Kristensen, S. E., Nilsson, I., Samuelsberg, T., Svånå, T. A., Stemmerik, L., and Worsley, D., 2005, Upper Palaeozoic Lithostratigraphy of the southern part of the Norwegian Barents Sea, p. 1-43.

Larssen, G. B., Elvebakk, G., Henriksen, L. B., Kristensen, S. E., Nilsson, I., Samuelsberg, T. J., Svånå, T. A., Stemmerik, L., and Worsley, D., 2002, Upper Paleozoic lithostratigraphy of the Southern Norwegian Barents Sea: Norwegian Petroleum Directorate Bulletin 9, p. 76.

Lees, A., and Buller, A. T., 1972, Modern temperate-water and warm-water shelf carbonate sediments contrasted: Marine Geology, v. 13, p. 67–73.

Lewis, C., 1997, Seismic attributes for reservoir monitoring: A feasibility study using forward modeling: The Leading Edge, v. 16, no. 5, p. 459-470.

Linari, V., Santiago, M., Pastore, C., Azbel, K., and Poupon, M., 2003, Seismic facies analysis based on 3D multiattribute volume classification, La Palma Field, Maracaibo, Venezuela: The Leading Edge, v. 22, no. 1, p. 32-36.

Lindstrom, S., 2003, Carboniferous palynology of the Loppa High Barents Sea, Norway: Norwegian Journal of Geology, v. 83, no. 4, p. 333-349.

Lønøy, A. 1988: Environmental setting and diagenesis of Lower Permian Palaeoaplysina buildups and associated sediments from Bjørnøya, Implications for exploration of the Barents Sea: Journal of Petroleum Geology, v. 11, p. 141–156.

Loucks, B., and Handford, C. R., 1992, Origin and recognition of fractures, breccias, and sediment fills in paleocave-reservoir networks, in Candelaria, M. P., and Reed, C. L., eds., Paleokarst, karst related diagenesis and reservoir development: examples from Ordovician-Devonian age strata of west Texas and the mid-continent: Permian Basin Section SEPM Publication 92-33, p. 31-44.

Loucks, R. G., 1999, Paleocave carbonate reservoirs; origins, burial-depth modifications, spatial complexity, and reservoir implications: AAPG Bulletin, v. 83, no. 11, p. 1795-1834.

Loucks, R. G., and Mescher, P. K., 1997, Interwell scale architecture, heterogeneity, and pore-network development in paleocave reservoirs: Dallas Geological Society and SEPM Field Trip 11, p. unpaginated.

Lucia, F. J., 1995, Lower Paleozoic cavern development, collapse, and dolomitization, Franklin Mountains, El Paso, Texas, in Budd, D. A., Saller, A. H., and Harris, P. M., eds., Unconformities and porosity in carbonate strata: Tulsa, The American Association of Petroleum Geologist, AAPG Memoir 63, p. 279-300.

Mangerud, G. 1994, Palynostratigraphy or the Permian and lowermost Triassic succession, Finnmark Platform, Barents Sea: Review of Palaeobotany and Palinology, v. 82, p. 317–349.

Mazullo, S. J., and Chilingarian, G. V., 1996, Hydrocarbon reservoirs in karsted carbonate rocks, *in* G. V. Chilingarian, Mazullo, S. J., and Rieke, H. H., eds., Carbonate reservoir characterization: a geologic-engineering analysis, part II: Amsterdam, Elsevier, p. 797-685.

McMechan, G. A., Loucks, R. G., Zeng, X., and Mescher, P. K., 1998, Ground penetrating radar imaging of a collapsed-paleocave system in the Ellenburger dolomite, central Texas: Journal of Applied Geophysics, v. 39, p. 1-10.

Meldahl, P., Heggland, R., Bril, B., and De Groot, P., 2001, Identifying faults and gas chimneys using multiattributes and neural networks: The Leading Edge, v. 20, no. 5, p. 474-482.

Mitchum, R. M., Vail, P. R., and Sangree, J. B., 1977, Seismic Stratigraphy and Global Changes of Sea Level, Part 6: Stratigraphic Interpretation of Seismic Reflection Patterns in Depositional Sequences, *in* Payton, C., ed., Seismic Stratigraphy - application to hydrocarbon exploration, Volume Memoir 26: Tulsa, Oklahoma, American Association of Petroleum Geologists, p. 117 - 133.

Morin, J., Desrochers, A., and Beauchamp, B., 1994, Facies analysis of Lower Permian platform carbonates, Sverdrup Basin, Canadian Arctic Archipelago: Facies, v. 31, p. 105–130.

Mørk, A., Dallmann, W. K., Dypvik, H., Johannesen, E. P., Larssen, G., Nagy, J., Olaussen, S., Pcelina, T. m., and Worsley, D., 1999, Mesozoic lithostratigraphy, *in* Dallmann, W. K., ed., Lithostratigraphic Lexicon of Svalbard. Review and Recommendations for Nomenclature Use. Upper Paleozoic to Quaternary Bedrock: Tromsø, Norsk Polarinstitutt, p. 127-214.

Mutti, M., and Hallock, P., 2003, Carbonate systems along nutrient and temperature gradients: some sedimentological and geochemical constraints: International Journal of Earth Sciences (Geol Rundsch), v. 92, p. 465–475.

Nakazawa, T, Ueno, K., Kawahata, H., and Fujikawa, M., 2011, Gzhelian–Asselian Palaeoaplysina–microencruster reef community in the Taishaku and Akiyoshi limestones, SW Japan: Implications for Late Paleozoic reef evolution on mid-Panthalassan atolls, Palaeogeography, Palaeoclimatology, Palaeoecology, v. 310, p. 378–392.

Nakrem, H. A., 1991, Conodonts from the Permian succession of Bjørnøya (Svalbard): Norsk Geologisk Tidsskrift, v. 71, p. 235-248.

Neal, J., and Abreu, V., 2009, Sequence stratigraphy hierarchy and the accommodation succession method: Geology, v. 37, no. 9, p. 779-782.

Nelson, C. S., 1988a, An introductory perspective on non-tropical shelf carbonates, in Nelson, C. S., ed., Non-Tropical Shelf Carbonates-Modern and Ancient, Sedimentary Geology, v. 60, p. 3–14

Nelson, C. S., 1988b, Non-tropical carbonate deposits on the modern New Zealand shelf, in Nelson, C. S., ed., Non-Tropical Shelf Carbonates-Modern and Ancient, Sedimentary Geology, v. 60, p. 71–94.

Palmer, A., 1981, A Geological Guide to Mammoth Cave National Park, Teaneck: New Jersey, Zephyrus Press.

Palmer, A. N., 1989, Geomorphic history of the Mammoth Cave System, *in* White, W. B., and White, E. L., eds., Karst Hydrology: Concepts from the Mammoth Cave Area: New York, Van Nostrand Reinhold.

Palmer, A. N., 1991, Origin and morphology of limestone caves: Geological Society of America Bulletin, v. 103, no. 1, p. 1-21.

Palmlöv, E., 1995, Seismic stratigraphy and tectonics of the Loppa High, western Barents Sea.

Pomar, L., 2001, Types of carbonate platforms: a genetic approach: Basin Research, v. 3, p. 313–334.

Pomar, L., and Kendall, C., 2007, Architecture of carbonate platforms: a response to hydrodynamics and evolving ecology, in J. Lukasik, and A. Simo, eds., Controls on Carbonate Platform and Reef Development: SEPM Special Publication, 89, p. 187–216.

Prosser, S., 1993, Rift-related linked depositional systems and their seismic expression: Geological Society, London, Special Publications, v. 71, no. 1, p. 35-66.

Purdy, E. G., 1974, Reef configurations: cause and effect, in Laporte, L. F., ed., Reefs in Time and Space, Volume Special Publication 18: Tulsa, Society of Economic Palaeontologists and Mineralogists.

Purdy, E. G., and Waltham, D., 1999, Reservoir implications of modern karst topography: Aapg Bulletin, v. 83, no. 11, p. 1774-1794.

Purser, B. H., Barrier, P., Montenat, C., Orszag-Sperber, F., D'Estevou, P. O., Plaziat, J. C., and Philobbos, E., 1998, Carbonate and siliciclastic sedimentation in an active tectonic setting: Miocene of the north-western Red Sea rift, Egypt, in Purser, B., and Bosence, D. J., eds., Sedimentation and Tectonics in Rift Basins Red Sea:- Gulf of Aden, Springer Netherlands, p. 239-270.

Purser, B. H., and Bosence, D., 1998, Sedimentation and Tectonics of Rift Basins: Red Sea–Gulf of Aden, London (UK), Chapman Hall-Kluwers.

Purves, W. J., Burnitt, L. R., Weathers, L. R., and Wipperman, L. K., 1992, Cave/pillar definition in the Ordovician Ellenburger reservoir by 3-D seismic, Pegasus field Midland and Upton counties, Texas, AAPG Annual Meeting Program and Abstracts p. 108.

Quinlan, J. F., and Ewers, R. O., 1989, Subsurface drainage in the Mammoth Cave area, in White, W. B., and White, E. L., eds., Karst Hydrology: Concepts from the Mammoth Cave Area: New York, Van Nostrand Reinhold.

Raeuchle, S. K., Hamilton, D. S., and Uzcategui, M., 1997, Integrating 3-D seismic imaging and seismic attribute analysis with genetic stratigraphy; implications for infield reserve growth and field extension, Budare Field, Venezuela: The Leading Edge, v. 16, no. 9, p. 1338-1339.

Rafaelsen, B., Elvebakk, G., Andreassen, K., Stemmerik, L., Colpaert, A., and Samuelsberg, T. J., 2008, From detached to attached carbonate buildup complexes — 3D seismic data from the upper Palaeozoic, Finnmark Platform, southwestern Barents Sea: Sedimentary Geology, v. 206, no. 1-4, p. 17-32.

Read, J. F., 1985, Carbonate platform facies models: AAPG Bulletin, v. 69, p. 1–21.

Reid, C. M., James, N. P., Beauchamp, B., and Kyser, T. K., 2007, Faunal turnover and changing oceanography: Late Palaeozoic warm-to-cool water carbonates, Sverdrup Basin, Canadian Arctic Archipelago: Palaeogeography, Palaeoclimatology, Palaeoecology, v. 249, p. 128–159.

Rønnevik, H., and Jacobsen, H. P., 1984, Structural highs and basins in the western Barents Sea, in Spencer, A. M., ed., Petroleum Geology of North European Margin: London, Graham & Trotman, p. 19-32.

Ruiz-Ortiz, P. A., Bosence, D. W. J., Rey, J., Nieto, L. M., Castro, J. M., and Molina, J. M., 2004, Tectonic control of facies architecture, sequence stratigraphy and drowning of a Liassic carbonate platform (Betic Cordillera, Southern Spain): Basin Research, v. 16, no. 2, p. 235-257.

Saggaf, M. M., Toksoz, M. N., and Marhoon, M. I., 2003, Seismic facies classification and identification by competitive neural networks: Geophysics, v. 68, no. 6, p. 1984-1999.

Samuelsberg, T. J., Elvebakk, G., and Stemmerik, L., 2003, Late Paleozoic evolution of the Finnmark Platform, southern Norwegian Barents Sea: Norwegian Journal of Geology v. 83, p. 351-362.

Sarg, J. F. R., and Schuelke, J. S., 2003, Integrated seismic analysis of carbonate reservoirs: From the framework to the volume attributes: The Leading Edge, v. 22, no. 7, p. 640-645.

Sayago, J., Di Lucia, M., Mutti, M., Cotti, A., Sitta, A., Broberg, K., Przybylo, A., Buonaguro, R., and Zimina, O., 2012, Characterization of a deeply buried paleokarst terrain in the Loppa High using core data and multiattribute seismic facies classification: AAPG Bulletin, v. 96, no. 10, p. 1843-1866.

Schlager, W., 1989, Drowning unconformities on carbonate platforms, in Crevello, P., Wilson, J. L., Sarg, J. F., and Read, J. F., eds., Controls on Carbonate Platforms and Basin Development, Volume 44, SEPM Spccial Publication p. 15-25.

Schlager, W., 2003, Benthic carbonate factories of the Phanerozoic: International Journal of Earth Sciences (Geol Rundsch), v. 92, p. 445–464.

Scotese, C. R., and McKerrow, W. S., 1990, Revised World maps and introduction: Geological Society, London, Memoirs, v. 12, no. 1, p. 1-21.

Scotese, C. R., and Langford, R. P., 1995, Pangea and the palaeogeography of the Permian, in P. A. Scholle, T. M. Peryt, and D. S. Ulmer-Scholle, eds., The Permian of Northern Pangea. Volume 1: Paleogeography, Paleoclimates, Stratigraphy, Springer-Verlag, Berlin, p. 3–18.

Sharp, I. R., Gawthorpe, R. L., Underhill, J. R., and Gupta, S., 2000, Fault-propagation folding in extensional settings: Examples of structural style and synrift sedimentary response from the Suez rift, Sinai, Egypt: Geological Society of America Bulletin, v. 112, no. 12, p. 1877-1899.

Skaug, M., Dons, C. E., Lauritzen, Ø., and Worsley, D., 1982, Lower Permian Palaeoaplysina bioherms and associated sediments from central Spitsbergen: Polar Research, v. 2, p. 57–75.

Skirius, C., Nissen, S., Haskell, N., Marfurt, K., Hadley, S., Ternes, D., Michel, K., Reglar, I., D'Amico, D., Deliencourt, F., Romero, T., D'Angelo, R., and Brown, B., 1999, 3-D seismic attributes applied to carbonates: The Leading Edge, v. 18, no. 3, p. 384-393.

Smelror, M., Petrov, O., Larssen, G. B., and Werner, S., 2009, ATLAS: geological history of the Barents Sea: Geological Survey of Norway. Trondheim.

Sohregan, G. S., and Giles, K. A., 1999, Amplitudes of Late Pennsylvanian glacioeustacy: Geology, v. 27, p. 255-258.

Soudet, H. J., Sorriaux, P., and Rolando, J. P., 1994, Relationship between Fractures and Karstification - the Oil - Bearing Paleokarst of Rospo Mare (Italy): Bulletin des Centres de Recherches Exploration-Production Elf Aquitaine, v. 18, p. 97-257.

Steel, R. J., and Worsley, D., 1984, Svalbard's post-Caledonian strata - an atlas of sedimentational patterns and paleogeographic evolution, in Spencer, A. M., Holter, E., Johnsen, S. O., Mørk, A., Nysæther, E., Songstad, P., and Spinnangr, A., eds., Petroleum Geology of the North European Margin: London, Graham&Trotman, p. 109-135.

Stemmerik, L., and Worsley, D., 1989, Late Paleozoic sequence correlation, North Greenland and the Barents Shelf, in Collinson, J. D., ed., Correlation in Hydrocarbon exploration: London, Graham & Trotman, p. 100-113.

Stemmerik, L., Vigran, J. O., and Piasecki, S., 1991, Dating of late Paleozoic rifting events in the North Atlantic: New biostratigraphic data from the uppermost Devonian and Carboniferous of East Greenland: Geology, v. 19, no. 3, p. 218-221.

Stemmerik, L., and Larssen, G. B., 1993, Diagenesis and Porosity Evolution of Lower Permian Palaeoaplysina Buildups, Bjornoya, Barents Sea: An Example of Diagenetic Response to High Frequency Sea Level Fluctuations in an Arid Climate: Chapter 12: , Diagenesis, Sequence Stratigraphy, and Changes in Relative Sea Level, AAPG Special Volumes.

Stemmerik, L., P. A. Larson, G. B. Larssen, A. Mørk, and B. T. Simonsen, 1994, Depositional evolution of Lower Permian Palaeoaplysina build-ups, Kapp Duner Formation, Bjørnøya, Arctic Norway: Sedimentary Geology, v. 92, p. 161–174.

Stemmerik, L., Nilsson, I., and Elvebakk, G., 1995, Gzelian-Asselian depositional sequences in the western Barents Sea and North Greenland, Norwegian Petroleum Society Special Publications, Volume 5, Elsevier, p. 529-544.

Stemmerik, L., and Worsley, D., 1995, Permian history of the Barents Shelf area, *in* Scholle, P. A., Peryt, T. M., and Ulmer-Scholle, D. S., eds., The Permian of Northern Pangea, Volume 2. Sedimentary Basins and Economic Resources: Berlin, Springer-Verlag, p. 81-97.

Stemmerik, L., Håkansson, E., Madsen, L., Nilsson, I., Piasecki, S., Pinard, S., and Rasmussen, J. A., 1996, Stratigraphy and depositional evolution of the Upper Palaeozoic sedimentary succession in eastern Peary Land, North Greenland: Bulletin Grønlands Geologiske Undersøgelse, v. 171, p. 45-71.

Stemmerik, L., 1997, Permian (Artinskian-Kazanian) cool-water carbonates in North Greenland, Svalbard and the western Barents Sea, in James, N. P., and Clarke, J. A. D., eds., Cool-water Carbonates, Society of Economic Paleontologists and Mineralogists Special Publication 56, p. 349-364.

Stemmerik, L., Elvebakk, G., Nilsson, I., and Olaussen, S., 1998, Comparison of upper Bashkirian-upper Moscovian high frequency sequences between Bjørnøya and the Loppa High, western Barents Sea, *in* Gradstein, F. M., Sandvik, K. O., and Milton, N. J., eds., Sequence Stratigraphy – concepts and applications, Volume NPF Special Publication 8: Amsterdam, Elsevier, p. 215-227.

Stemmerik, L., Elvebakk, G., and Worsley, D., 1999, Upper Palaeozoic carbonate reservoirs on the Norwegian Arctic Shelf: delineation of reservoir models with application to the Loppa High: Petroleum Geoscience, v. 5, no. 2, p. 173-187.

Stemmerik, L., 2000, Late Palaeozoic evolution of the North Atlantic margin of Pangea: Palaeogeography, Palaeoclimatology, Palaeoecology, v. 161, no. 1-2, p. 95-126.

Stemmerik, L., and Worsley, D., 2000, Upper Carboniferous cyclic shelf deposits, Kapp Kåre Formation, Bjørnøya, Svalbard: response to high frequency, high amplitude sea level fluctuations and local tectonism: Polar Research, v. 19, no. 2, p. 227-249.

Stemmerik, L., 2003, Controls on localization and morphology of Moscovian (Late Carboniferous) carbonate buildups, southern Amdrup Land, North Greenland, in W. M. Ahr, P. M. Harris, W. A. Morgan, and I. D. Somerville, eds, Permo-Carboniferous Carbonate Platforms and Reefs. SEPM Special Publication no. 78, p. 253–265.

Stemmerik, L., and Worsley, D., 2005, 30 years on - Artic Upper Paleozoic stratigraphy, depositional evolution and hydrocarbon prospectivity: Norwegian Journal of Geology, v. 85, p. 151-168.

Stemmerik L., 2008, Influence of late Paleozoic Gondwana glaciations on the depositional evolution of the northern Pangean shelf, North Greenland, Svalbard, and the Barents Sea, in C. R. Fielding, T. D. Frank, and J. L. Isbell, eds., Resolving the Late Paleozoic Ice Age in Time and Space: Geological Society of America Special Publication, 441, p. 205–217.

Taner, M. T., Koehler, F., and Sheriff, R. E., 1979, Complex seismic trace analysis: Geophysics, v. 44, no. 6, p. 1041-1063.

Tebo, J. M., and Hart, B. S., 2005, Use of Volume-Based 3-D Seismic Attribute Analysis to Characterize Physical-Property Distribution: A Case Study to Delineate Sedimentologic Heterogeneity at the Appleton Field, Southwestern Alabama, U.S.A: Journal of Sedimentary Research, v. 75, no. 4, p. 723-735.

Tinker, S. W., Ehrets, J. R., and Brondos, M. D., 1995, Multiple karst events related to stratigraphic cyclicity: San Andres Formation, Yates field, west Texas, *in* Budd, D. A., Saller, A. H., and Harris, P. M., eds., Unconformities and porosity in carbonate strata, AAPG Memoir 63, p. 213-238.

Tucker, M. E., and Wright, V. P., 1990, Carbonate sedimentology: Blackwell, Oxford, 496 p.

Vachard, D., and Kabanov P., 2007, Palaeoaplysina gen. nov. and Likinia Ivanova and Ilkhobskii, 1973 emend., from the type Moscovian (Russia) and the algal affinities of the ancestral palaeoaplysinaceae n. comb.: Geobios, v. 40, p. 849–860.

Vail, P., and Mitchum, R., 1977, Seismic Stratigraphy and GLobal Changes of Sea Level, Part 3: Relative Changes of Sea Level from Coastal onlap: Exxon Mobil, p. 1-19.

Viniegra, O. F., and Castillo-Tejero, C., 1970, Golden Lane fields, Veracruz, Mexico, *in* Halbouty, M. T., ed., Geology of giant petroleum fields: Tulsa, The American Association of Petroleum Geologist, AAPG Memoir 14, p. 25-309.

Wahlman, G. P., 2002, Upper Carboniferous–Lower Permian (Bashkirian–Kungurian) mounds and reefs, in W. Kiessling, E. Flügel, and J. Golonka, eds., Phanerozoic Reef Patterns: SEPM Special Publication, 72, p. 271–338.

Warren, J. K., 2006, Evaporites: Sediments, Resources and Hydrocarbons, Heidelberg, Springer, 1035 p.

Williams, H. D., Burgess, P. M., Wright, V. P., Della Porta, G., and Granjeon, D., 2011, Investigating carbonate platform types: multiple controls and a continuum of geometries: Journal of Sedimentary Research, v. 81, p. 18–37.

White, E. L., and White, W. B., 1969, Processes of cavern breakdown: National Speleothem Society Bulletin, v. 31, p. 83-96.

White, R. E., 1991, Properties of instantaneous seismic attributes: The Leading Edge, v. 10, no. 7, p. 26-32.

White, W. B., 1988, Geomorphology and hydrology of karst terrains, New York, University Press, 464 p.

Worsley, D., 2006, The post-Caledonian geological development of Svalbard and the Barents Sea: Norsk Geologisk Forening, Abstracts and Proceedings, no. 3.

Worsley, D., 2008, The post-Caledonian development of Svalbard and the western Barents Sea: Polar Research, v. 27, no. 3, p. 298-317.

Worsley, D., Agdestein, T., Gjelberg, J., Kirkemo, K., Mørk, A., Nilsson, I., Olaussen, S., Steel, R. J., and Stemmerik, L., 2001, The geological evolution of Bjørnøya, Artic Norway: implications for the Barents Shelf: Norwegian Journal of Geology, v. 81, p. 195-234.

Wright, V. P., Esteban, M., and Smart, P. L., 1991, Paleokarst and Paleokarstic Reservoirs: University of Reading, PRIS Contribution 152, p. 157.

Wright, V. P., 1992, Speculations on controls on cyclic peritidal carbonates: ice-house versus greenhouse eustatic controls: Sedimentary Geology, v. 76, p. 1-5.

Wright, V. P., and T. P. Burchette, 1996, Shallow-water carbonate environments, in H. G. Reading, ed., Sedimentary Environments: Processes, Facies and Stratigraphy, Blackwell Science Ltd, Oxford, p. 325–394.

Wright, V. P., and T. P. Burchette, 1996, Carbonate ramps: an introduction, in V. P. Wright, and T. P. Burchette, eds., Carbonate Ramps, Geological Society of London, Special Publication, v. 149, p. 1–5.

Yuan, D., 1991, Karst of China, Beijing, Geological Publishing House, 224 p.:

Zhemchugova, V. A., and Schamel, S., 1994, Carboniferous-Lower Permian Carbonate Reservoirs of the Timan-Pechora Basin: International Geology Review, v. 36, no. 1, p. 15-23.